Department of Civil and Environmental Engineering

Stanford University

Seismic Performance of Steel Corrugated Shear Walls

By

László Gergly Vigh,
Abbie Liel,
Steve Tipping,
Eduardo Miranda,
and Gregory G. Deierlein

Report No. 178
August 2012

The John A. Blume Earthquake Engineering Center was established to promote research and education in earthquake engineering. Through its activities our understanding of earthquakes and their effects on mankind's facilities and structures is improving. The Center conducts research, provides instruction, publishes reports and articles, conducts seminar and conferences, and provides financial support for students. The Center is named for Dr. John A. Blume, a well-known consulting engineer and Stanford alumnus.

Address:

The John A. Blume Earthquake Engineering Center
Department of Civil and Environmental Engineering
Stanford University
Stanford CA 94305-4020

(650) 723-4150
(650) 725-9755 (fax)
racquelh@stanford.edu
http://blume.stanford.edu

Abstract

A new approach to develop seismic response factors for the design of structural systems has recently been developed by the Applied Technology Council in ATC Project 63. Referred to as FEMA P695, the assessment methodology provides a comprehensive and objective approach to evaluate the performance factors based on non-linear structural analysis and considering the uncertainties in design requirements, supporting test data, and the non-linear model. The basis of the methodology is to ensure an acceptably low likelihood of structural collapse under extreme (rare) earthquake ground motions. The methodology is based on the design and assessment of representative archetypical building designs, whose collapse performance is evaluated through a series of non-linear static and dynamic analyses using numerical models that are calibrated to experimental test data. This methodology is applied to evaluate the seismic performance factors for a new light-framed steel shear wall seismic force resisting system, developed by Tipping Mar and Associates of Berkeley, California. The system consists of a steel corrugated sheet shear wall for use in mid-size residential and commercial structures. Calibration of the non-linear analysis model parameters to test data is done using genetic algorithms. The system archetypes evaluated in this study are shown to meet the FEMA P695 acceptance criteria for a seismic response modification factor of R equal to 4.

Acknowledgements

The authors express their thanks to The Thomas Cholnoky Foundation for sponsoring Laszlo Vigh's study sojourn at Stanford University, in the framework of the Dr. Imre Koranyi Scholarship.

Table of contents

List of figures

List of tables

1. Introduction

1.1. Purpose and objectives

Tipping Mar + Associates, Berkeley, California has recently developed a light-gage steel shear wall system for use in mid-size residential and commercial earthquake-resistant buildings. [1]

This research aims to estimate the global seismic performance parameters of the newly developed system, *e.g.* R factor, through collapse analyses of archetype buildings. The parameter quantification is being completed in accordance with the method developed by Applied Technology Council Project 63 and published in FEMA P695 [2], which has strong relation to performance based earthquake engineering methodology, and focuses on assessing collapse risk to establish acceptable life safety performance [2].

The purpose of this study is two-fold: a) to provide an appropriate value of the response modification factor R, by which the shear wall system is deemed to have acceptable collapse safety; b) as one of the first practical applications, to demonstrate the FEMA P695 methodology and outline the practically arising complications.

1.2. Shear wall system description

The shear wall system proposed in [1] utilizes low profile corrugated steel sheet as sheathing, which is fastened to cold-formed steel framing with screws. Vertical studs are located at every 610 mm (2 ft) on center; and horizontal end tracks are applied at the top and bottom of the wall. The configuration, corrugation geometry and typical connection details are shown in Figure 1-1 and 1-2.

By changing the thickness of the corrugated plate, boundary members, screw size and spacing various load capacities can be achieved. The sheathing can be placed either one or both sides of the boundary members. Gypsum finishing can be also added. The configurations of proposed – and experimentally tested – assemblies are listed in Table 1-1. Groups indicated by red color – based on the ductility observed in test – are not recommended for practical use, as will be described later. Based on the test results, design strengths for various combinations of sheathing thickness, stud thickness and screw spacing are recommended for practical application [1]. Application for seismic design by elastic analysis (e.g., equivalent lateral force procedures) requires the establishment of appropriate seismic performance factors to adjust the force and displacement demands from elastic analysis to account for inelastic effects.

Note that the sheathing corrugation runs horizontally, providing the same strength against both positive and negative loading. (An inclined configuration would provide maximum shear strength in one direction and a reduced capacity in the other. In such case, sheathing should be placed in pairs in order to avoid the unsymmetrical global behavior.)

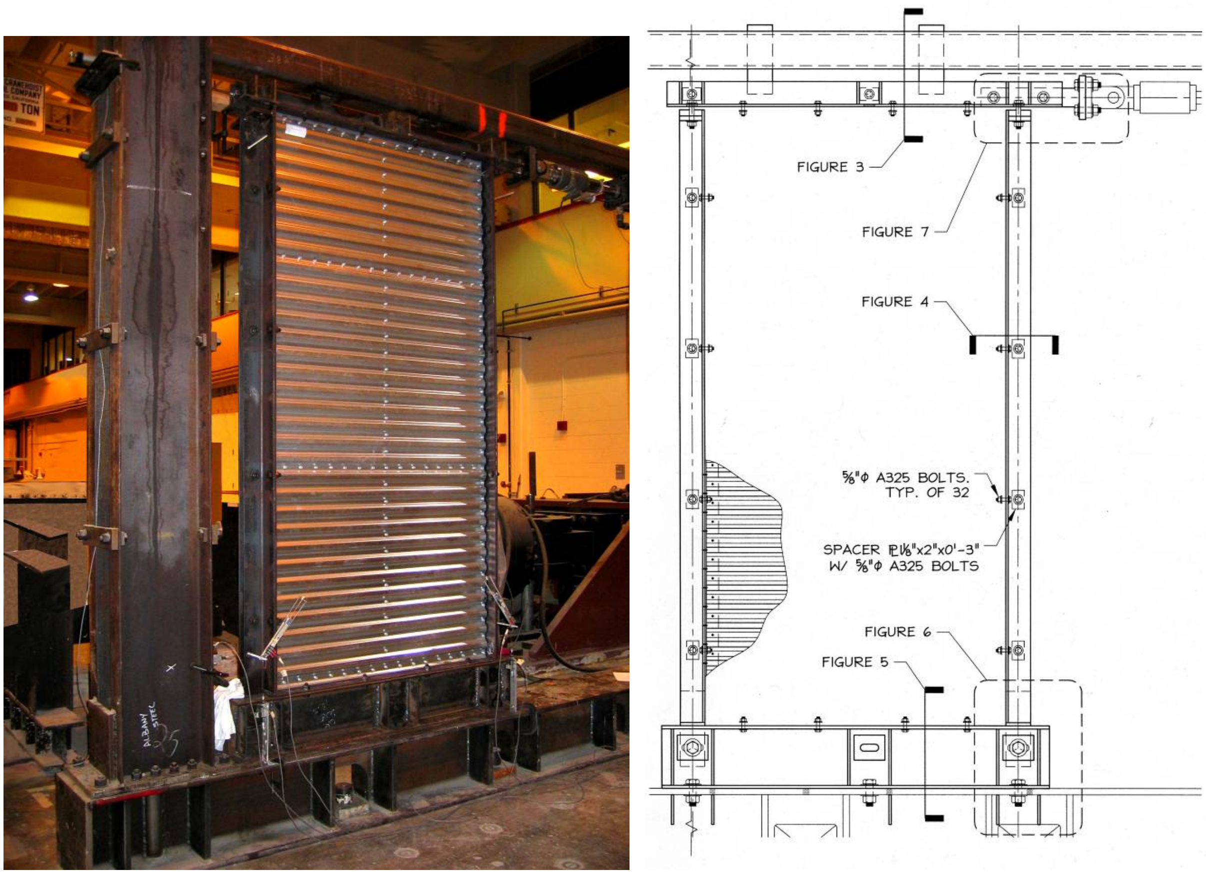

Figure 1-1. Shear wall – test configuration. [1]

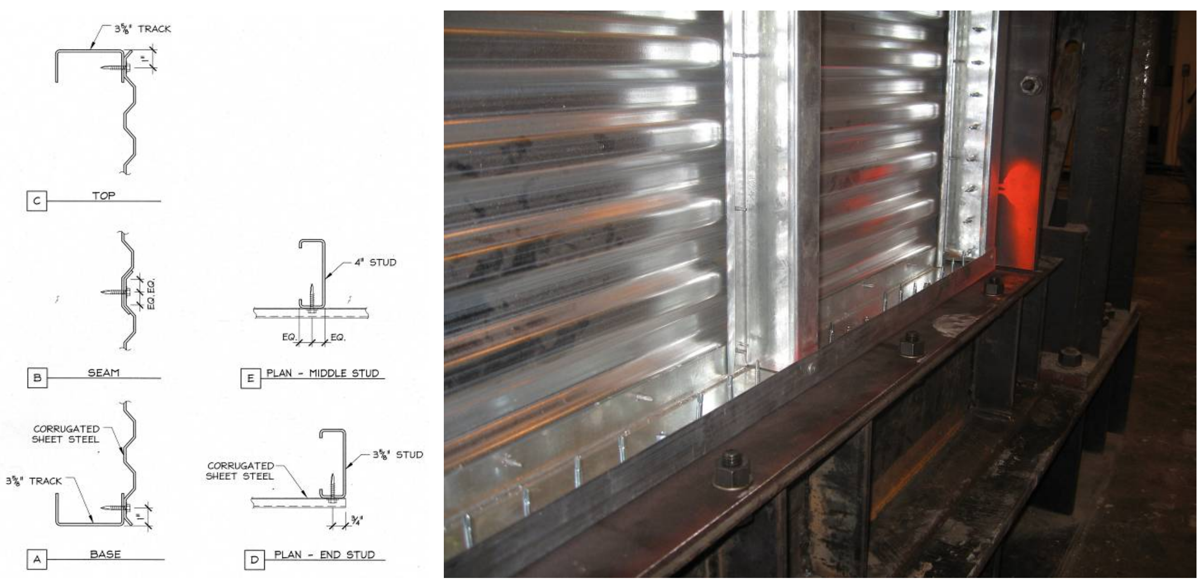

Figure 1-2. Shear wall – details. [1]

Table 1-1. Proposed shear wall configurations (Group Index Matrix). [1]

Assembly	stud gauge	20	18	16	16
	screw size	12	12	12	14
sheathing	screw spacing	Group #			
22	6"	1	25	7	
22	3"	3	6	8	
18	3"		13	14	16

(Note: groups in red are not recommended for practical application)

1.3. Seismic performance quantification by FEMA P695

FEMA P695 [2] provides a comprehensive general framework for seismic performance evaluation of new systems. The methodology achieves the primary life safety performance objective by requiring an acceptably low probability of collapse of the seismic force resisting system for maximum considered earthquake (MCE) ground motions. It presumes that the structural system is clearly defined and so-called archetype buildings that well represent the application fields are determined. For this family of archetype buildings, common performance factors, such as the response modification factor R, the overstrength factor Ω_0 and the displacement modification factor C_d are estimated by the method. The method consists of the following steps:

1) Multiple realizations of idealized archetypical lateral systems are designed, covering the expected range of building heights, bay widths, gravity load ratios, seismic design categories, etc. Typically 20-30 different building archetypes are designed in accordance to design provisions and assuming certain performance parameters.
2) Analytical model of the building archetypes are developed and calibrated to test data (Figure 1-3a).
3) By means of nonlinear static pushover analysis (Figure 1-3b) the overstrength factor and the global ductility are determined for each archetype.
4) Nonlinear incremental dynamic analysis (IDA, Figure 1-4) is completed for each archetype model, using 22 pairs of ground motion records that are specified by the FEMA P695 document.
5) Based on the IDA results, adjusted fragility curves (Figure 1-4b) are derived and the adjusted collapse margin ratio (ACMR) – the ratio of the median collapse intensity and MCE – is calculated. If ACMR exceeds the minimum acceptable value given by FEMA P695, the collapse probability is acceptably low and the seismic performance factors assumed in the designs are deemed to be appropriate. The acceptable values of ACMR account for the uncertainties in the model, control of failure modes, quality of experimental data, etc. If the required ACMR is not met, then one has to restart with the archetype design using a decreased R-value.

In the above process, the analytical model development and calibration of the model is a key issue. The model should capture all the relevant failure modes and represent the hysteretic behavior of the structure. It should also be as simple as possible (to facilitate the large number of analysis to be completed), while faithfully representing the collapse response. In this study shear wall is modeled by single uniaxial elements, as Figure 1-3a illustrates. The shear wall is the primary design element, and possible contributions from the columns and beams are conservatively ignored. The properties of the model are described in more detail later.

For further details on the methodology refer to [2] and [3].

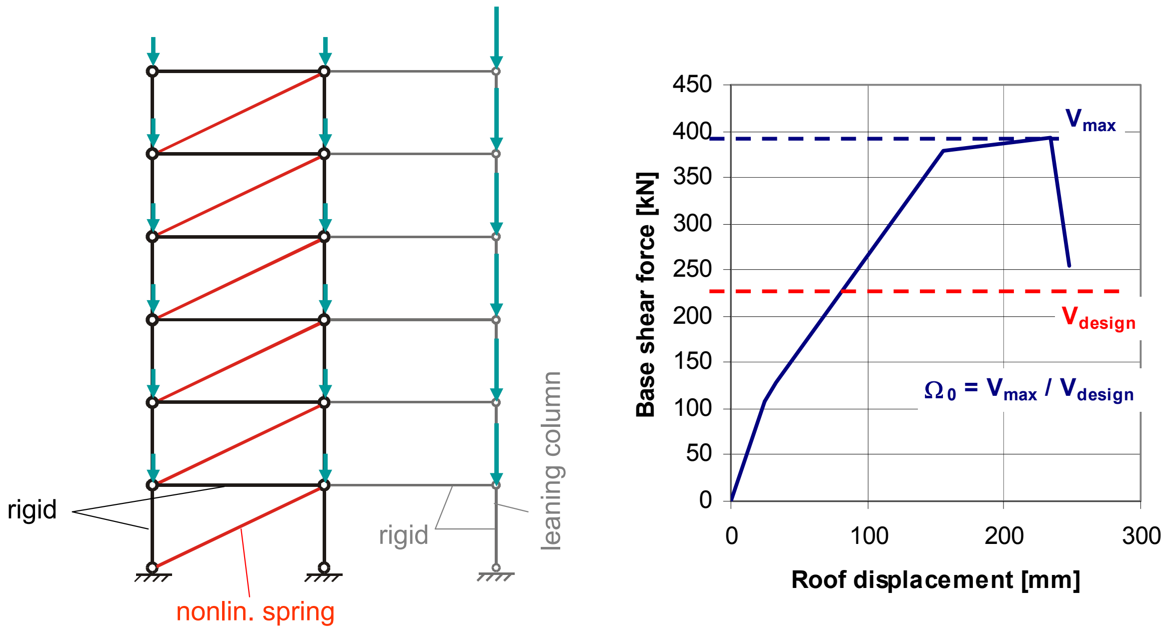

a) numerical model b) capacity curve from pushover analysis

Figure 1-3. Archetype building model and nonlinear static (pushover) analysis.

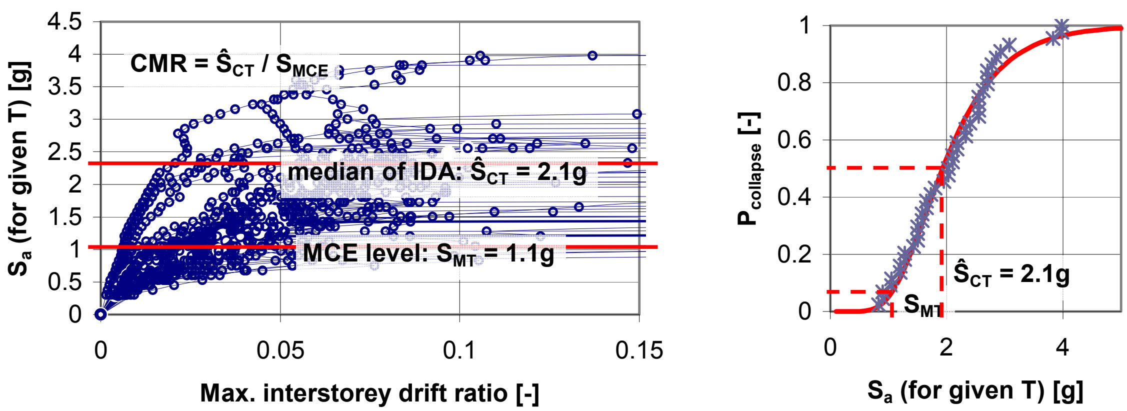

a) IDA result b) collapse fragility curve

Figure 1-4. Results of nonlinear incremental dynamic analysis for an individual archetype building.

2. Experimental results

2.1. Test configuration and test program

The analytical model is calibrated to test data. The experimental research is shortly summarized hereafter. For the detailed experimental program refer to [1].

Cyclic tests on corrugated panels (Figure 1-1 and 2-1) measuring approximately 1.2 m wide and 2.5 m high were completed by Stojadinovic et al. [1] at the University of California, Berkeley. Altogether, 44 specimens (24 groups) were tested to investigate six design parameters:

1. corrugated sheet thickness,
2. gauge of studs and tracks,
3. screw type/size,
4. fastener spacing,
5. inclusion of gypsum board,
6. one-sided or double-sided corrugated sheet application.

The AC154 [12] cyclic loading protocol was applied and no monotonic testing was completed. The basic configurations – one-sided sheathing with no gypsum board – are tabulated in Table 2-1; these assemblies provide a design basis. For further reference, the assembly group numbers are also indicated in the table. Note that Group #25 is listed in the table, but was not actually tested.

Table 2-1. Tested configurations of shear walls (Group Index Matrix).

Assembly	stud gauge	20	18	16	16
	screw size	12	12	12	14
sheathing	**screw spacing**	**Group #**			
22	**6"**	1	25	7	
22	**3"**	3	6	8	
18	**3"**		13	14	16

Figure 2-1. Test configuration. [1]

2.2. Result summary

Figure 2-2 illustrates the typical hysteresis curve of the shear wall. Figure 2-3 showing the cyclic envelope curves draws a general idea on the shear strength and ductility of the assemblies relative to each other. The cyclic envelope curve (or group backbone curve) was calculated in accordance to AC154; the test data of specimens in the same group were averaged [1, 12]. In this figure, the concentrated force applied during the tests is converted to a linear force per unit wall length.

The typical failure sequence of the shear wall developed in the tests as follows (Figure 2-4):

- due to the cyclic loading, failure starts at the connection zones: gouging of decking is observed at the screws,
- as the holes elongate, screws start to pull out, followed by screw tilt, which results in lower shear load resistance of the connection zone (cyclic degradation),
- because of the screw pull-out lateral support of the sheathing is drastically reduced; and ultimately, plate buckling of the partially restrained corrugated panel develops.

During the tests, no failure of the boundary members, *i.e.* studs, was observed. The failure always initiated in the connection zones, and plate buckling occurred as a consequence of the connection failure. Note that screw connections in the vicinity of the corners failed, indicating non-uniform load distribution. The plate buckling and warping of the panel typically develops after the failure of the connection zones in the vicinity of the corners, and thus it has little influence on the load capacity.

From Figure 2-2, the pinching characteristics of the hysteresis behavior can be observed. It can be also stated that although strength and ductility differ, in general the experimented behavior is very similar to the one of typical wooden shear walls made of OSB panels [2] as a consequence of the similar failure mechanism and component performance.

Table 2-2 summarizes the nominal shear capacity of the different assemblies. Each assembly group differs by sheathing thickness, stuck thickness, screw size and screw spacing. Typically, three duplicate specimens were conducted in each configuration and results were averaged. The nominal shear capacities were calculated in accordance to AC130 [13] protocol [1]. The design strength for ASD design (Table 2-3) is derived from the nominal values by applying a safety factor of 2.5.

The experimental research and its findings are detailed in [1].

Note for readers: From Section 3 onward (except for Section 5.1 dealing with archetype design), results will be reported in SI units instead of imperial units.

Table 2-2. Nominal shear capacity. [1]

Assembly	**stud gauge**	**20**	**18**	**16**	**16**
	screw size	**12**	**12**	**12**	**14**
sheathing	**screw spacing**	**Shear (plf)**			
22	**6"**	1173	1505	1836	
22	**3"**	2165	3227	3290	
18	**3"**		4144	5164	5874

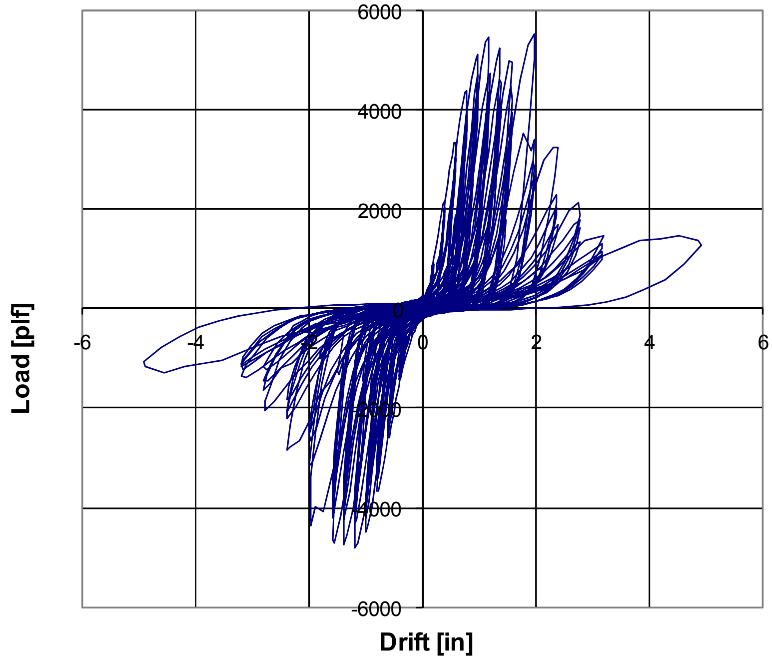

Figure 2-2. Typical hysteresis curve. [1]

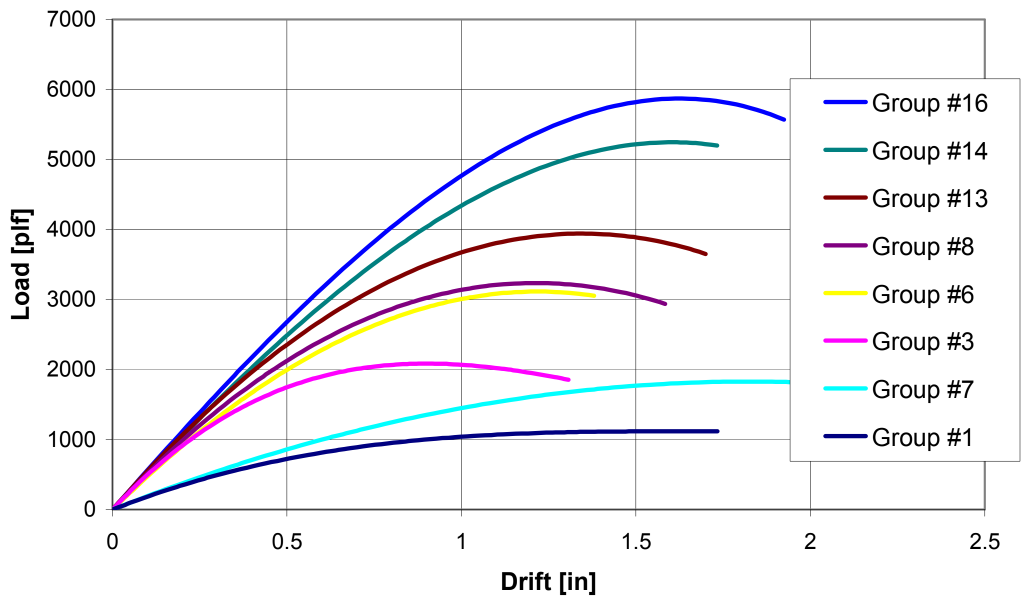

Figure 2-3. Cyclic envelope capacity curves for averages of different groups of specimens. [1]

a) bearing b) screw pull-out / tilt

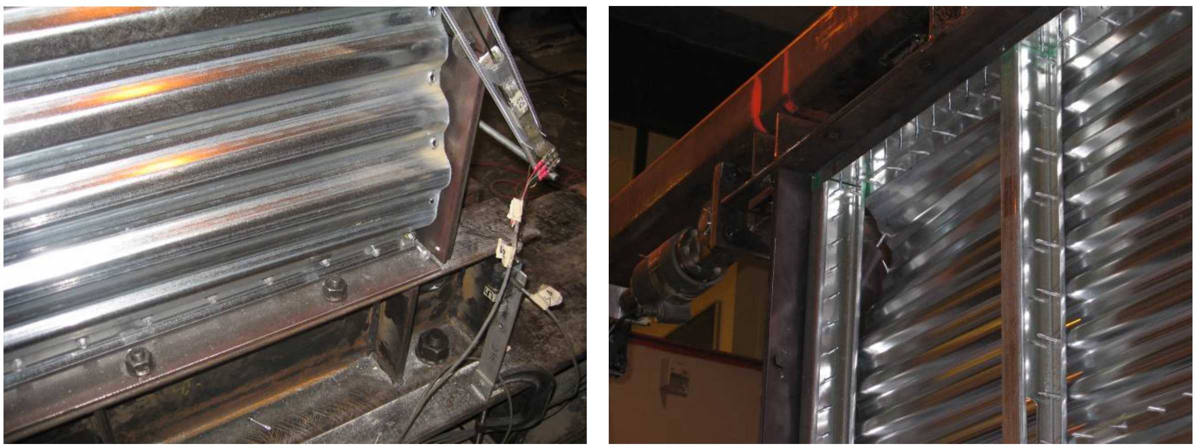

c) buckling and warping of corrugated sheet after screw pull-out

Figure 2-4. Observed failure sequence. [1]

Table 2-3. ASD design strength. [1]

Assembly	**stud gauge**	**20**	**18**	**16**	**16**
	screw size	**12**	**12**	**12**	**14**
sheathing	**screw spacing**	**Fasd (plf)**			
22	**6"**	469	602	706	
22	**3"**	866	1225	1316	
18	**3"**		1658	1835	2176

3. Shear wall behavior – estimation of monotonic backbone curve

3.1. Problem statement

The FEMA P695 methodology is based on the results of nonlinear static (pushover) and dynamic analyses of the archetype models. The monotonic pushover analysis is invoked for the evaluation of system overstrength and system ductility, while the ground motion intensity at collapse level can be calculated by the incremental nonlinear dynamic analysis.

In order to achieve an analytical model that reliably and accurately captures the actual behavior, accurate estimation of the monotonic backbone curve is necessary. Although the computationally intensive incremental dynamic analyses are carried out using a simplified model in *OpenSees* (see Section 4 and Figure 1-3a), a finite element model is developed first to predict monotonic behavior of the walls that captures the primary non-linear behavioral effects. On the one hand, it is straightforward that monotonic pushover analysis requires good representation of the component behavior under monotonic loading. On the other hand, it is also a key issue in the nonlinear dynamic analysis. Typically, structural analysis software requires the definition of a set of parameters characterizing the monotonic behavior and – in relation to this backbone curve – cyclic degradation parameters. The model calibration cannot be completed only on the basis of cyclic test results, as those are dependent on the load protocol. Calibration of the analysis model is complicated by the fact that the same cyclic results can be obtained with different sets of capping point locations (monotonic backbone curve) and degradation properties (i.e. infinite number of solution may be present). The challenge is to back-calculate a set of parameters that are generally applicable for any loading history.

Typically, the backbone curve parameters are outcomes of monotonic test results. Since monotonic tests were not conducted on the steel panel walls, separate detailed nonlinear static analysis is completed. The purpose is three-fold: a) to study the overall and local behavior and failure mechanism of the shear wall; b) to extend the results to longer wall configurations; c) to provide an estimation of the monotonic backbone curve.

3.2. Shear wall modeling technique

The test results proved that the connection zone failure dominates in the overall failure of the shear wall while buckling or overall yielding of the corrugated sheet does not play role. Consequently, for the detailed numerical modeling reliable representation of the screw connection behavior is required.

The shear walls are modeled in ANSYS [4], using shell elements, beam element and nonlinear springs to represent the sheathing, boundary members and the screw connections, respectively (Figure 3-1).

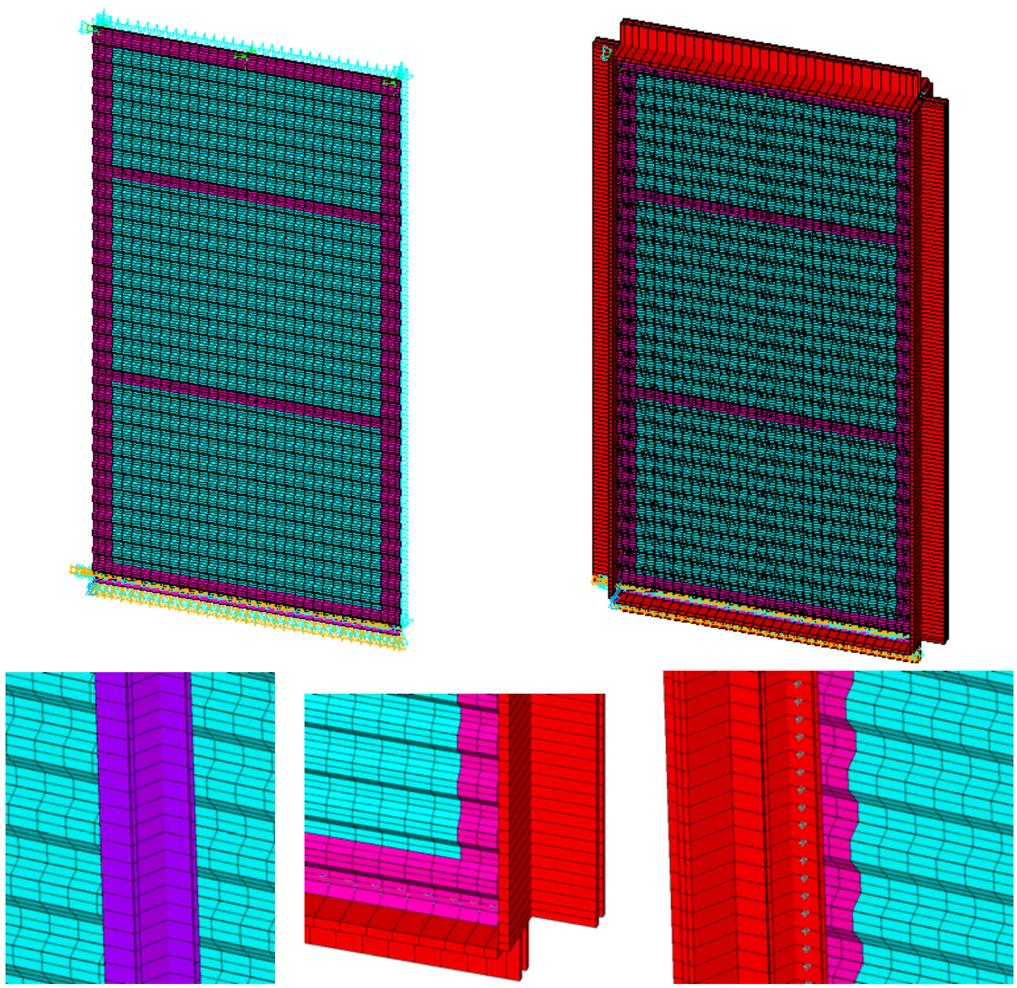

Figure 3-1. Shell-element model for global shear wall analysis.

A trilinear elastic-plastic material model is applied for the shell elements with the parameters: Young's modulus of E = 210 GPa; measured mean yield stress of f_y = 330, 330, 365 MPa for Groups #1, #8 and #14, respectively; and measured average tensile strength of f_u = 406, 406, 448 MPa for Group #1, #8 and #14, respectively. In the vicinity of the screw connections, the elements are assigned elastic material, because gouging of the deck is represented in the connection zone behavior through the nonlinear spring element.

Since the boundary member failure was not observed during the tests, elastic beam elements are sufficient; which was also certified by preliminary analysis.

As mentioned, screw connections are modeled with nonlinear spring elements. At each screw location three springs are placed: two springs for the in-plane degrees of freedom, and one for the out-of-plane degrees of freedom. With each spring a nonlinear force-displacement characteristics is associated. The relatively accurate estimation of this relation is a significant issue; the applied approach is detailed in the following sections.

An equivalent geometric imperfection is built in the model. The equivalent geometric imperfection substitutes for the total effect of geometric and other nature of imperfections (e.g. residual stresses due to welding, manufacturing). The first buckling mode that is dominant with respect to the shear ultimate capacity is chosen as imperfection, with an amplitude of 5 mm.

Based on a convergence study, it is found that a shell mesh size of 50 mm and 20 mm is reasonable in the horizontal (parallel to the corrugation) and vertical direction, respectively; and still relatively effective with respect to calculation time needs.

3.3. Single screw connection behavior and analysis

To accurately estimate the screw connection performance and develop a representative numerical model is not an easy task. The major challenge is that at large deck deformations due to bearing screw pull-out may randomly develop. As a consequence of this, a unique force-deflection relation does not exist; both the strength and ductility of the tested systems vary significantly. This problem is illustrated by tests performed by Dubina et al. (Figure 3-2, [5]).

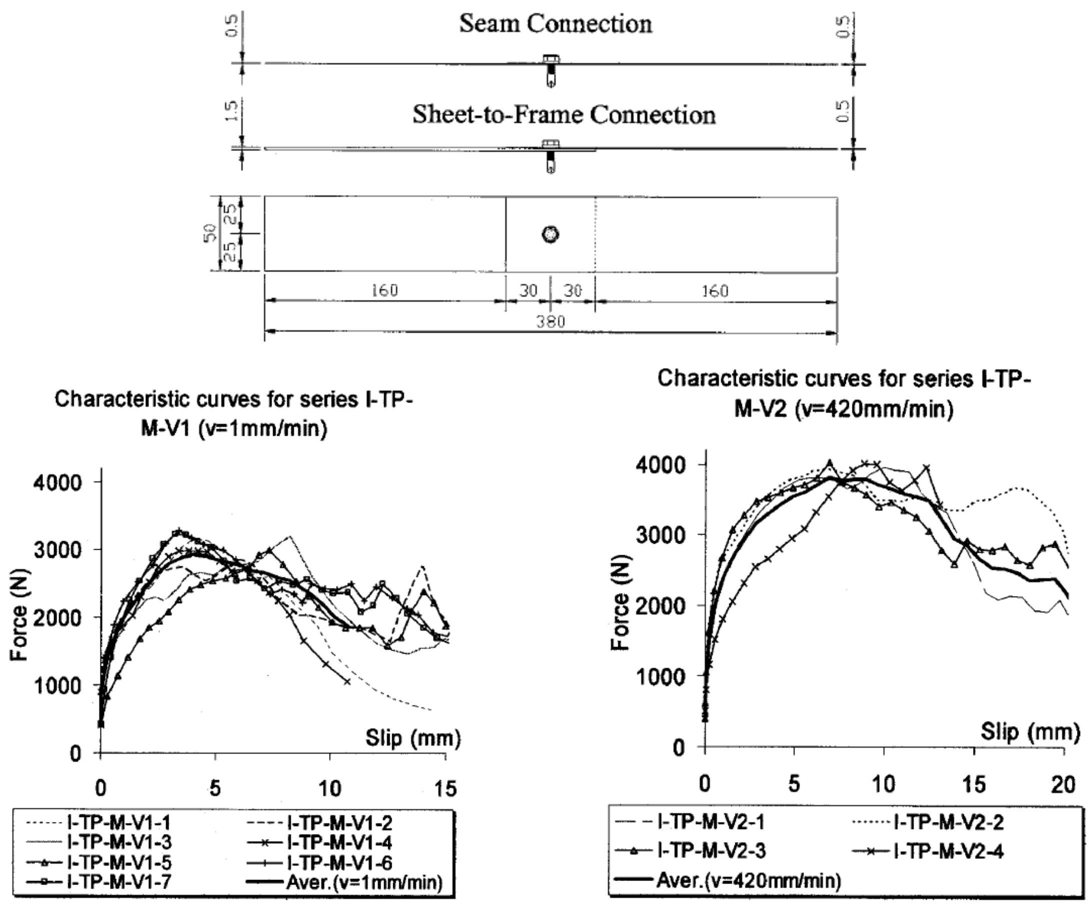

Figure 3-2. Connection test by Dubina et al. [5].

For the nonlinear models applied in FEMA P695, a mean characteristic behavior is to be considered. To find this representative characteristics, the following approaches are invoked:

- by literature review on related researches, a general idea on connection behavior, rigidity, strength and ductility can be drawn, which also provides a solid basis for further engineering judgments,
- strength data for the actual connections are available in literature,
- Eurocode 3 Part 1-3 (EC3-1-3, [6]) provides strength calculation method for such connections,
- by nonlinear submodel the ultimate capacity and ductility can be estimated.

Anderson and Peyton performed monotonic static test on thin-walled plates connected by screw. The investigated configurations cover a wide range of practical applications. The obtained shear, as well as pull-out resistances, are tabulated in Table 3-1. Note that the listed values are design strengths determined from the test results in accordance with the AISI code. To approximately back-calculate the nominal strength one has to multiply the given design resistance with the ratio of actual and characteristic yield strength, and with the safety factor 3.

The method proposed by EC3-1-3 is not detailed here. It can be stated that this method – compared to the above-discussed one – typically gives lower resistances for both shear and pull-out failures. In pull-out resistance the difference is substantial, even double in certain cases.

The above calculations provide guideline to the following adjustment procedure.

As shown in Figure 3-3, a submodel of small connection specimen is developed by the authors: one single plate with a hole is modeled. On the perimeter of the hole, compression-only rigid radial supports are placed. In this way, the single bearing resistance of the connection can be analyzed, and thus an upper boundary of the connection strength and rigidity and a lower boundary of the ductility can be estimated. If actual measured material properties are considered, the actual strength of the connection cannot be larger than the so calculated one. It can be stated that this value should be close enough to the actual strength, given that large tilting and pull-out do not influence the connection static behavior (this is assumed to be valid up to a relatively large deformation level before any screw pulls fully out). The typical outcome of this analysis is illustrated on Figure 3-4. (Note that the figure represents analyses with different material models for the steel plate: a) elastic-perfectly plastic and b) material model with defined yield plateau and strain hardening). Tilting and pull-out significantly – and almost unpredictably – effect the rigidity and specially the ductility.

As a consequence of the above investigations, a relatively good estimation for the mean strength of the screw connection can be made. However, with respect to rigidity and ductility, further model adjustment is required. For this purpose, the calculated force-displacement relation is built into the overall shear wall model, and the spring model is adjusted in the framework of an iterative procedure, on the basis of comparison of the tested and simulated overall behavior (Figure 3-6). In this procedure, it is assumed that cyclic degradation does not take place up to a certain level of deformation/loading, which basically means that the adjusted model shall follow the envelope curve determined by cyclic tests approximately up to its peak. Different spring characteristics are considered, whether including or eliminating the post-capping negative slope.

The results for different shear wall configurations indicate that there is no large difference between the cyclic and the monotonic maximum strength. This also means that consideration of negative slope in the spring characteristics hardly influences the strength. However, it does effect the capping point location (displacement at ultimate strength) and thus the ductility. The amount of the post-capping strength degradation on the connection level is not well studied; in lack of corresponding data its effect cannot be directly considered in this level. Alternatively, one may reduce the calculated capping displacement based on engineering judgments.

The performed analysis consequently does not give information on the overall post-capping behavior of the shear wall either.

The authors would like to emphasize that testing the actual screw connections would efficiently reduce the discussed uncertainties and would enable more accurate analysis capturing a wider range of the backbone curve.

Note that on component level, the connection strength depends on the thickness and strength of the connected materials and the screw size. Among the studied shear wall assemblies, there are only three different connection types. For the global analysis of the shear wall, a non-linear spring is applied to represent the behavior of the screw connection zone. The simplified spring characteristics (Figure 3-5) is derived from the submodel analysis. To capture the actual – measured – rigidity of the wall, the simplified spring model is adjusted for two basic wall assemblies (Group #14 and Group #1). As shown in Figure 3-6, the adjustment is completed in a way that the wall model provides the same overall wall rigidity and early plastic behavior as observed in the tests. The adjusted models are then applied in other assemblies: the calculated backbone curves well fit the tested cyclic envelope curves, which validates the applicability of the developed model.

Table 3-1. Strength of single screw connection, [10].

TABLE #1 (Anderson-Peyton Proposed Modified Screw Capacity)
ALLOWABLE SHEAR & PULLOUT VALUES
FOR A SINGLE SCREW CONNECTING LIGHT GAUGE STEEL[1,3,5]
NORTH AMERICAN SPECIFICATION FOR THE DESIGN OF COLD-FORMED STEEL MEMBERS
AISI Standard - 2001 Edition - Section E4 and Nominal Screw Test Strength[7]

			#8 screw		#10 screw		#12 screw	
Nominal Screw Strength Test Data[6]								
Ps screw test (Nominal Strength) =			**900**	**1615**	**1500**	**2515**	**2250**	**3665**
Allowable Value 0.8*Ps test / FS[7] =			**240**	**431**	**400**	**671**	**600**	**977**
	Design	**Material**	DIA.[4] =0.164		DIA.[4] =0.190		DIA.[4] =0.216	
Thick-ness MILS	**Thick-ness**[5] INCHES	**Ultimate Strength**[2] F_u- (KSI)	V SHEAR (LBS)	T PULL-OUT (LBS)	V SHEAR (LBS)	T PULL-OUT (LBS)	V SHEAR (LBS)	T PULL-OUT (LBS)
18 (25 GA)	0.0188	45	66	39	71	46	75	52
27 (22 GA)	0.0283	45	121	59	131	69	139	78
33 (20 GA)	0.0346	45	164	72	177	84	188	95
43 (18 GA)	0.0451	45	**240** ***(244)***	94	263	109	280	124
54 (16 GA)	0.0566	65	**240** ***(496)***	171	**400** ***(534)***	198	569	225
68 (14 GA)	0.0713	65	-NA-	-NA-	**400** ***(755)***	249	**600** ***(805)***	284
97 (12 GA)	0.1017	65	-NA-	-NA-	**400** ***(1130)***	356	**600** ***(1285)***	405

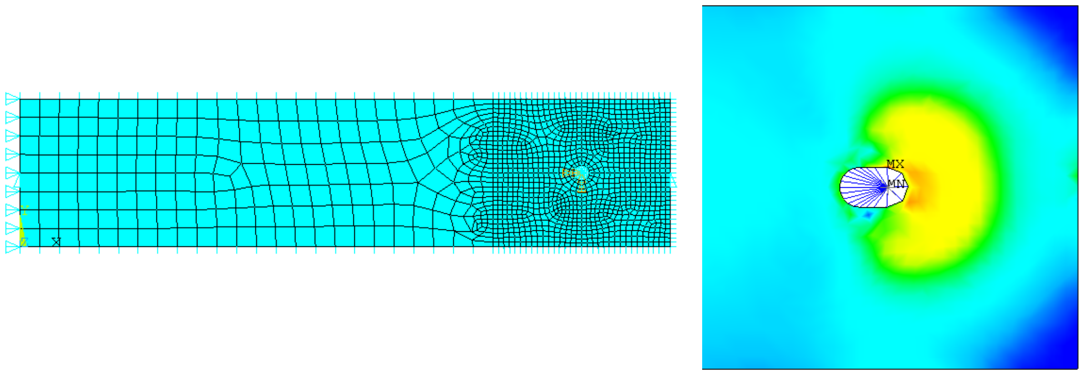

Figure 3-3. 2-D model and nonlinear analysis of screw single connection (submodel), showing bearing failure.

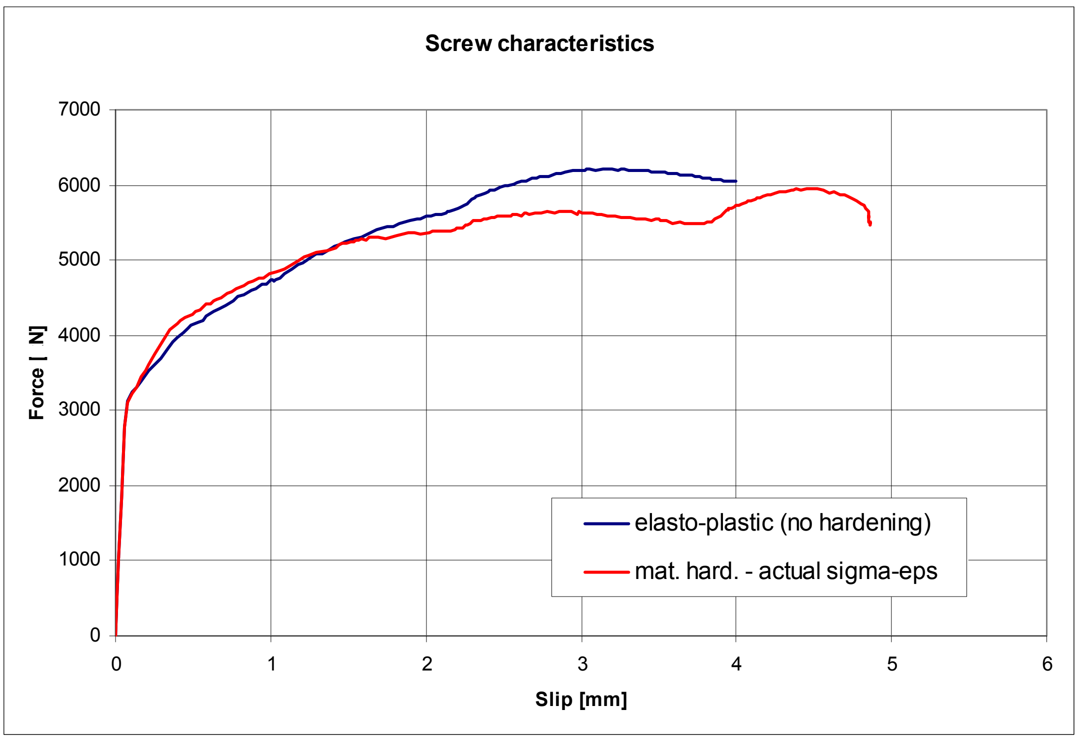

Figure 3-4. Screw characteristics from connection submodel analysis.

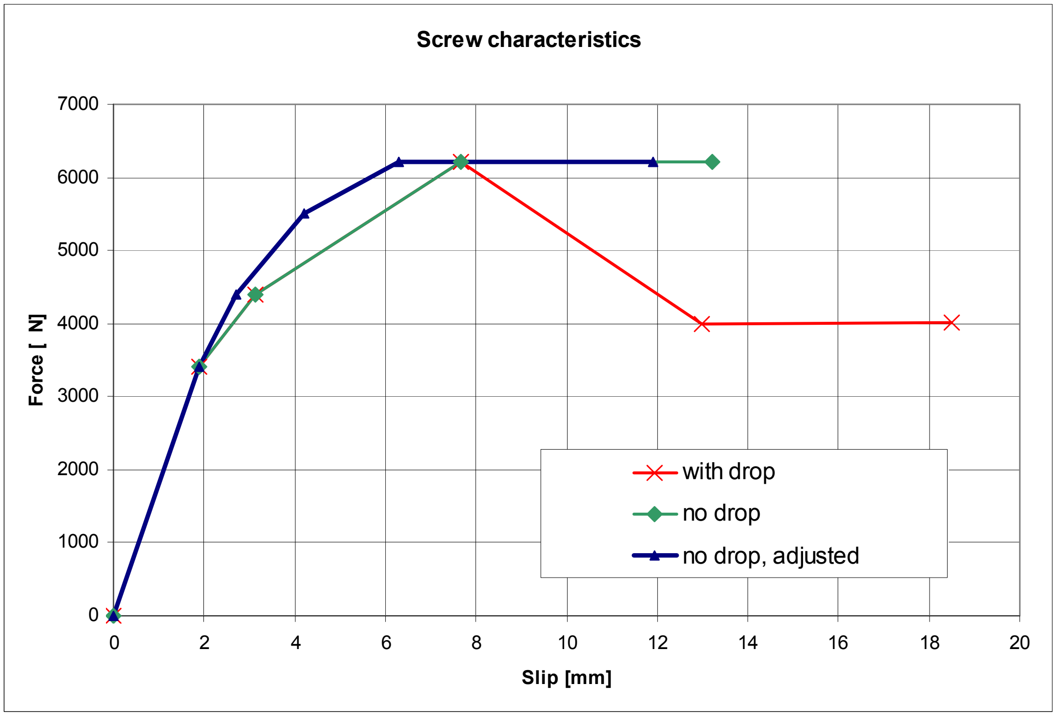

Figure 3-5. Simplified screw characteristics for global wall analysis.

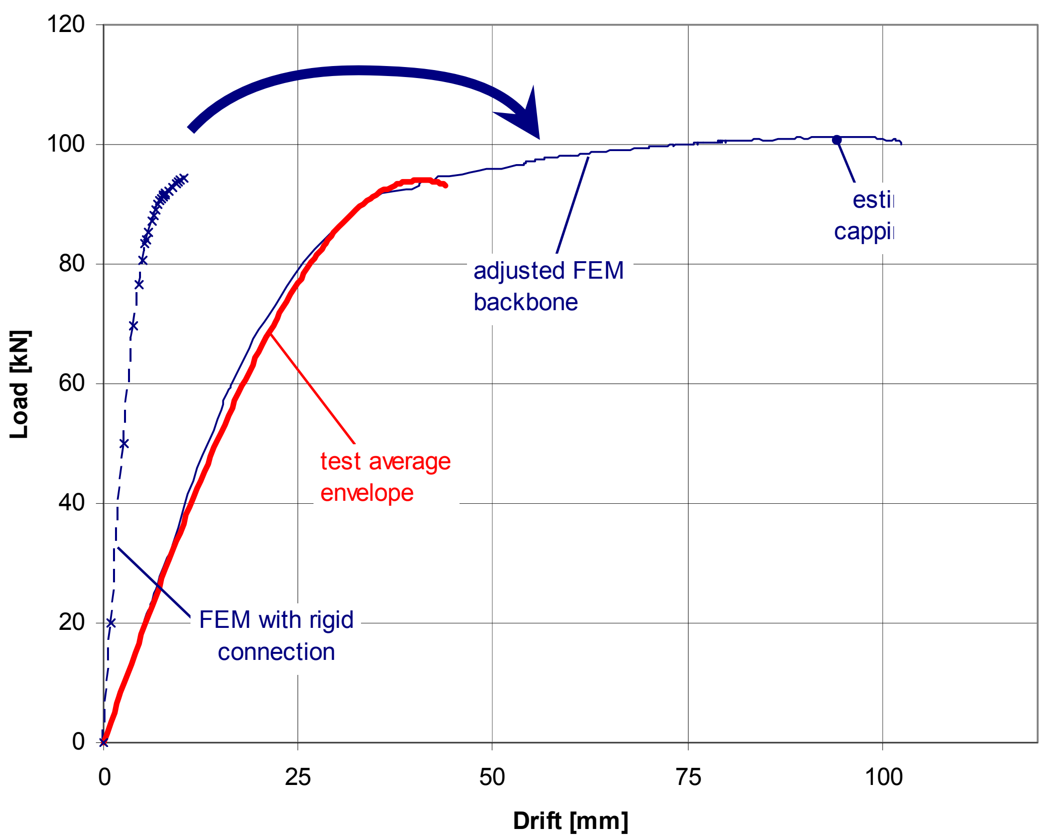

Figure 3-6. Monotonic backbone curve adjustment – Group #14.

3.4. Shear wall behavior and analysis

Beside the backbone curve estimation, the ANSYS model also helped the authors to better understand the overall wall behavior.

The results of the nonlinear analysis confirm that the corrugated sheet remains elastic even at large deformations and that the connection zone controls the failure initiation with the modes of bearing, tilting and finally pull-out. The screw pull-out is accompanied by the increased shear buckling deformations of the panel. The non-uniform load distribution along the boundaries is also observed, leading to a screw failure sequence similar to the one experienced by tests.

Additional linear buckling analysis is also completed. The typical buckling shape shown in Figure 3-7 well indicates the presence of overturning bending moment, which certainly reduces the shear capacity of the wall. Important to note that although plate buckling is dominant in the buckled shape, it interacts with the buckling of the vertical stud.

These observations raise the question whether the failure mode remains the same at other (longer) shear walls and so the tested results and the calibrated numerical models can be automatically extended to those cases.

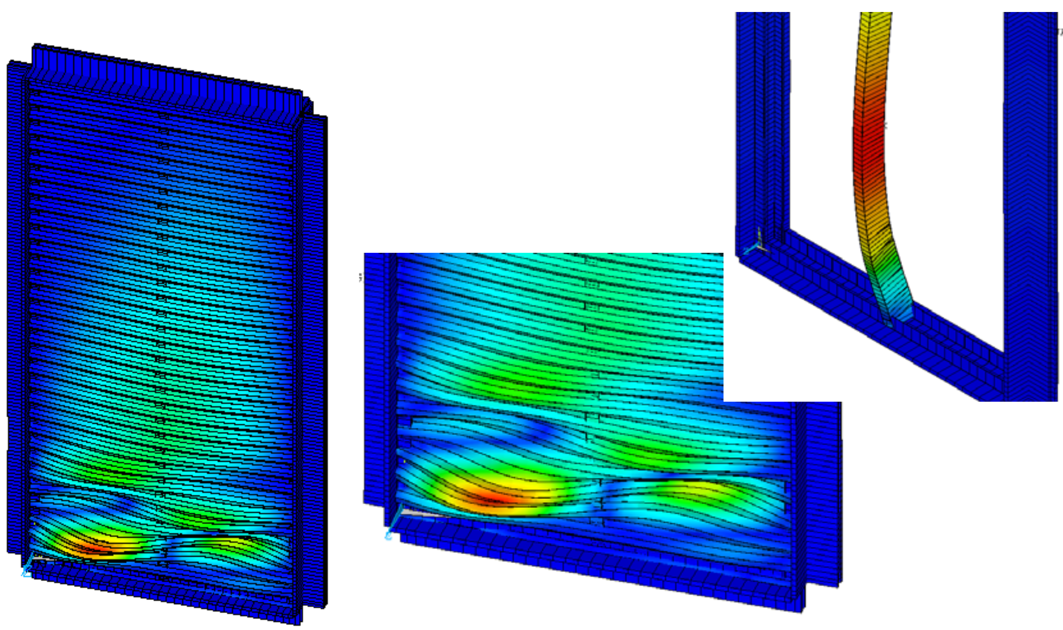

Figure 3-7. Buckling pattern of the tested wall – Group #14.

3.5. Extension to longer walls

Beyond calibration of the backbone curve parameters, the ANSYS model also provided information to examine walls with different aspect ratios. This is important, since the walls in the archetype designs are much longer than those tested. Whereas the tests had height-to-length ratios of 2:1, the more typical configurations have aspect ratios less than 1:1 and are longer (typically 8 ft ~ 32 ft or 2.4 ~ 9.7m). Therefore, as already mentioned, the calibrated models (after proper transformation) can only be applied in the global analysis if the same failure mechanism dominates the behavior of the longer walls as the tested ones.

Analysis of up to 32-feet long shear walls is completed by the shell-element model. In order to reduce the calculation demands, for the very long walls equivalent elastic orthotropic shell elements are employed in place of the previously shown detailed corrugated geometry. This simplification is reasonable due to the fact that excessive plate yielding is not expected.

Analysis of the shell-element model confirmed that connection failure is the governing failure mode of the longer wall, as observed in the short test panel. Although one may expect an increasing role of overall shear buckling in the long wall, the change in buckling capacity is negligible below an aspect ratio of 1. This is also justified by a parametric study based on a calculation method proposed by Eurocode 3 Part 1-5 [11].

Figure 3-8 compares the calculated shear load – drift relations. The numerical study helps to justify the assumption that the shear panel strength is linearly related to its length. Interestingly, the ratio of the strengths of the 8-feet (2.4 m) and 4-feet (1.2 m) walls is larger than 2 (approximately by a factor of 4/3), but beyond 8 feet the tendency becomes nearly linear in relation to the 8-feet case. It appears that the occurring overturning moment reduces the capacity in case of shorter walls, while its effect is vanishes at larger spans. Calculated buckling shapes (Figure 3-9 ~ 11) confirm this assumption. This allows for higher strengths in longer walls (lower aspect ratios) by applying a strength enhancement factor of α_L. [8]

It is also certified that ductility (and generally the occurring displacements) hardly changes when varying the wall length.

On the base of these observations, it is stated that the results of shorter walls can be extended to longer cases, either by linear strength transformation or considering the factor of 4/3 illustrated in the analyses.

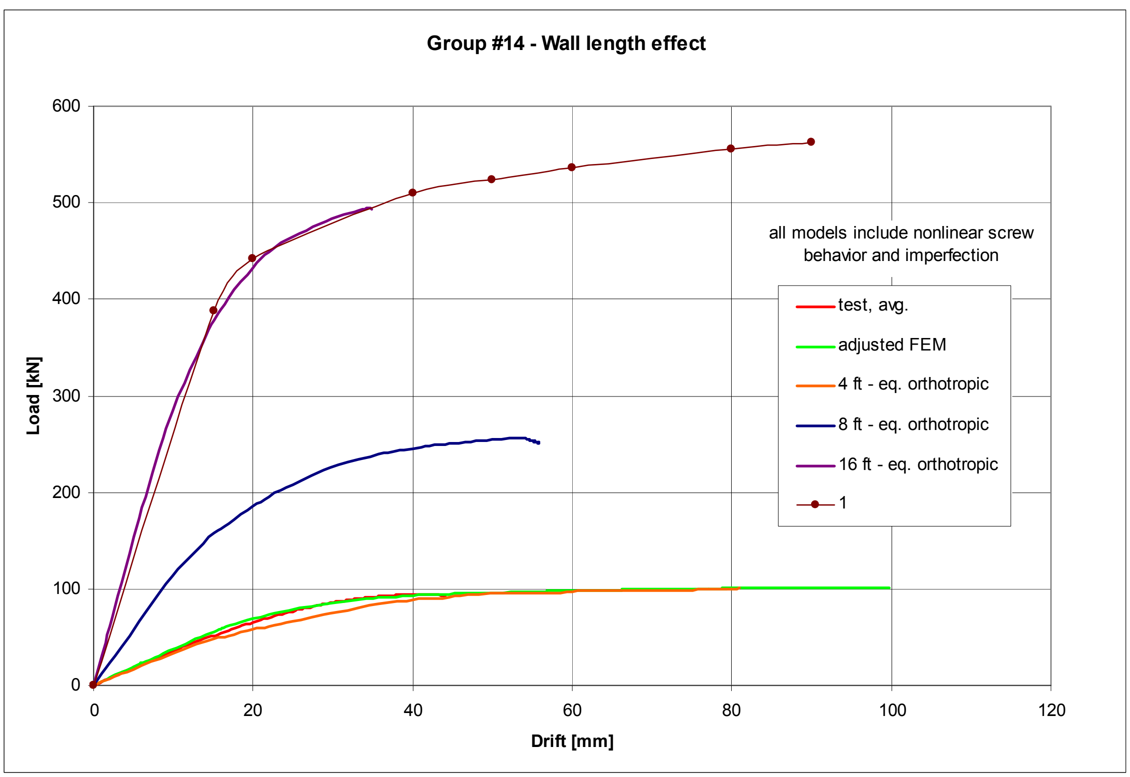

Figure 3-8. Wall length effect.

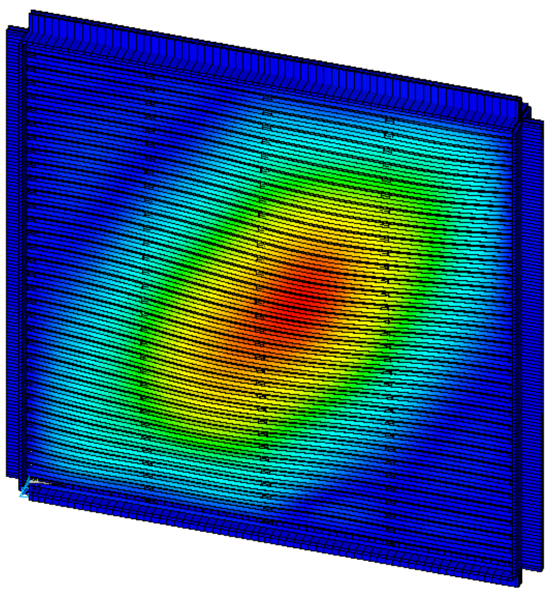

Figure 3-9. Buckling shapes of 8'-long wall.

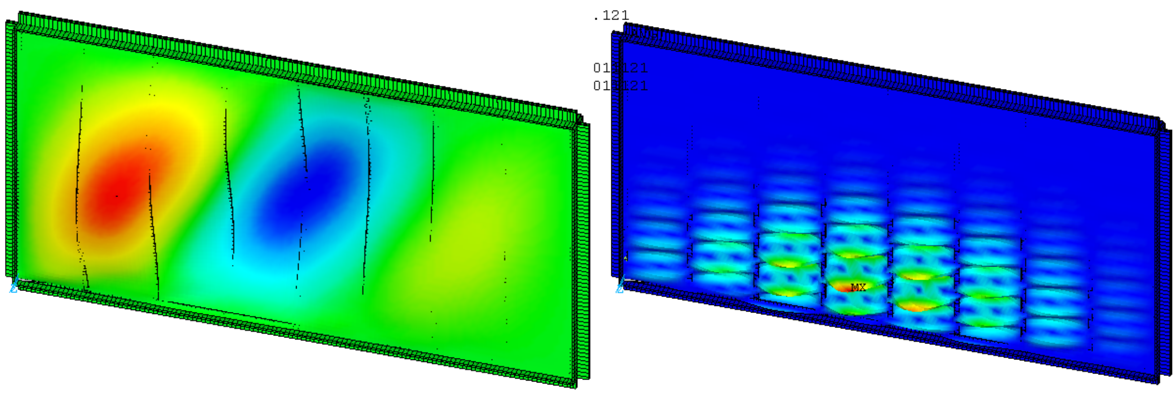

Figure 3-10. Buckling shapes of 16'-long wall.

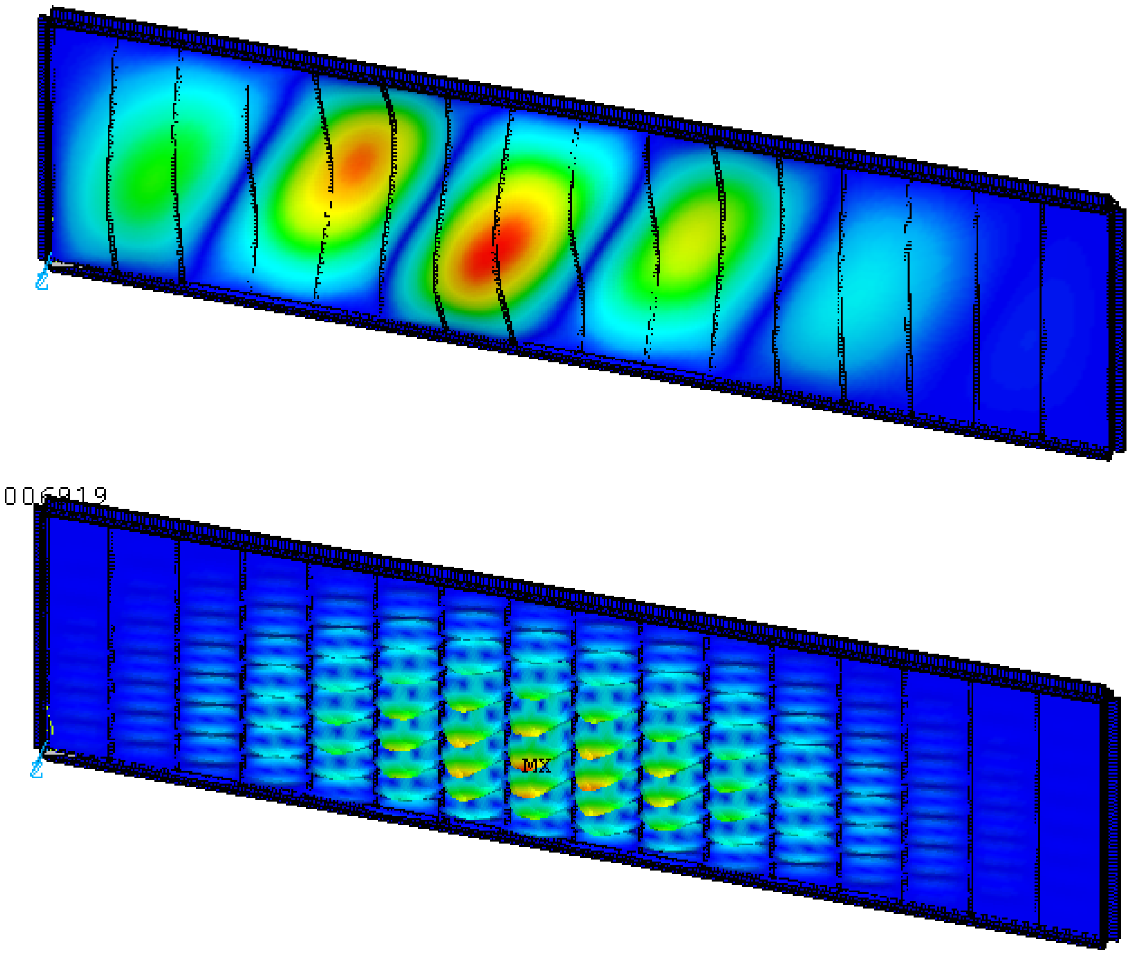

Figure 3-11. Buckling shapes of 32’-long wall.

4. Model calibration

4.1. Overview and approach of model calibration

The nonlinear model shall effectively serve both the pushover and the nonlinear dynamic analyses, meaning that it should reliably capture the monotonic and the cyclic behavior, including cyclic degradations as well. The software selected for the structural analysis is the Open Systems for Earthquake Engineering Simulation (OpenSees, [7]). As shown in Fig. 1-3a, the shear wall is represented by 2D truss, where the diagonal strut properties are calibrated to reflect the non-linear shear wall response (experimental data from [3]); other elements (including beams, columns and leaning column) are all elastic pin-connected members. Consequently, possible contributions from the columns and beams are conservatively ignored. A leaning column (pinned, rigid elements) is used to account for the masses that – in a vertical sense – are not directly transferred to the columns of braced bay, but are tributary to the bracing wall system with respect to lateral inertial load effects.

The calibration of the diagonal strut properties is complicated by the fact that large number of parameters is to be determined and that the backbone curve is not fully known. To perform the calibration, a genetic optimization algorithm is invoked.

4.2. Representative nonlinear numerical model of shear wall

The monotonic and cyclic behavior of the wall is modeled by the substitutive link element. Monotonic behavior is represented by the so-called backbone curve, and the hysteretic response is derived from the monotonic curve by means of cyclic loading and degradation parameters. The test results (referring back to Figure 2-2) show that the behavior is non-linear from the very beginning, which results in an unloading stiffness steeper than the effective (secant) initial stiffness. As mentioned, the shear wall itself is modeled by single uniaxial truss elements in the global archetype models. The pinching characteristics of the material behavior is clearly observable. It is also found that the characteristic curve is nonlinear from the very beginning, which results in an unloading stiffness steeper than the effective (secant) initial stiffness. In order to capture this behavior, two materials are combined in parallel, resulting in a short, steep initial part, as shown in Figure 4-1. To simulate cyclic degradation, the Ibarra-Medina-Krawinkler [8] model is applied. The resulting combined model can be described by 15 independent parameters:

a) parameters for the backbone curve (yield and ultimate loads F_{y1}, F_{y2}, F_u and corresponding displacements δ_{y1}, δ_{y2}, δ_m, capping slope α_C and residual r);

b) pinching parameters (α_p and β_p, refer to Figure 4-2);

c) cyclic degradation parameters (c, γ_A, γ_S, γ_D, γ_K, see Figure 4-3).

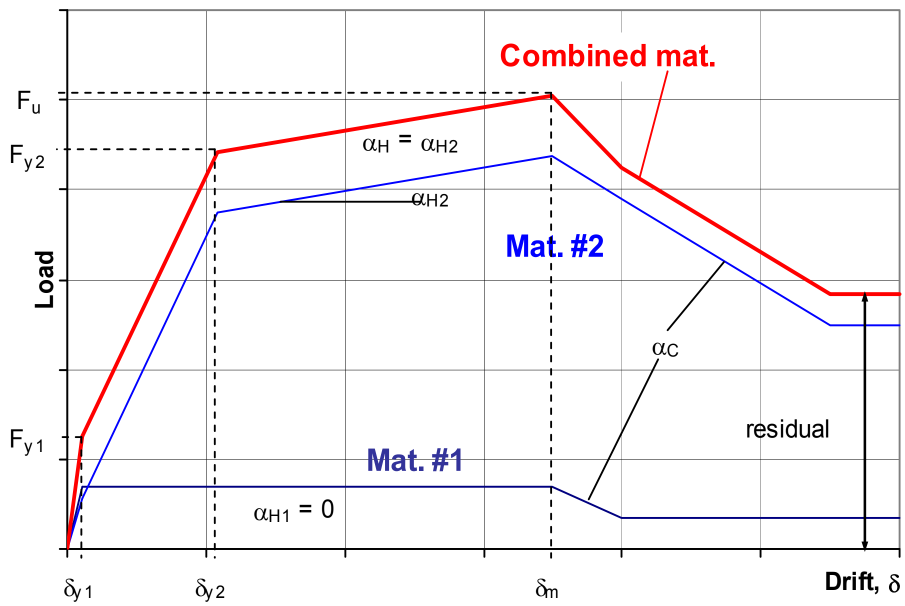

Figure 4-1. Response of two material springs defined in parallel to represent shear wall response at each story.

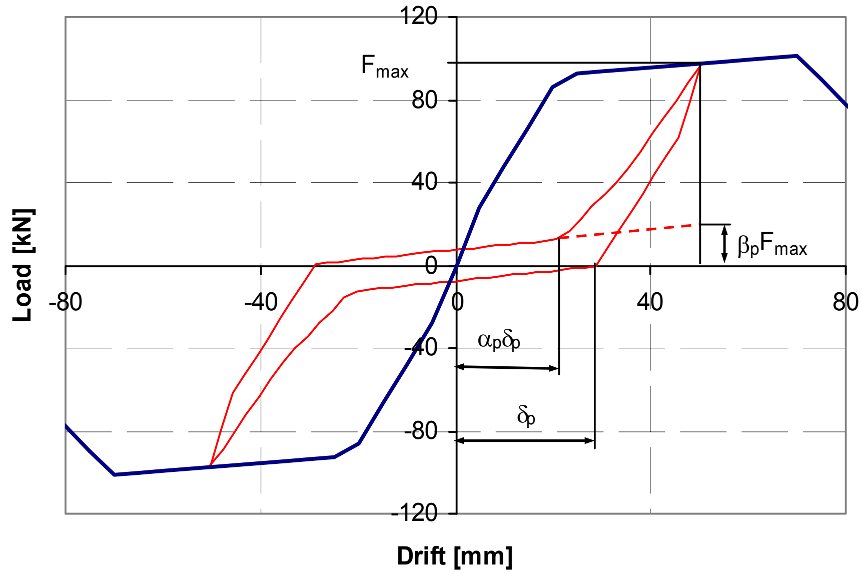

Figure 4-2. Illustration of pinching parameters.

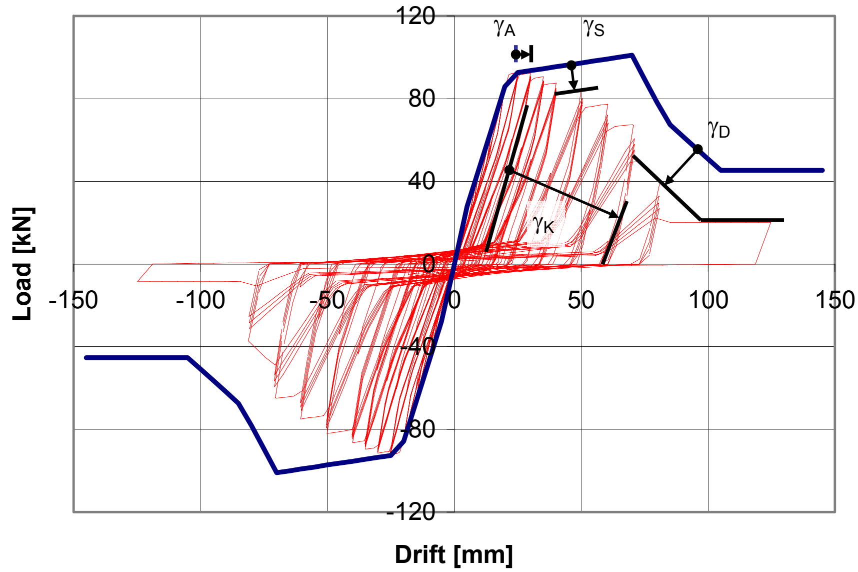

Figure 4-3. Illustration of cyclic degradation parameters.

4.3. Estimation of monotonic backbone curve

The backbone curve estimation for the different assembly groups is completed in accordance with finite element modeling results described Chapter 3. The nonlinear models should be calibrated to represent the mean properties of the structural components, so the models are adjusted to the average cyclic envelope curves (i.e. average of the specimens in the same assembly group). The calculated capping displacement is conservatively reduced in order to take the connection post-capping effect into account.

As an example, Figure 4-4 compares the calculated monotonic backbone and tested cyclic envelope curves for three different groups.

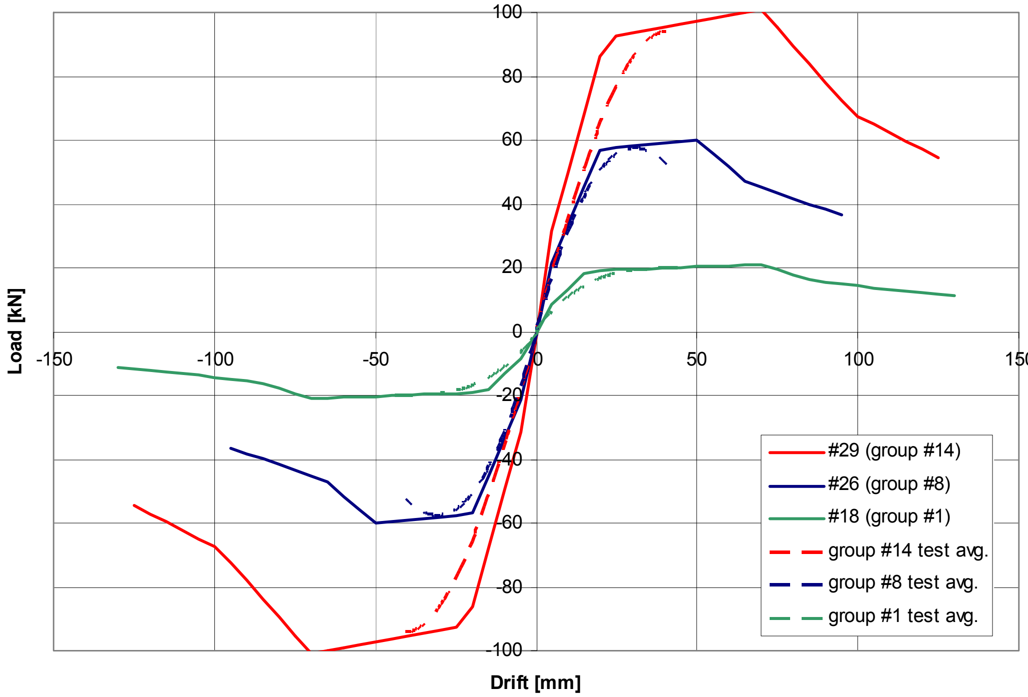

Figure 4-4. Monotonic backbone curves: test and numerical results are indicated by dashed and continuous lines, respectively.

4.4. Calibration of model parameters using genetic algorithm

Given that the monotonic backbone curve is known up to the capping point, the remaining unknown parameters to define are: the capping slope α_C, the residual r, pinching (α_P, β_P), and cyclic degradation parameters (γ_A, γ_S, γ_D). As described below, these parameters are determined by calibration of the inelastic cyclic strut model to the shear wall cyclic tests.

To overcome the indeterminacy of the parameter calibration process, a genetic algorithm (GA) is applied for determining the post-capping and cyclic response parameters. The objective function is the weighted sum of square errors of the tested and calibrated load values for given displacement. The error function is weighted with the displacements in order to increase the role of the final – degraded – parts of the hysteresis curve.

Using the GA structure and parameters given in Figure 4-5, a population size of 20 is found eligible. As Figure 4-6 shows, after approximately 100 generations an optimal solution can be found with this parameter set. Figure 4-7 demonstrates the tested and analytical hysteresis curves for three calibrated specimens, and Table 4-1 summarizes the corresponding model parameters for those particular specimens.

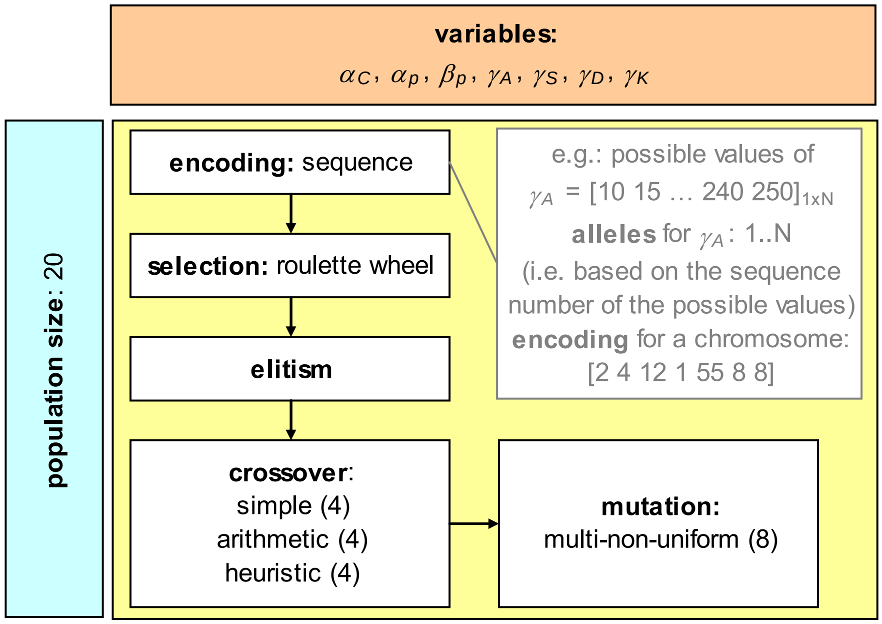

Figure 4-5. Structure of genetic algorithm.

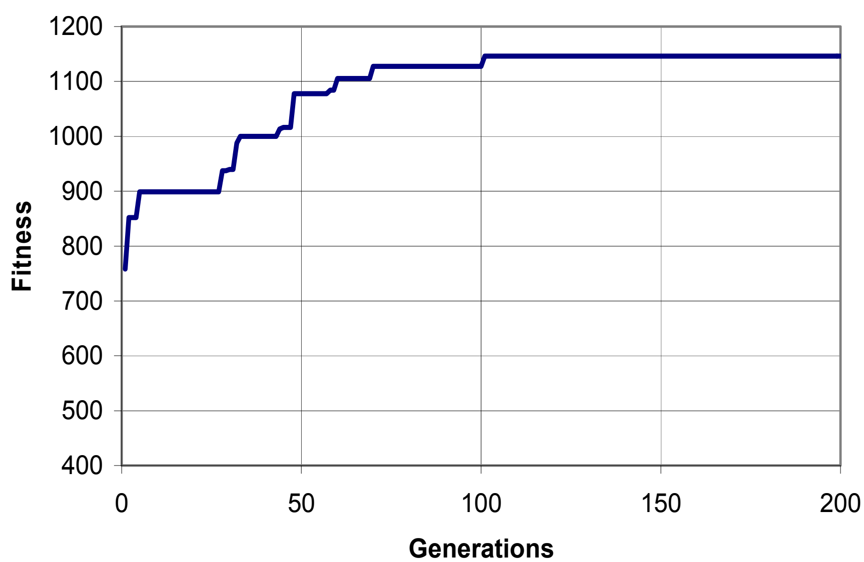

Figure 4-6. Convergence of optimization.

Table 4-1. Calibrated model parameters.

			Group #1	Group #8	Group #14
		Opt	**Spec. #18**	**Spec. #26**	**Spec. #29**
$\mathbf{F_{y1}}$	[kN]	0	5.0	16.3	25.0
$\mathbf{e_{y1}}$	[mm]	0	1.58	2.90	3.27
$\mathbf{F_{y2}}$	[kN]	0	19.0	57.0	92.0
$\mathbf{e_{y2}}$	[mm]	0	16.00	20.00	21.60
$\mathbf{F_{y3}}$	[kN]	0	21.0	60.0	101.0
$\mathbf{e_{y3}}$ (δ_{cap})	[mm]	0	70.00	50.00	70.00
α_{H2}	[–]	0	0.00	0.00	0.00
α_{C}	[–]	1	-0.10	-0.15	-0.15
$\alpha_{C,ratio}$	[–]	0	1.00	1.00	1.00
α_{pinch}	[–]	1	0.75	0.75	0.95
β_{cap}	[–]	1	0.20	0.25	0.15
c	[–]	0	1.00	1.00	1.00
λ_{S}	[–]	1	∞	∞	∞
λ_{K}	[–]	0	∞	∞	∞
λ_{A}	[–]	1	50.0	30.0	12.0
λ_{D}	[–]	1	50.0	30.0	11.0
r	[–]	1	0.60	0.65	0.60

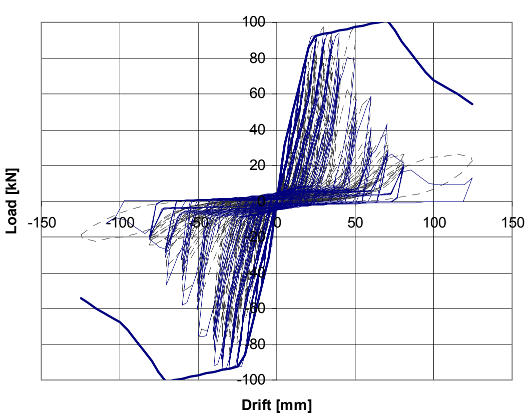

a) test #29 (group #14)

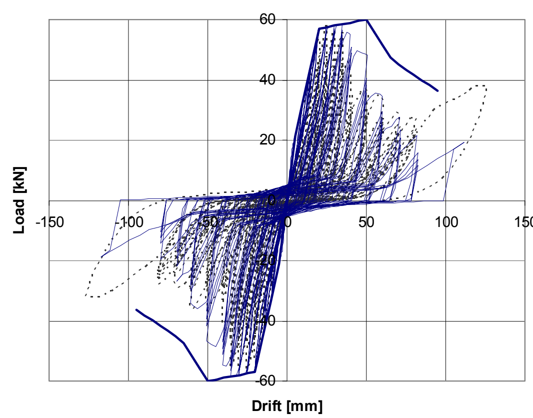

b) test #26 (group #8)

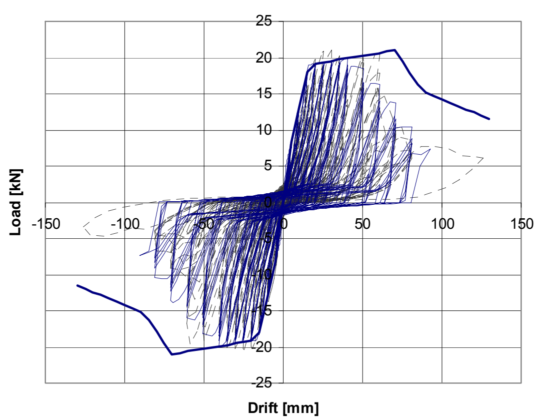

c) test #18 (group #1)

Figure 4-7. Calibrated models.

4.5. Final model for archetype study

Further study confirmed that, although the exact calibrated parameters differ from specimen to specimen, a single cyclic model can be effectively applied for most of the specimens. The uniform model is derived from the slightly modified Group #8 model. Models for other groups can be determined by linearly changing the load ordinates of the curve in accordance with the strength ratio of the group under consideration and Group #8. All other parameters, such as the displacement values, ductility, degradation or residual, are unchanged. As Figure 4-8 ~ 4-15 show, this simplified model is conservative for Groups #1, #7, slightly overestimating for Groups #13 and #14 and #16. In these cases, the approximation is reasonable; moreover, regarding the full shear wall assembly set, can be considered as a mean characteristic model.

Note that this model cannot be applied for Group #3 and #6, but these groups are outside of our range interest, because their application is not recommended due to the small ductility.

It is shown in Chapter 3 that longer wall may have an extra – 4/3 times – shear capacity. This increase is considered in the further analyses.

In Chapter 6, the model parameter sensitivity on collapse intensity is briefly discussed.

Table 4-2. Uniform model.

	Uniform
$\mathbf{F_{y1}}$	$= \alpha_{F,i} F^{(8)}_{y1} = \alpha_{F,i} 25.0$
$\mathbf{e_{y1}}$	3.99
$\mathbf{F_{y2}}$	$= \alpha_{F,i} F^{(8)}_{y2} = \alpha_{F,i} 56.0$
$\mathbf{e_{y2}}$	20.00
$\mathbf{F_{y3}}$	$= \alpha_{F,i} F^{(8)}_{y3} = \alpha_{F,i} 60.0$
$\mathbf{e_{y3}}$ (δ_{cap})	60.00
α_{H2}	0.00
α_{C}	-0.05
$\alpha_{C,ratio}$	1.00
α_{pinch}	0.60
β_{cap}	0.21
c	1.00
λ_{S}	∞
λ_{K}	20.0
λ_{A}	20.0
λ_{D}	20.0
r	0.65

$$\alpha_{F,i} = \frac{F^{(i)}_{ASD}}{F^{(8)}_{ASD}}$$

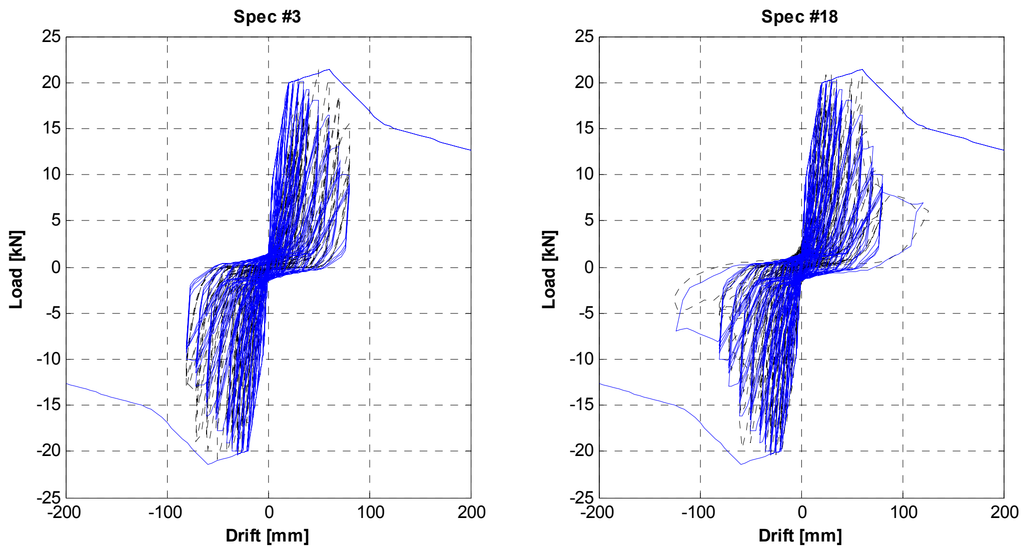

Figure 4-8. Test vs. uniform model – Group #1.

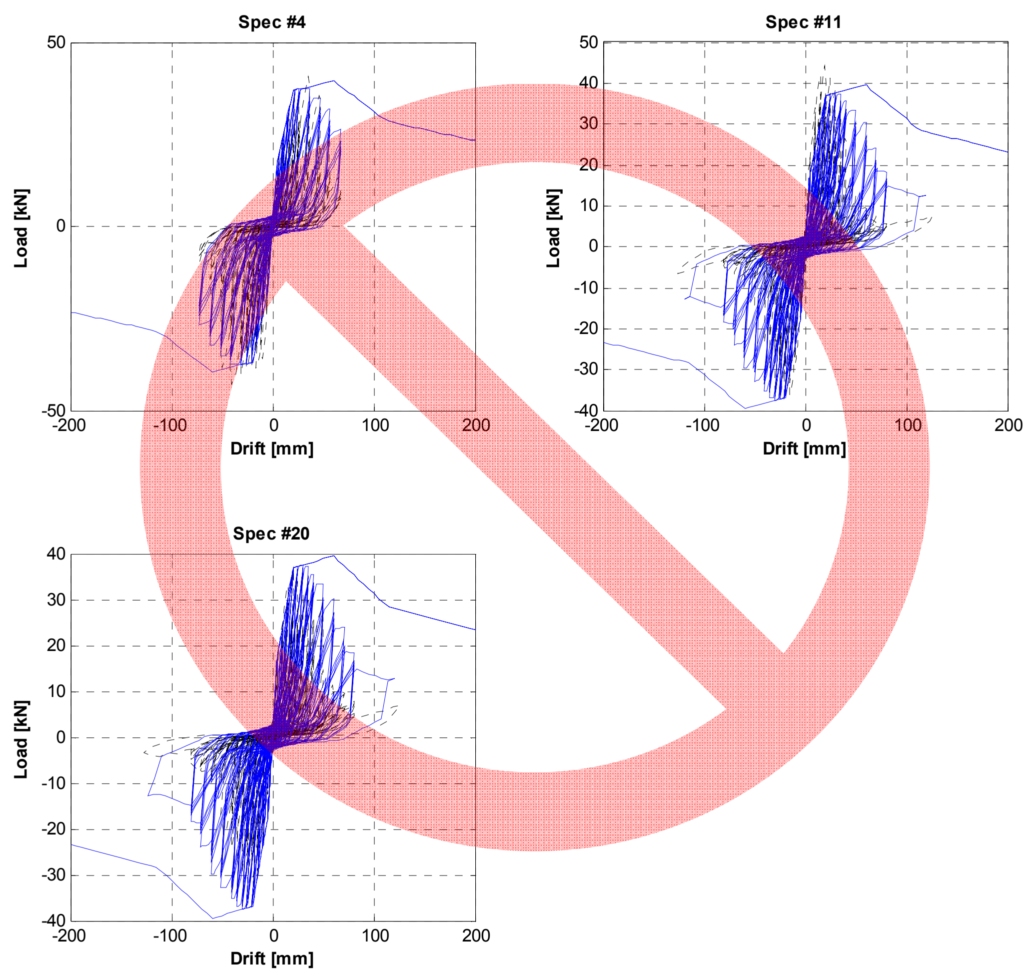

Figure 4-9. Test vs. uniform model – Group #3. This figure is crossed out because this configuration is not recommended for use in design because of its low ductility; in addition, the model does not capture the actual behavior of these specimens.

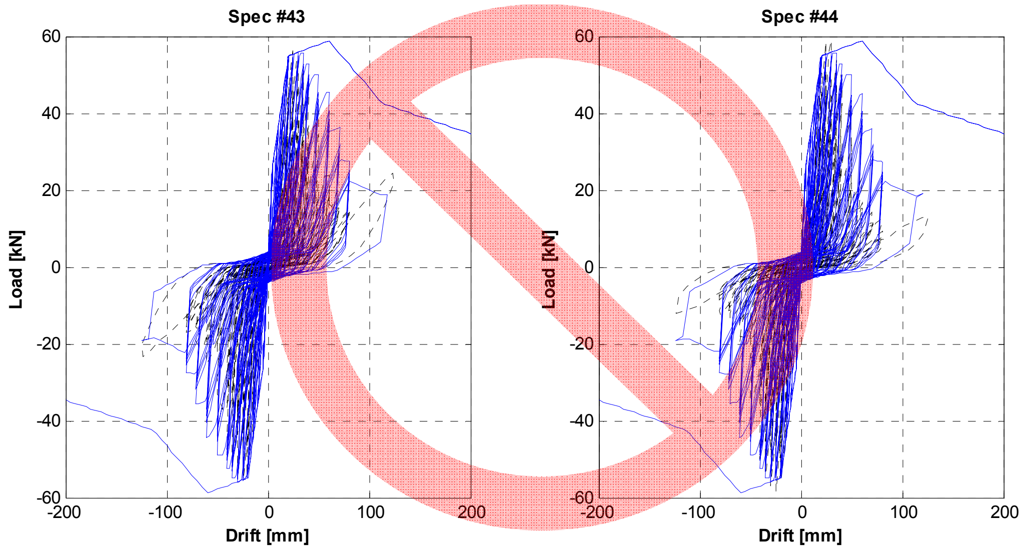

Figure 4-10. Test vs. uniform model – Group #6. This figure is crossed out because this configuration is not recommended for use in design because of its low ductility; in addition, the model does not capture the actual behavior of these specimens.

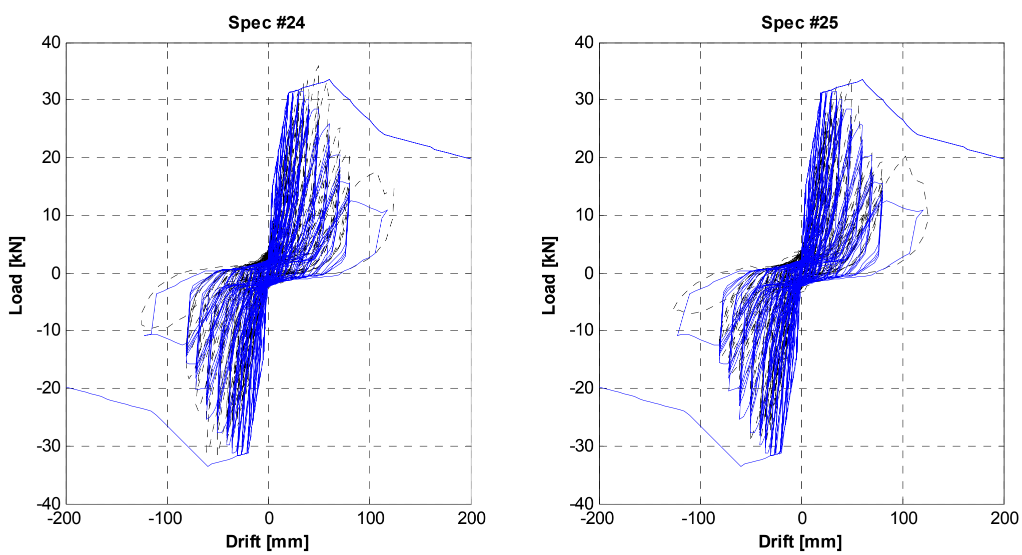

Figure 4-11. Test vs. uniform model – Group #7.

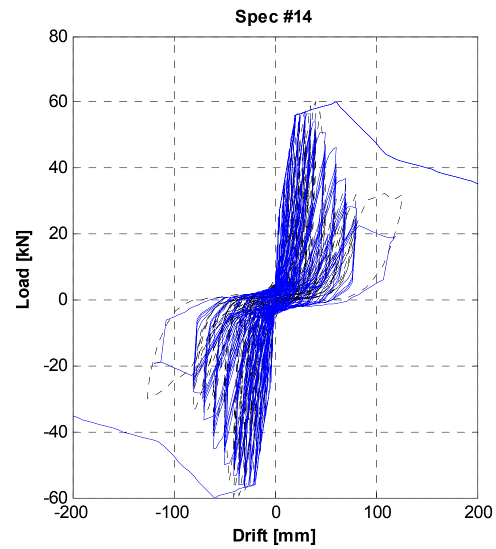

Figure 4-12. Test vs. uniform model – Group #8.

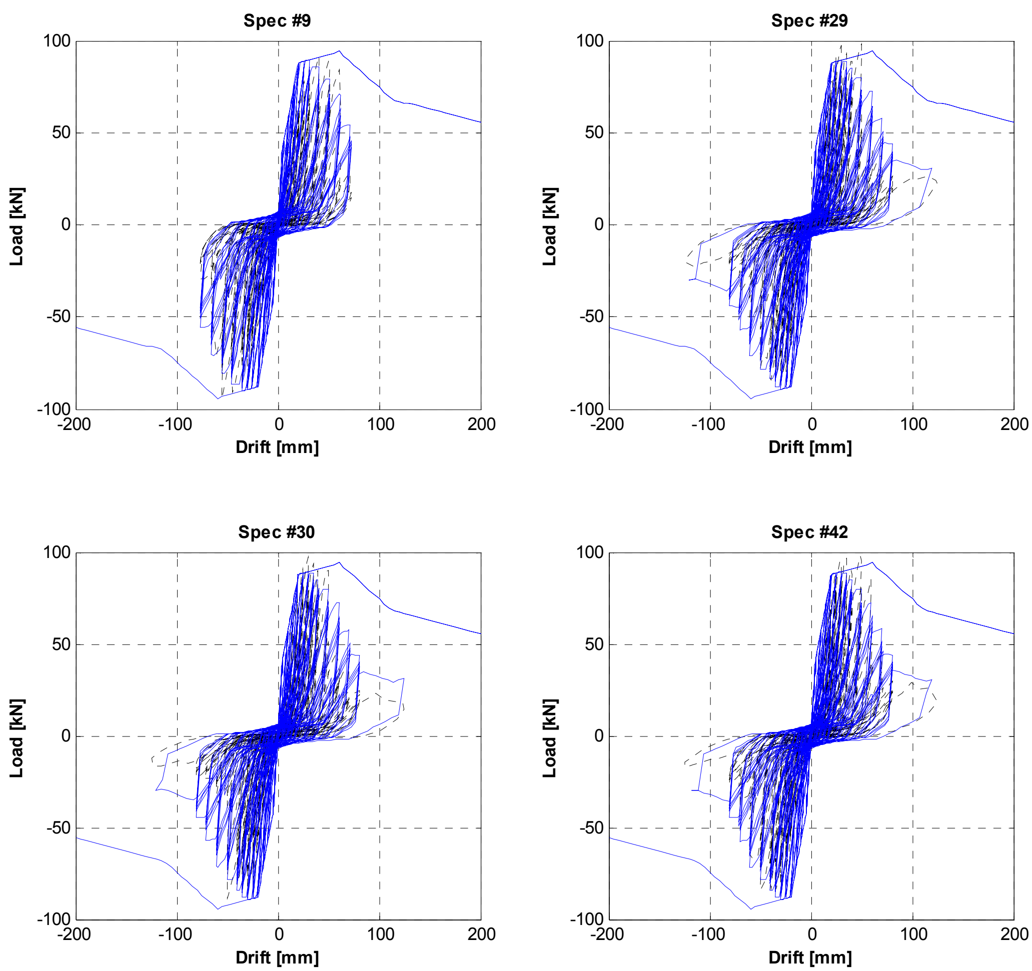

Figure 4-13. Test vs. uniform model – Group #14.

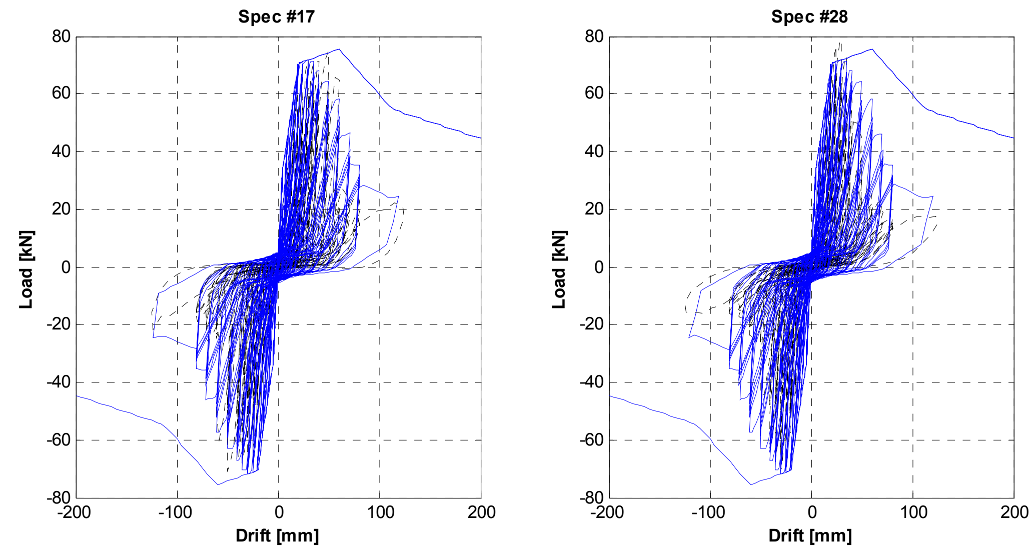

Figure 4-14. Test vs. uniform model – Group #13.

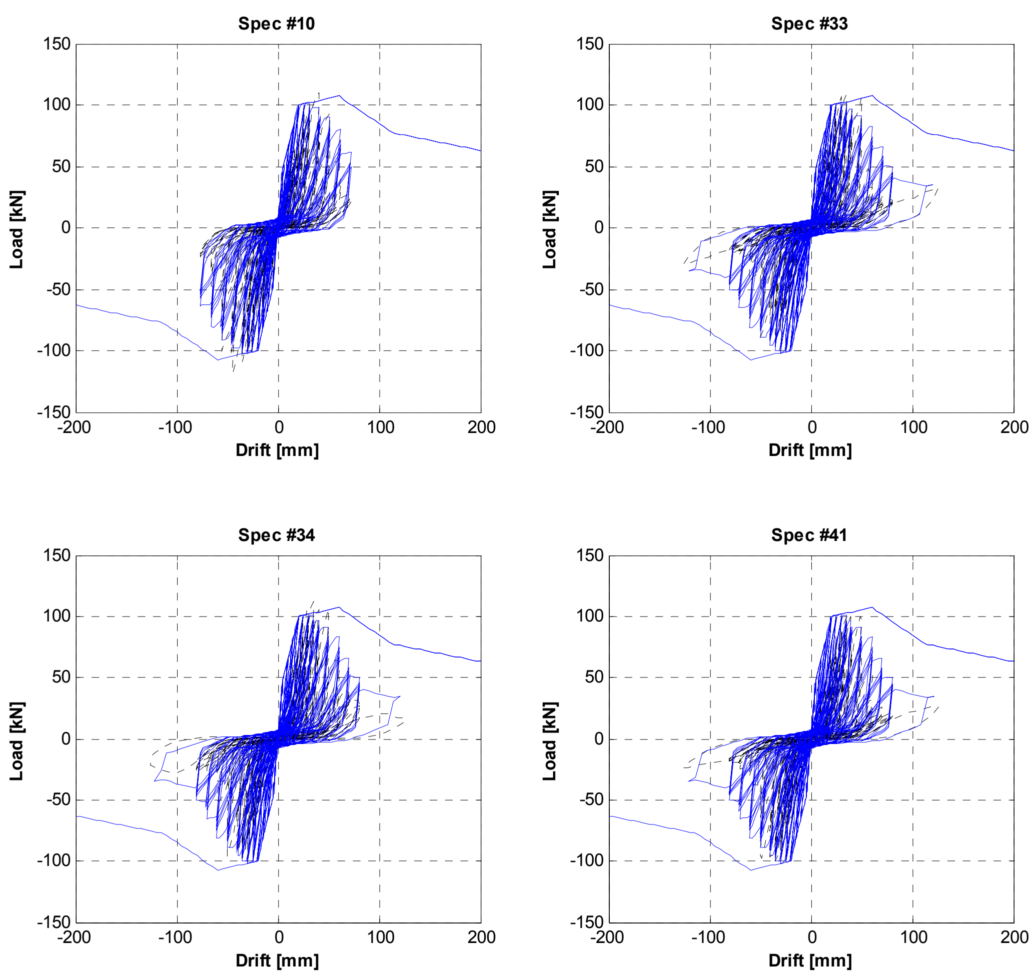

Figure 4-15. Test vs. uniform model – Group #16.

5. Building archetype analysis and seismic performance quantification

5.1. Building archetypes

5.1.1. Identification of archetype configurations

In many aspects, the scope and application field of the steel shear wall system is similar to wooden shear walls (e.g. OSB panels). Based on this observation, for definition of archetypical buildings for the steel shear wall systems are modelled after the OSB-panel example described in the FEMA P695 document [1]. Accordingly, the following assumptions are made in the archetype definition:

- Two major building functions are distinguished: residential and commercial (Figure 5-1). The function also defines the plan and the size of the building. According to the function, two groups of archetypes, termed “performance groups”, are defined.
- Number of stories: 1 ~ 10. Note that according to current U.S. codes [4], the system cannot be applied in buildings taller than 5 stories; however, for completeness the system is evaluated for systems up to 10 stories. For this reason, Performance Group II is further divided into two subgroups IIa and IIb with number of stories 1~5 and 6~10, respectively.
- Seismic Design Category: The archetypes are designed for seismic design category (SDC) D in ASCE 7-05, which has an MCE of $S_{MT} = 1.5g$ for short-period buildings. [4]

Shear walls are assumed on the perimeter of the building. The seismic mass is 30 psf on both the commercial and the multi-family residential buildings, while 10 psf is considered for the smaller residential ones. The highest seismicity is considered with SDC D category; lower seismicity regions are not included in this study.

The effect of wall finishes – that are not engineered – is not studied.

Tables 5-1 and 5-2 summarize the defined building archetypes – the archetype indexing suits to the one applied in the wood study.

Note that the system is non-redundant, i.e. failure of any shear wall directly leads to global collapse; contribution of framing is not taken into account. Therefore, changing the tributary area and/or the seismic mass cannot lead to significant dispersion in the global system performance, provided that the shear walls are accordingly designed – unless P-Δ effect becomes dominant. Thus, it is expected that the results of the two major archetype performance groups (residential or commercial) are essentially similar, but may vary with storey number. Also note that torsional effects are not considered.

a) residential building

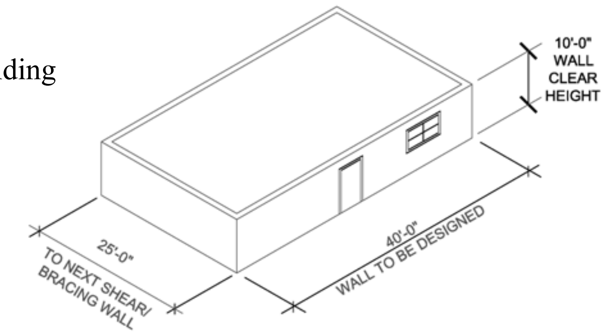

b) commercial building

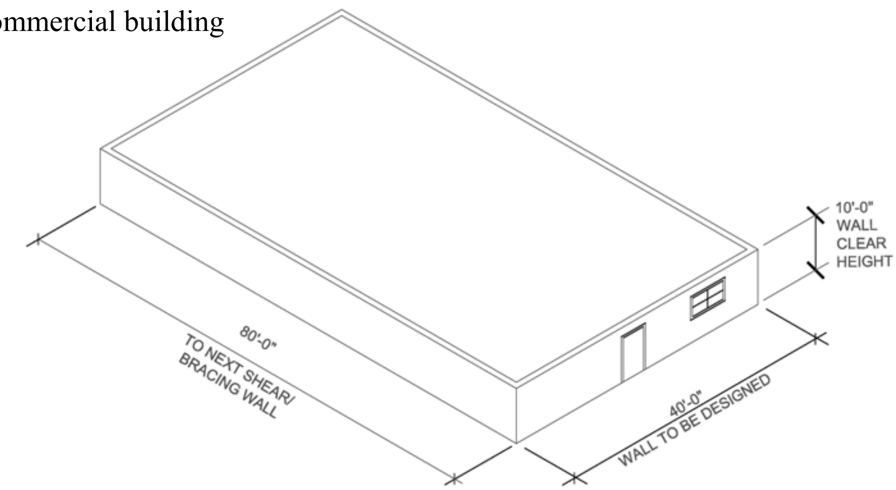

Figure 5-1. Building configurations. [2]

Table 5-1. Building archetypes and seismic design.

R = 4 High seismic (SDC Dmax)

S_S = 1.5, S_1 = 0.9 (S_{DS} = 1.0, S_{D1} = 0.6)

Archetype	Story #	Function	A_{floor} [sqft]	seismic weight [psf]	Period T_{design} [s]	S_{MT} [g]	C_s [-]	Design base shear [kip]	wall length [ft]	C_v [-]	wall type	UF [%]
1	1	Commercial	1600	30	0.16	1.50	0.25	12	12	1	7	97
5	2	Commercial	1600	30	0.19	1.50	0.25	24	24	0.667 0.333	25 7	79 97
9	3	Commercial	1600	30	0.26	1.50	0.25	36	20	0.5 0.333 0.167	7 8 8	88 81 98
2	1	1&2 Family	500	10	0.112	1.50	0.25	1.25	8	1	1	24
6	2	1&2 Family	500	10	0.19	1.50	0.25	2.5	8	0.667 0.333	1 1	32 48
10	3	Multi-Family	500	30	0.26	1.50	0.25	11.25	12	0.5 0.333 0.167	1 25 7	71 93 91
13	4	Multi-Family	500	30	0.32	1.50	0.25	15	16	0.4 0.3 0.2 0.1	1 25 7 7	57 78 82 91
15	5	Multi-Family	500	30	0.38	1.50	0.25	18.75	20	0.333 0.267 0.2 0.133 0.067	1 1 25 7 7	48 86 89 85 91

Table 5-2. Further building archetypes – Taller buildings.

R = 4 High seismic (SDC Dmax)

S_S = 1.5, S_1 = 0.9 (S_{DS} = 1.0, S_{D1} = 0.6)

Archetype	Story #	Function	A_{floor} [sqft]	seismic weight [psf]	Period T_{design} [s]	S_{MT} [g]	C_s [-]	Design base shear [kip]	wall length [ft]	C_v [-]	wall type	UF [%]
17	6	Multi-Family	500	30	0.431	1.50	0.25	22.5	24	0.286	1	41
										0.238	1	75
										0.19	25	79
										0.143	7	78
										0.095	7	87
										0.048	7	91
18	7	Multi-Family	500	30	0.484	1.50	0.25	26.25	26	0.25	1	38
										0.214	1	71
										0.179	25	77
										0.143	25	94
										0.107	7	88
										0.071	7	95
										0.036	7	98
19	8	Multi-Family	500	30	0.535	1.50	0.25	30	30	0.224	1	34
										0.195	1	64
										0.167	1	89
										0.139	25	86
										0.111	7	81
										0.083	7	89
										0.055	7	95
										0.027	7	97
20	9	Multi-Family	500	30	0.584	1.50	0.25	33.75	20	0.204	1	52
										0.180	25	77
										0.157	7	89
										0.134	8	62
										0.110	8	72
										0.087	8	80
										0.065	8	86
										0.042	8	90
										0.021	8	92
21	10	Multi-Family	500	30	0.632	1.42	0.237	35.58	20	0.187	1	51
										0.167	25	75
										0.148	7	87
										0.128	8	61
										0.109	8	71
										0.089	8	80
										0.07	8	87
										0.052	8	92
										0.034	8	95
										0.016	8	97

5.1.2. Design of archetype buildings

The identified building configurations shall conform the corresponding design codes. The structure shall safely carry the gravity loads and resist against lateral effects. In our study, since no contribution of the elements other than the shear wall is considered in the seismic performance (see the following section), design of columns, beams or their connections is not necessary; and in the analyses they are assumed rigid and pin-ended. All elements other than the shear wall are assumed to be accordingly designed to remain elastic.

In concept, the archetype analysis models are designed based on a tributary mass/gravity layout given by the archetype configurations. The total tributary seismic mass – which basically determines the seismic demand on the lateral resisting system – is the total mass that is stabilized by one shear wall, i.e. half of the floor area shall be considered in our case, regardless of the actual shear wall length. The total gravity load used for P-Delta effects is based on this seismic mass. A certain portion of the total load – that is tributary to the wall, thus proportional to the actual shear wall length – directly acts on the shear wall boundary members in the gravity sense.

The design of the shear wall as earthquake resisting system is completed in accordance with ASCE 7-10 [9]. LRFD design method is applied, for which the authors defined the design strength of a shear wall assembly as 1.4 times the ASD strength derived from test results, e.g.:

1. ultimate (nominal) strength = 5,000 plf (assume average from tests)
2. ASD design strength = 2,000 plf (derived from the test results; given in [1])
3. LRFD design strength = 1.4 ASD design strength = 2,800 psf (= 0.56 nominal strength)

The design is based on the equivalent lateral force method. The same wall length is applied along the building height, but the wall type is changed according to the seismic demand (Table 5-3). A sample calculation for Archetype #15 is provided in Appendix A. The major design parameters and the corresponding wall schedule are summarized in Table 5-1 ~ 5-2.

Note that the amount of seismic demand depends on the period, for which ASCE 7-10 proposes the following approximation:

$T_a = C_t \cdot H^{x_c} = 0.02 \cdot H^{0.75}$, where H stands for the building height in feet.

On the conservative side, this approximate period is applied as the base of design and of seismic record scaling (cf. upper limit in ASCE 7-10). As it is proved, the way of period approximation may influence the performance evaluation (refer to Chapter 6).

Table 5-3. Seismic design – Archetype #15.

Story	EQ loading [kip]	demand, V_u [lbs]	[plf]	wall type (group#)	V_{nom} [plf]	V_{ASD} [plf]	V_{LRFD} [plf]
R	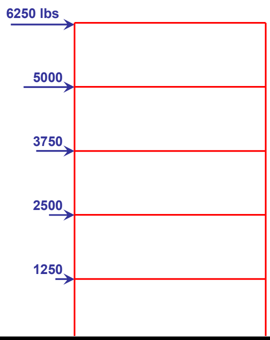	6250	**312**	1	1173	469	**657**
4		11250	**563**	1	1173	469	**657**
3		15000	**750**	25	1505	602	**843**
2		17500	**875**	7	1836	734	**1028**
1		18750	**937**	7	1836	734	**1028**

5.2. Representative numerical model for building archetypes

As mentioned, the software selected for the structural analysis is the Open Systems for Earthquake Engineering Simulation (OpenSees, [7]).

The 2-D archetype analysis model is shown in Figure 5-2, where the primary component is the diagonal spring (spring element – referred as *zeroLength* in OpenSees – or uniaxial truss element – referred as *corotTruss*) that is calibrated to simulate the nonlinear shear panel response. The associated material model (combined *Pinching*) is the one discussed in Chapter 4.5. Beams (*corotTruss*) are pin-ended and are not intended to play a substantial role in the model. Similarly, seismic resistance contribution of the vertical boundary columns is eliminated: columns are also pin-ended (*corotTruss*). Both the beams and columns are rigid. Alternative to this method would be the usage of elastic member as column, where the member has low flexural stiffness and whose axial stiffness is representative of the real member; the axial stiffness might be tuned to account for the base uplift. Advanced modeling would represent nonlinear behavior of the column, either by fiber type model or inelastic springs. Such modeling would enable to capture not only the nonlinear performance of the column (that would be necessary when columns are considered as part of the lateral resisting system), but also the possible redistribution of forces after failure of a shear wall element. Present study does not take such effects into account, but assumes that all elements other than the shear walls are accordingly designed and remain elastic / rigid.

A "leaning column" (*corotTruss*) is used to apply vertical gravity loads that are stabilized by the wall but not tributary to the wall. Basically, the total gravity load (the sum of forces applied to the wall and leaning column) should equal the vertical load associated with the seismic mass. The goal of the model is to capture deformations (including P-delta effects) associated with wall shear only (axial boundary member flexibility and axial flexibility of the boundary base are excluded).

Masses are associated with the nodes only.

The calibrated model shown in the previous chapter corresponds to the horizontal response of 4-feet wide and 8-feet tall shear wall panels. Therefore, a conversion of the load-displacement characteristics is required as follows:

1., Conversion from 4-feet to a length of B_{wall}:

The preliminary study showed that with lengthened wall (>8ft) there is an extra shear capacity that can be expressed by a factor of 4/3. Additionally, it was found that the ductility of the wall does not change. Thus, the factors for the conversion of forces

($\alpha_{F,1}$), displacements ($\alpha_{D,1}$) and rigidities ($\alpha_{K,1}$):

$$\alpha_{F,1} = \frac{4}{3}\frac{B_{wall}}{4\text{ft}}; \quad \alpha_{D,1} = 1; \quad \alpha_{K,1} = \frac{\alpha_{F,1}}{\alpha_{D,1}} = \frac{4}{3}\frac{B_{wall}}{4\text{ft}}\text{, respectively.}$$

2., Conversion from horizontal to diagonal axis:

$$\alpha_{F,2} = \frac{\sqrt{h_{storey}^2 + B_{wall}^2}}{B_{wall}}; \quad \alpha_{D,2} = \frac{B_{wall}}{\sqrt{h_{storey}^2 + B_{wall}^2}}; \quad \alpha_{K,2} = \frac{\alpha_{F,2}}{\alpha_{D,2}} = \frac{h_{storey}^2 + B_{wall}^2}{B_{wall}^2},$$

where h_{storey} is the storey height.

3., Total conversion:

$$\alpha_F = \alpha_{F,1}\alpha_{F,2}; \quad \alpha_D = \alpha_{D,1}\alpha_{D,2}; \quad \alpha_K = \alpha_{K,1}\alpha_{K,2}$$

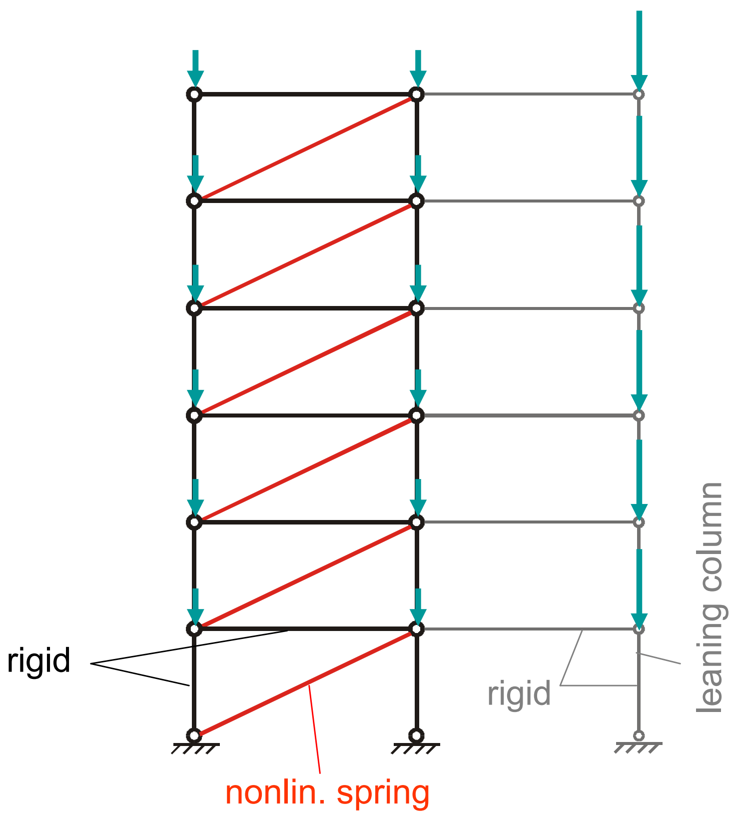

Figure 5-2. Archetype model.

5.3. Pushover analysis and overstrength factor

5.3.1. Pushover analysis

Nonlinear static (pushover) analysis is carried out a) to generally characterize the given structural system, in terms of overstrength factor, ductility as well as b) to draw a general idea on the collapse mechanism.

Beside the gravity loads, the same load pattern is to be applied as used for the archetype code design (Table 5-2).

Displacement controlled static analysis is performed; one of the nodes of the roof level is the control node. A general direct solver for banded matrices is applied to solve the linear equation systems. Generally, the Newton solution algorithm is used for the nonlinear problem. The convergence is checked on an energy basis, the goal tolerance is 10^{-8}. In case, either Broyden method or Newton with line search usually helps to overcome convergence problems that may occur at the descending region of the capacity curve.

A typical pushover curve – defined as base shear vs. roof displacement relation; also called capacity curve – is illustrated on Figure 5-3. Definitions of further parameters, such as overstrength factor, yield displacement and ultimate displacement are also introduced on the figure – further details are discussed in Chapter 6.

Figure 5-4 illustrates the collapse-characterizing deformed shape (at the maximum base shear).

5.3.2. Overstrength factor

The overstrength factor Ω_0 is defined as the ratio of the maximum base shear calculated by pushover analysis and the design base shear (Figure 5-3). For the studied archetypes, Table 5-4 summarizes the calculated overstrength factors. Typically, Ω_0 falls into the range of 2.40 ~ 2.60.

5.3.3. Ductility ratio and spectral shape factor

According to the FEMA P695 document, the ultimate displacement corresponds to the 80% of the maximum base shear, measured on the descending branch of the capacity curve (Figure 5-3). Similarly, to comprehensively define the yield displacement, one has to find an equivalent elastic-perfectly plastic capacity curve, where the elastic branch intersects the original curve at a load level of 60%; the yield displacement is then given by the intersection of the elastic slope and yield plateau, as shown in Figure 5-3.

The ductility ratio is the ratio of the ultimate and the yield displacements. In Table 5-4, the obtained values corresponding to the archetype models are also indicated. The ductility ratio values show large dispersion (2.72 ~ 6.31).

The spectral shape factor – discussed in the further sections – depends on the fundamental period and the system ductility. The large dispersion of the ductility ratios however do not lead to large differences in the spectral shape factors: its value is typically between 1.19 ~ 1.31.

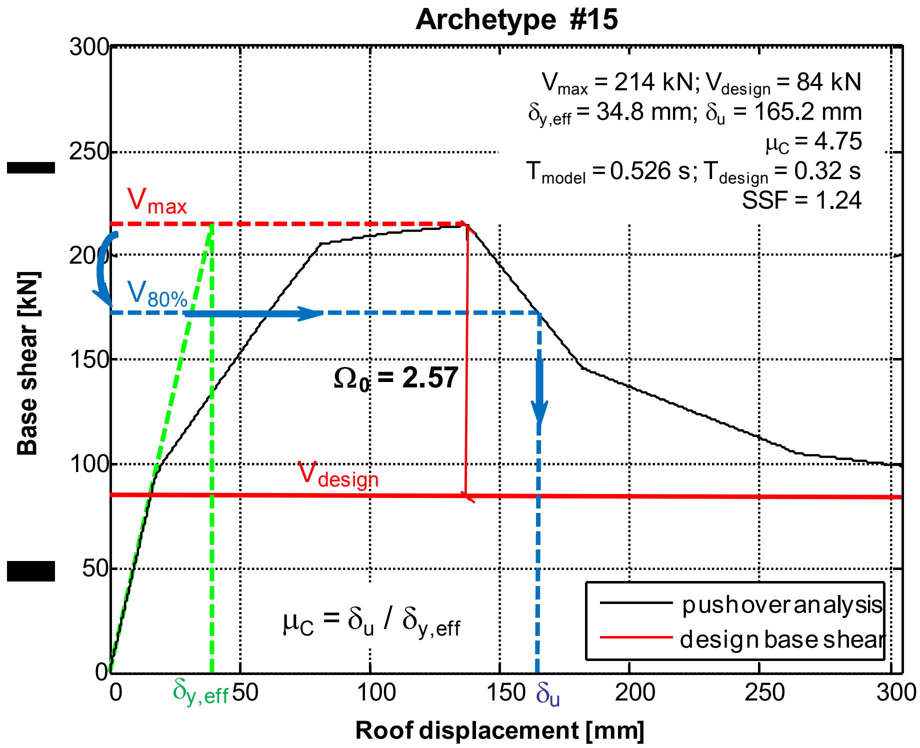

Figure 5-3. Typical capacity curve from pushover analysis – archetype #15.

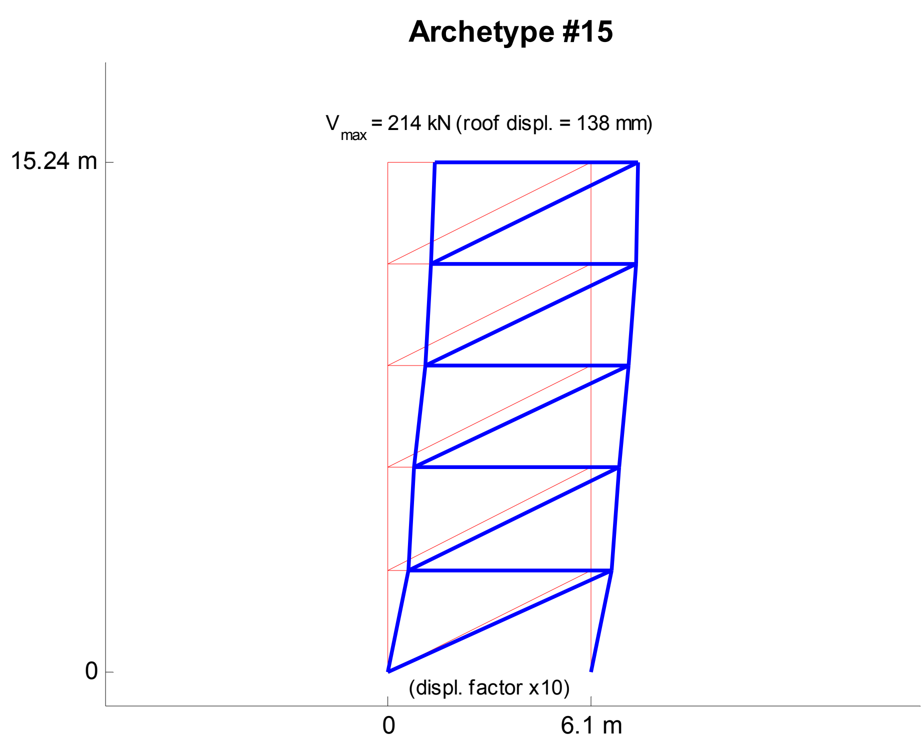

Figure 5-4. Deformed shape at ultimate load – archetype #15.

Table 5-4. Summary of collapse results.

R = 4 High seismic (SDC Dmax)

S_S = 1.5, S_1 = 0.9 (S_{DS} = 1.0, S_{D1} = 0.6)

Archetype	Storey #	Function	Ω [-]	μ_C [-]	SSF [-]	S_{MT} (T_{design}) [g]	SF_{anchor} [-]	β_{tot} [-]	$\hat{S}_{CT}$ [g]	CMR [-]	ACMR [-]		ACMR limit [-]	check (pass/fail)
1	1	commercial	2.38	10.28	1.33	1.50	2.10	0.70	**2.79**	1.86	**2.48**	**>**	**1.76**	**Pass**
5	2	commercial	2.40	7.05	1.31	1.50	1.97	0.70	**2.93**	1.95	**2.55**	**>**	**1.76**	**Pass**
9	3	commercial	2.39	5.74	1.27	1.50	1.88	0.70	**3.04**	2.03	**2.58**	**>**	**1.76**	**Pass**
										Mean	**2.54**	**>**	**2.38**	**Pass**

2	1	1&2 family	9.91	10.38	1.33	1.50	2.60	0.70	**4.85**	3.24	**4.30**	**>**	**1.76**	**Pass**
6	2	1&2 family	4.91	7.34	1.31	1.50	1.97	0.70	**4.44**	2.96	**3.89**	**>**	**1.76**	**Pass**
10	3	multi-family	2.52	6.95	1.30	1.50	1.88	0.70	**3.34**	2.23	**2.90**	**>**	**1.76**	**Pass**
13	4	multi-family	2.56	4.93	1.25	1.50	1.95	0.70	**3.01**	2.01	**2.50**	**>**	**1.76**	**Pass**
15	5	multi-family	2.57	4.75	1.24	1.50	2.00	0.70	**3.08**	2.05	**2.55**	**>**	**1.76**	**Pass**
										Mean	**3.23**	**>**	**2.38**	**Pass**

5.4. Incremental dynamic analysis

5.4.1. Incremental dynamic analysis – modeling and solution method

The same numerical model is applied for the incremental dynamic as for the pushover analysis.

Effective 3% Rayleigh damping calculated from the first and third eigenmode is considered.

Each ground motion record is applied uniformly at the support nodes. The record sets that are determined by FEMA P695 include a set of ground motions recorded at sites located greater than or equal to 10 km from fault rupture, referred to as the "Far-Field" record set. It includes twenty-two records (with two horizontal components, thus 44 individual components) selected from the PEER-NGA database using several criteria, such as code consistency, independency to structural type and site hazard, etc [2].

Time history analysis is conducted accounting material and geometrical nonlinearity. In each shear wall member, plastic deformations are not limited in the material model. Similarly, further non-simulated collapse mechanisms are not considered.

A general direct solver for banded matrices is applied to solve the linear equation systems. For the iteration the Newton solution algorithm is used. The convergence is checked on an energy basis, the goal tolerance is 10^{-8}. The transient analysis is solved by the help of Newmark-β time integrator with parameters $\gamma = 0.5$ and $\beta = 0.25$. Convergence analysis confirmed that for the time step double frequency as of the ground motion record is sufficient to obtain accurate solution.

5.4.2. Incremental dynamic analysis – scaling method

To find the median collapse intensity, an iterative procedure – incremental dynamic analysis – is to be completed for each archetype and earthquake record. Ground motion intensity is defined as the spectral acceleration S_T at the fundamental period of the structure under consideration. For the collapse evaluation of an individual archetype, a normalizing and scaling procedure is completed as follows (and consistent with recommendations from FEMA P695):

- Firstly, the records are normalized by the peak ground velocity (Figure 5-5).
- Secondly, the records are scaled in a way that the median intensity of the records meets the selected reference value at the fundamental period T (typically the maximum considered earthquake MCE spectral acceleration). This means that the records show dispersion even at T. Note that this scaling method (hereafter referred as ATC scaling) is different from the conventional ones (component scaling) where all the components are scaled to MCE level (i.e. no dispersion at T). This is illustrated in Figure 5-5.
- In the framework of IDA, the records are collectively scaled upward or downward to the median collapse intensity, i.e. to the point where 50% of the ground motions cause collapse. Practically, the analysis is started with a reference level (e.g. 0.1 times MCE) and then the intensity is gradually increased by simple algebraic scaling.

5.4.3. Incremental dynamic analysis – results

Typical time-history and hysteresis curves for various ground motion intensities are plotted in Figure 5-6 ~ 5-13. At the MCE level, plastic deformation may occur, but its magnitude does not extend the capping displacement. Primarily depending on the utilization factor (i.e. demand vs. capacity ratio) of the shear walls, failure initiation may be indicated at more than one story. However, at the collapse level, typically, failure of one story leads to global collapse due to global instability (represented by "infinitely" large drift due to global/local instability phenomena or any local failure that causes collapse). As the hysteresis plots prove, the collapse generally occurs after a few cycles only.

Using the discussed numerical model it is assumed that there is a residual strength in the post-capping region of the shear wall characteristics and that infinite "plastic flow" may take place. Fracture of a unit or other failure modes may be considered in the model or, alternatively, as a non-simulated collapse by declaring a drift limit associated with the collapse load. However, in our case this neglect does not cause significant error in the collapse intensity: the large deformations in a storey directly lead to collapse of the whole structure.

The validity of this assumption is confirmed by the IDA curves (maximum interstory drift vs. ground motion intensity – i.e. spectral acceleration at the fundamental period – relations), as shown in Figure 5-14 for Archetype #15. For each archetype, 44 IDA curves are calculated. The plateau of an IDA curve indicates the collapse. It can be observed that in the collapse intensity region small change in intensity may result in rapid increase of interstory drift.

Results well represent the expected behavior: the drift ratio at the MCE level is typically around 1~3% (for details refer to Appendix C), that is reasonable and acceptable.

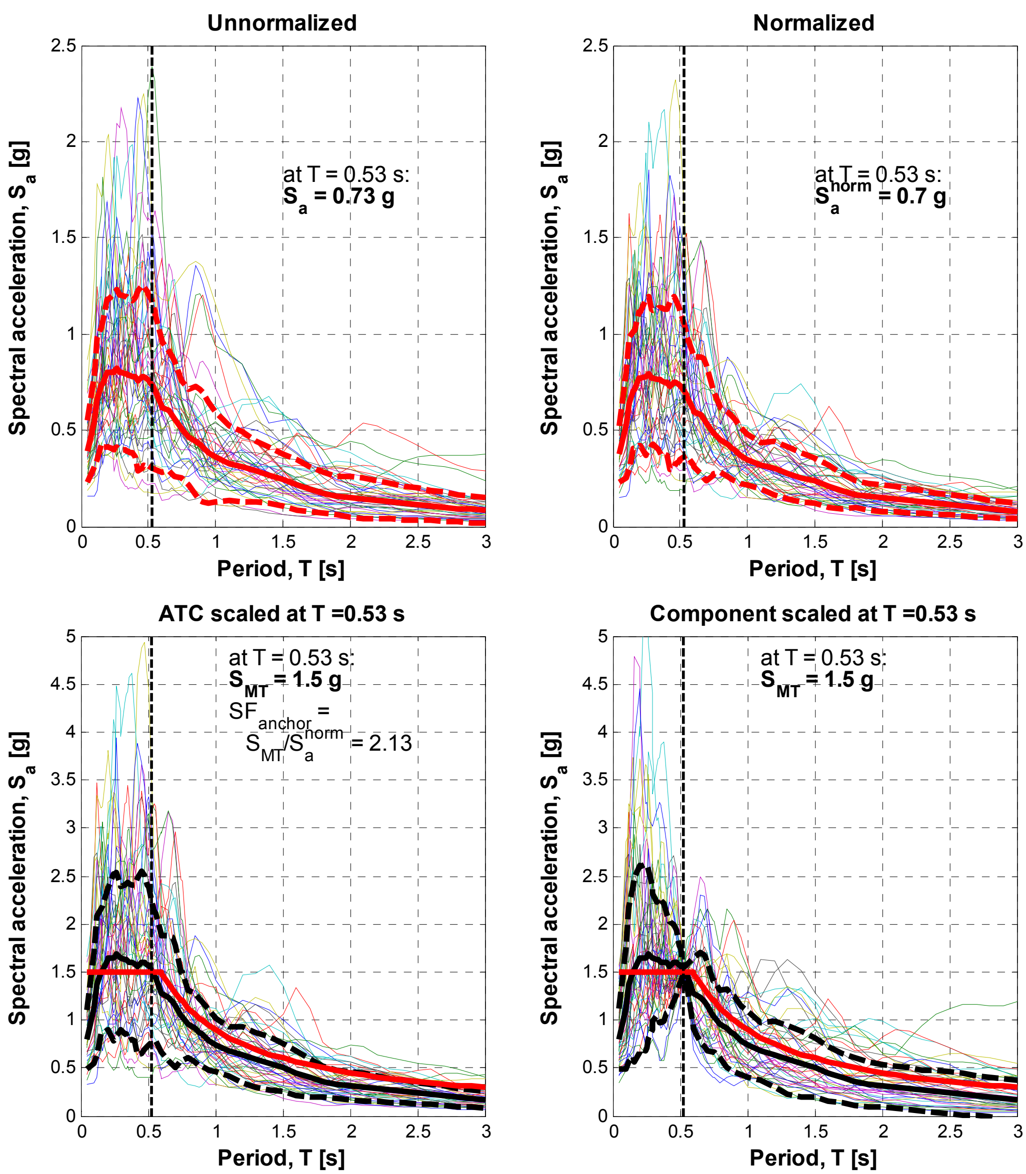

Figure 5-5. Ground motion normalization and scaling.

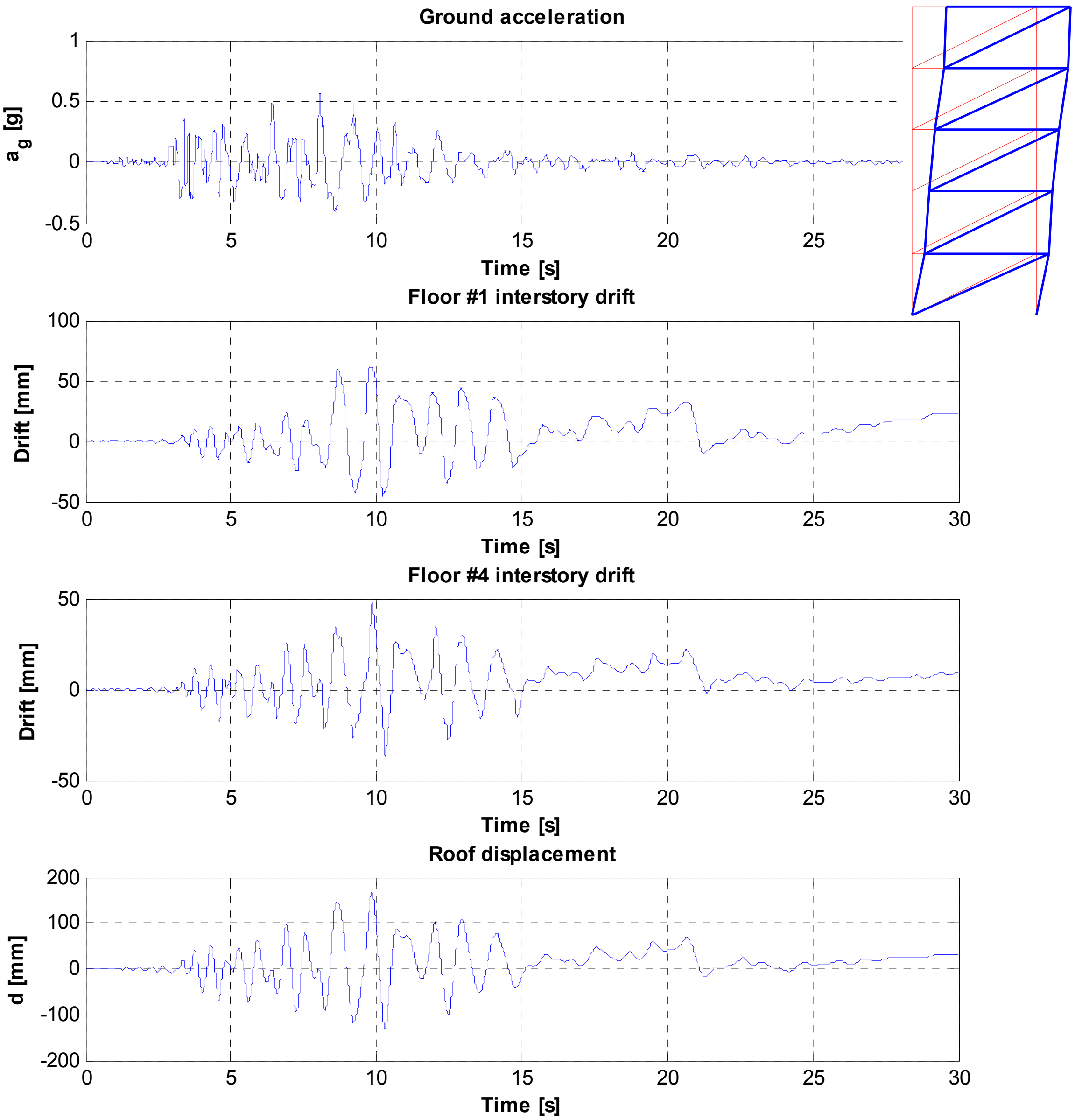

Figure 5-6. Response history of Archetype #15 – Record #1 – S_{CT} = 1.5 g (MCE level).

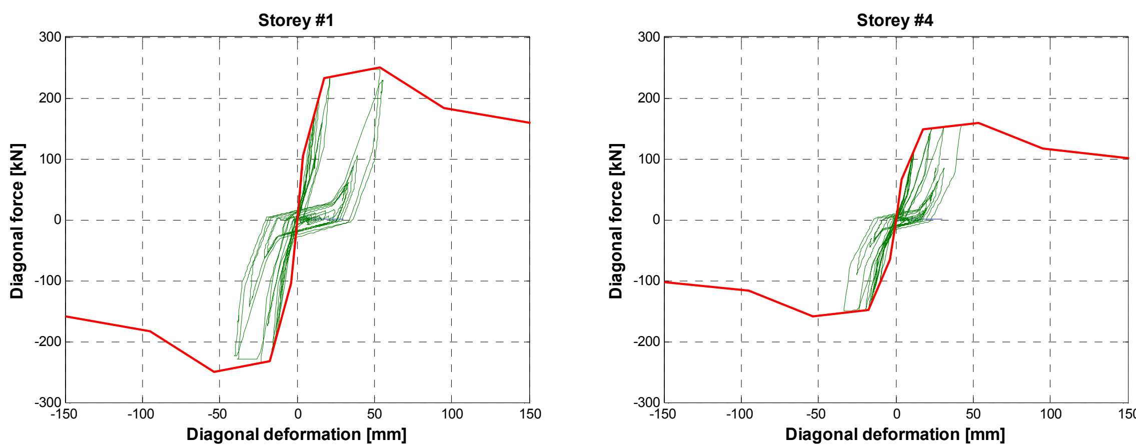

Figure 5-7. Hysteresis plots – Archetype #15 – Record #1 – S_{CT} = 1.5 g (MCE level).

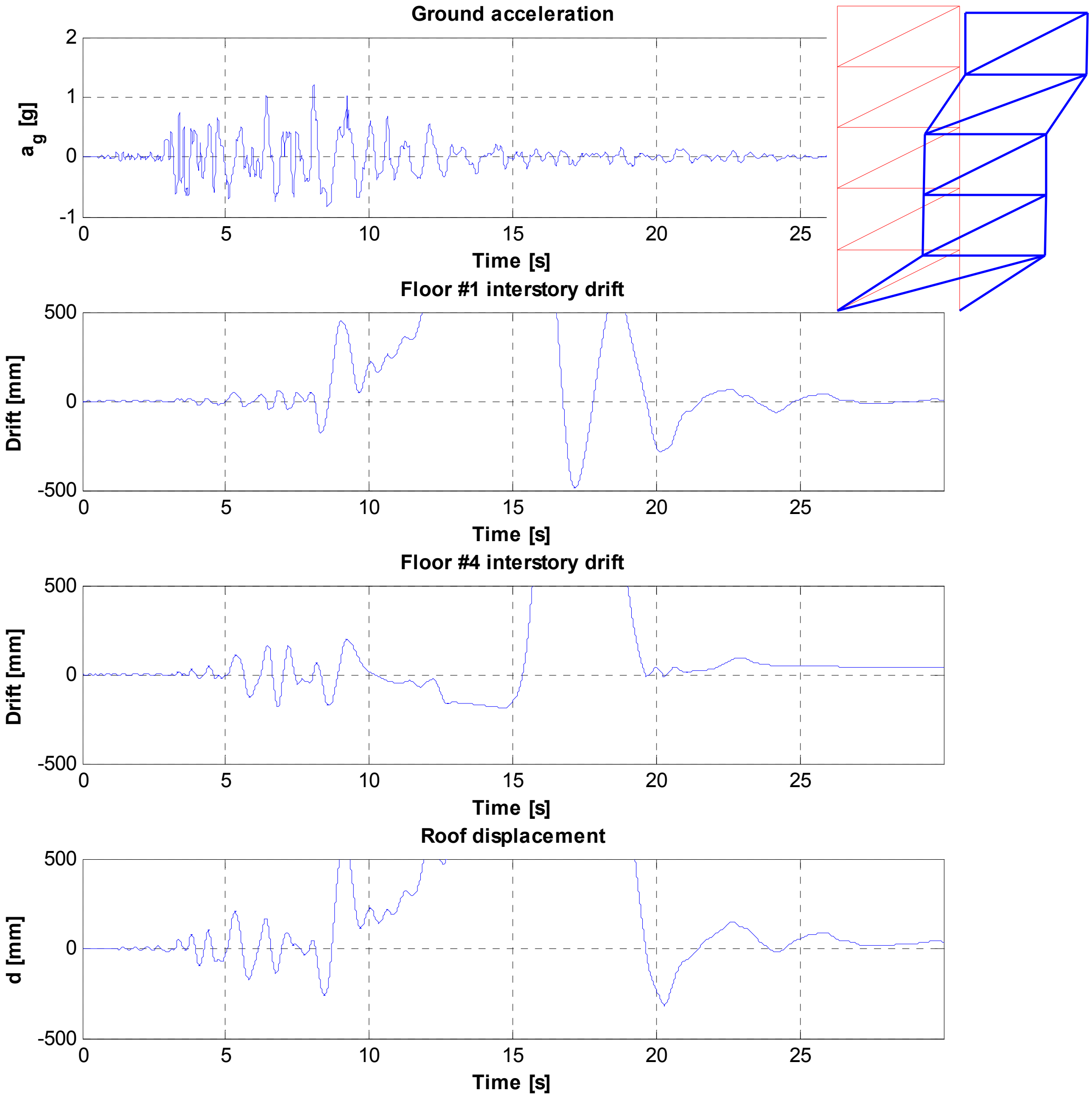

Figure 5-8. Response history curves of Archetype #15 – Record #1 – S_{CT} = 2.21 g (at collapse level).

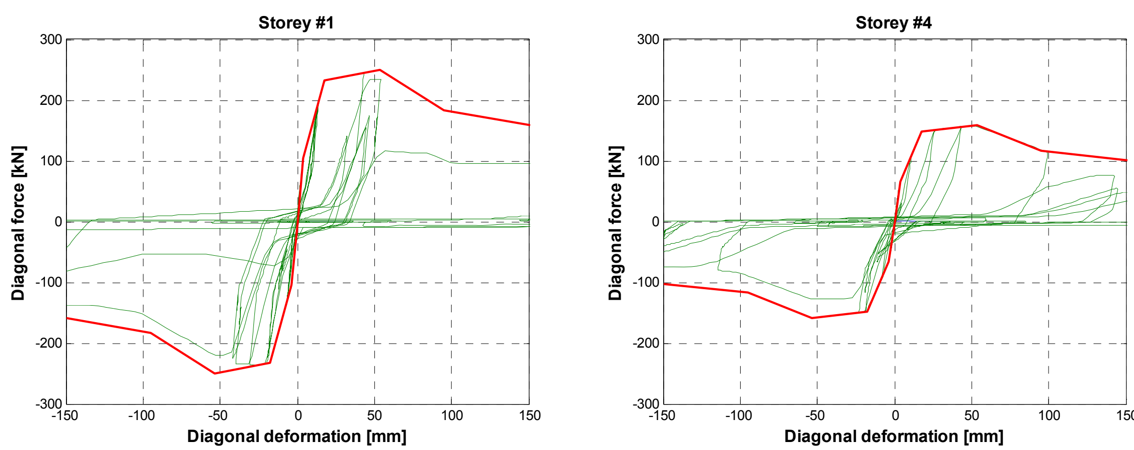

Figure 5-9. Hysteresis plots – Archetype #15 – Record #1 – S_{CT} = 2.21 g (at collapse level).

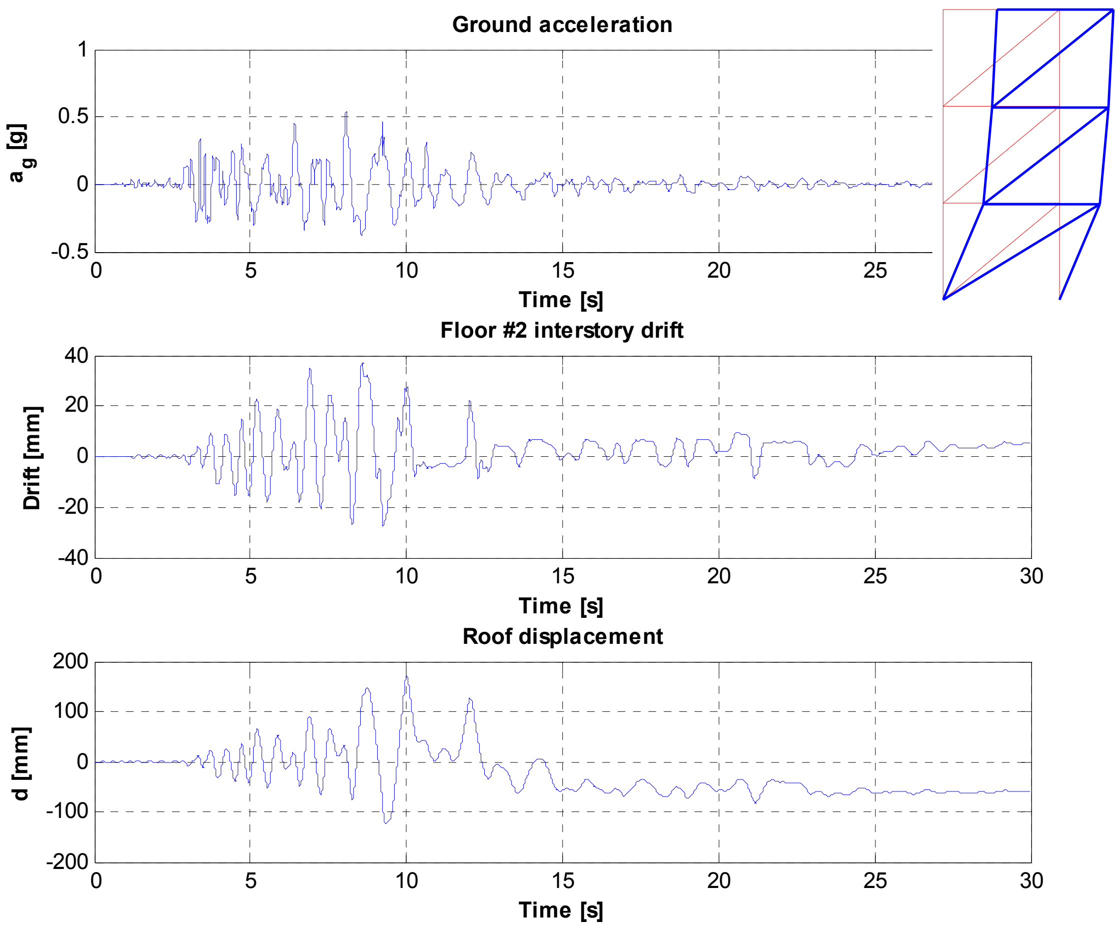

Figure 5-10. Time history curves – Archetype #10 – Record #1 – S_{CT} = 1.5 g (MCE level).

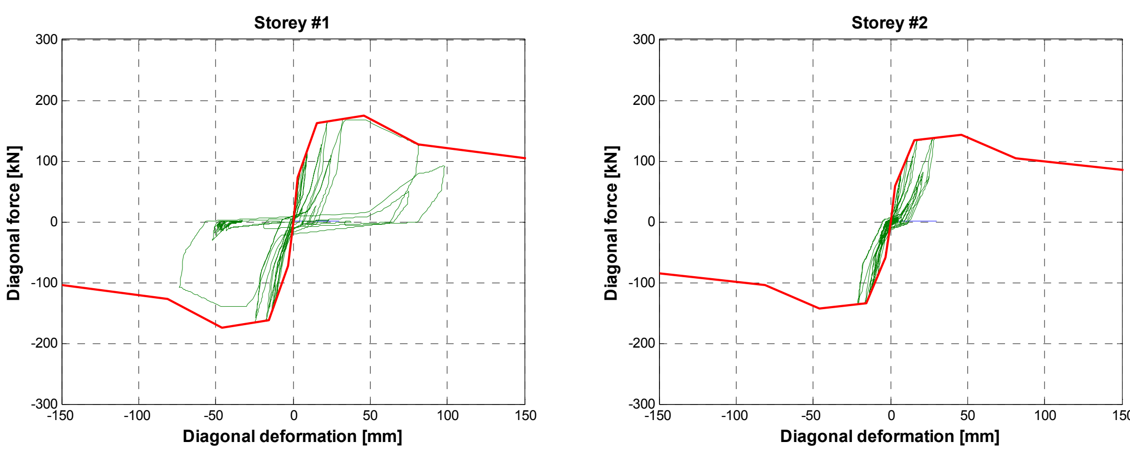

Figure 5-11. Hysteresis plots – Archetype #10 – Record #1 – S_{CT} = 1.5 g (MCE level).

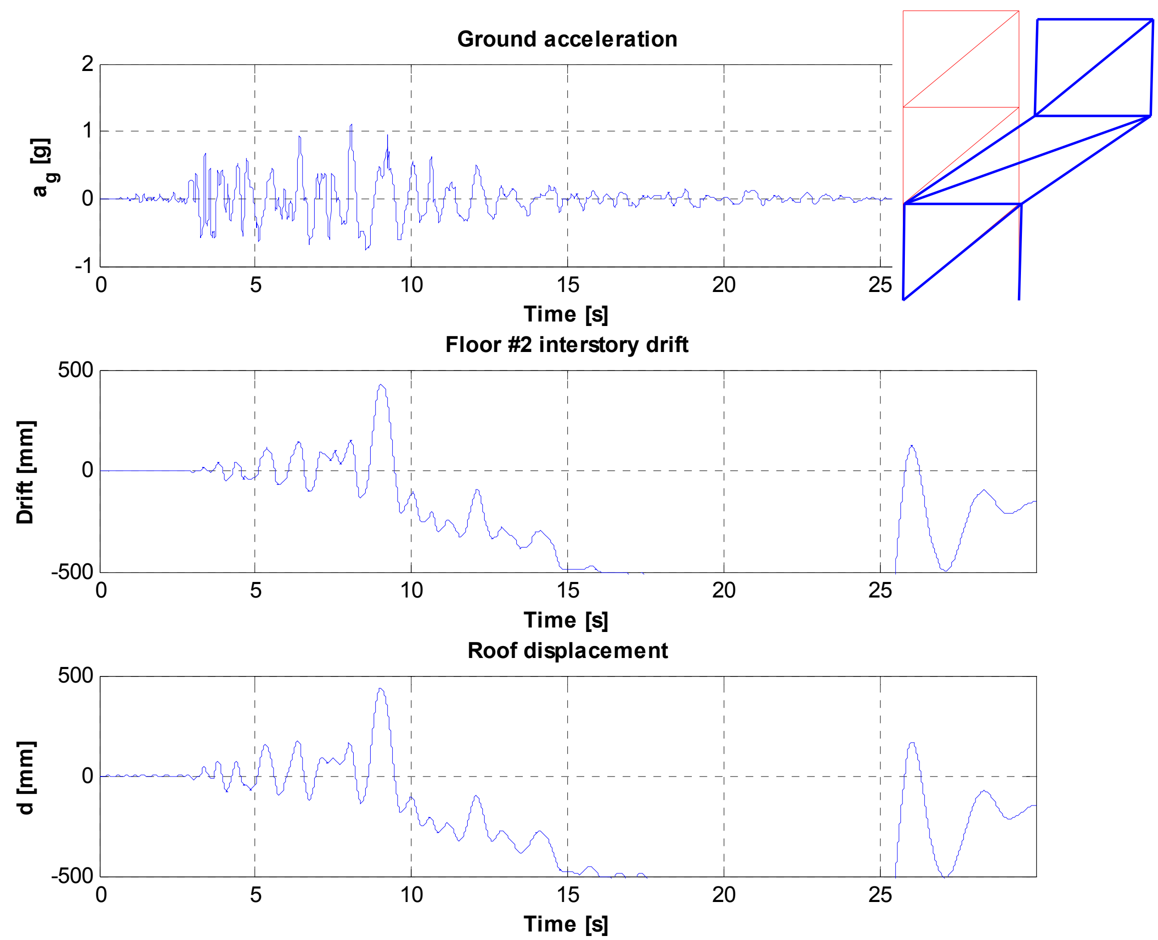

Figure 5-12. Response history curves for Archetype #10 – Record #1 – S_{CT} = 2.15 g (at collapse level).

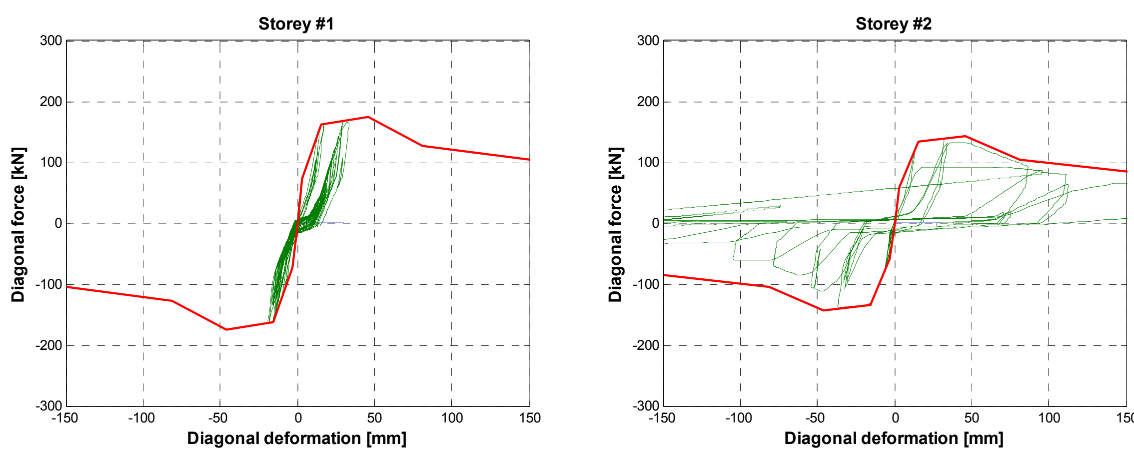

Figure 5-13. Hysteresis plots – Archetype #10 – Record #1 – S_{CT} = 2.15 g (at collapse level).

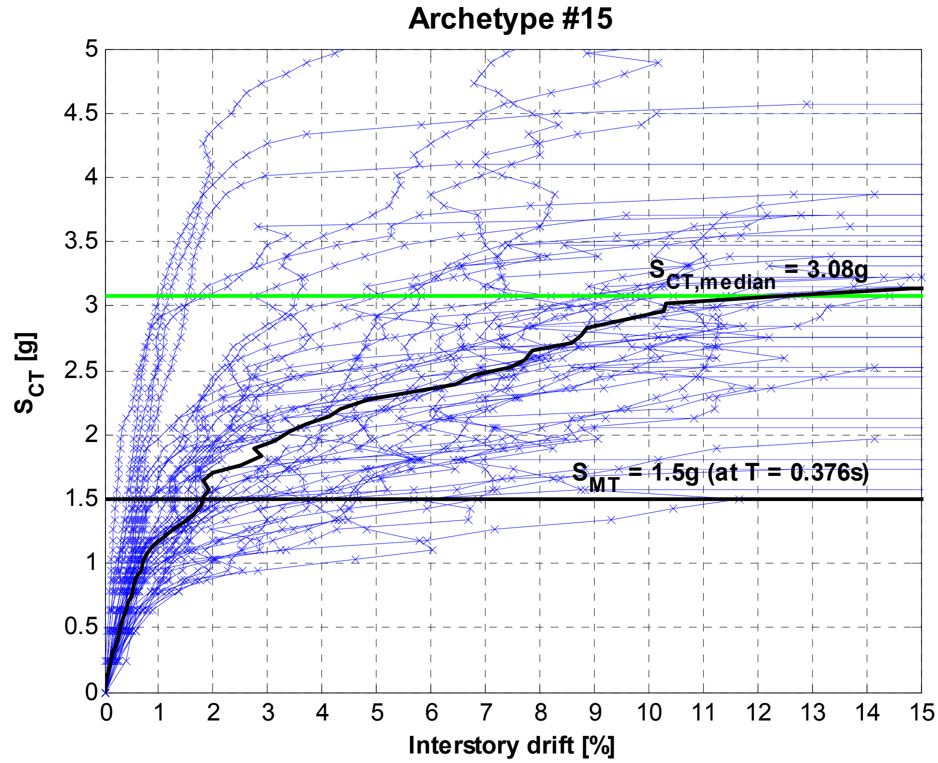

Figure 5-14. IDA results for archetype #15.

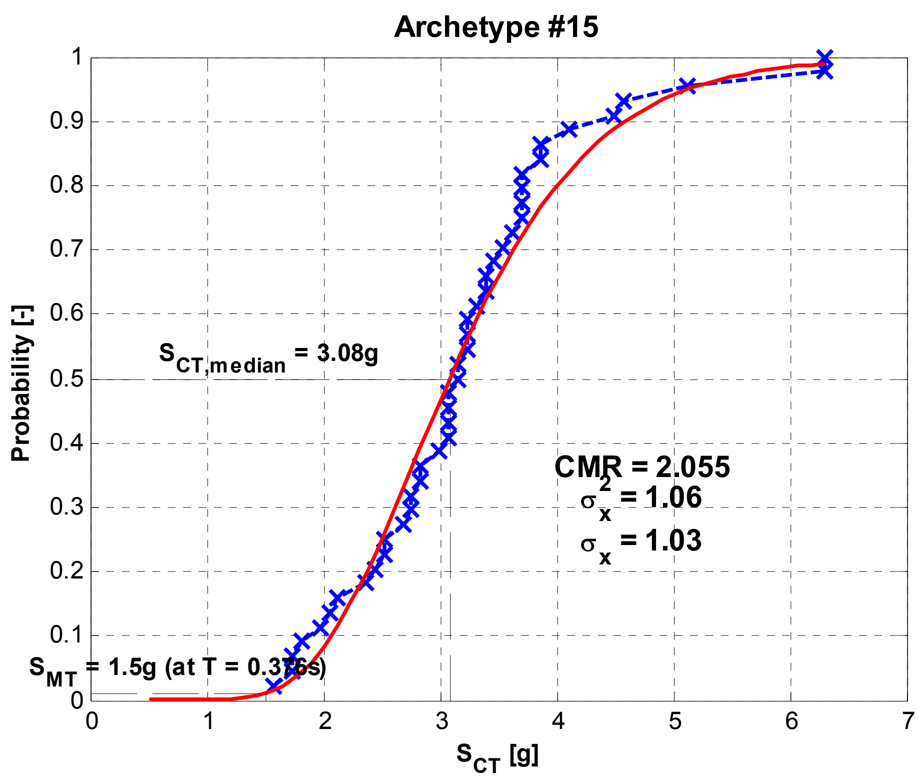

Figure 5-15. Fragility curve (not adjusted for spectral shape factor) – Archetype #15.

5.4.4. Collapse fragility curve

Based on the IDA curves, the collapse fragility curve – that shows the probability of collapse at variable earthquake intensities – of the archetype can be calculated: the cumulative distribution function of the collapse intensities defines the fragility curve (Figure 5-15). The discrete collapse intensities derived from the IDA analyses fit to a lognormal distribution, and thus the fragility curve can be characterized by its median and the standard deviation of the natural logarithm.

The record-to-record variability is accordingly represented in this fragility curve; however, further uncertainties (such as uncertainties in modeling, code, test data, etc) and the differences between the median spectral shape of records in the general far-field record set and the characteristics of the MCE hazard shall be also accounted for.

5.4.5. Collapse margin ratio and response modification factor

The ratio of the median collapse intensity to the MCE is the so-called collapse margin ratio (CMR, Table 5-4).

To overcome the above-mentioned problem that for rare ground motions the spectral shape can be much different than the shape of the design spectrum, the ATC methodology provides a simplified procedure using general sets of adjustment factors. The spectral shape adjustment factor (SSF) depends on the fundamental period and the structural ductility. Multiplying CMR with this factor results in the adjusted collapse margin ratio (ACMR). In this study, the SSF and the ACMR typically fall into the range of 1.24 ~ 1.33 and 2.48 ~ 4.30, respectively; however, the 1&2-family residential buildings have much higher ACMR values (Table 5-4).

As related to the FEMA P695 methodology, the above fragility curve is yet incomplete in respect to the variability in the collapse behaviour. While the obtained fragility curve reflects the dispersion due to ground motion record-to-record variability, the curve does not reflect other important sources of uncertainty associated with (a) the implementation of design and quality assurance requirements, (b) quality and completeness of the test data to characterize the structural behaviour, and (c) accuracy and variability of the structural analysis. Since these uncertainties are difficult, and for some sources impossible to quantify analytically, the FEMA P695 methodology relies upon judgment to establish the variability for these sources. The judgments are described in terms of ratings of design requirements, test data, and the non-linear analysis model. In each area, the ratings range from "excellent" (A) to "poor" (D), where an excellent (A) rating implies a low level of uncertainty and a poor (D) rating implies a high level of uncertainty.

Establishment of the quality ratings, and the resulting uncertainties, is somewhat subjective and worthy of more extensive discussion. For the purposes of the present study, the quality ratings are conservatively assumed as "fair"(C) for the design requirements and test data and "good" (B) across the board, for the analysis model. Following the FEMA P695 procedure, these ratings result in a total dispersion (standard deviation of the natural logarithm) of $\beta_{tot} = 0.675$. This dispersion affects the flatness of the fragility curve, which in turn determines the minimum permissible margin between the MCE ground motion intensity, S_{MT}, and the median collapse capacity, $\hat{S}_{CT}$. Assuming maximum failure probabilities at the MCE ground motions of 10% and 20%, the required margins for $\beta_{tot} = 0.675$ are 2.38 and 1.76, respectively.

If ACMR exceeds the minimum acceptable value given by FEMA P695, the collapse probability at the MCE level is acceptably low (i.e. 20% for an individual archetype and on average 10% for a performance group) and thus the seismic performance factors assumed in the designs are deemed to be appropriate. (If the required ACMR is not met, then one has to restart with the archetype design using a decreased R-value).

As Table 5-4 proves, both types of collapse-risk limiting criteria are met when designing with R = 4; accordingly, the response modification factor in practical design can be assumed as 4 for buildings up to 5 stories.

Note that structures in low seismic zone were not studied. However, based on the experiences of the wooden shear wall study – which shows similarities to our results –, it is likely that the required ACMR is met in low seismic zone as well.

5.4.6. Displacement modification factor

According to the FEMA P695 methodology, the displacement modification factor is equal to the response modification factor:

$$C_d = R$$

Note that the studied archetype buildings are short-period structures, thus the application of the equal displacement rule is questioned: the short-period effect may result in larger actual displacements.

6. Further studies

6.1. Constant wall strength

In practical design, under certain circumstances it may be more efficient or economic to use single shear wall type in the whole building, instead of adjusting the shear capacity to the demand at each floor. Figures 6-1 and 6-2 compare the pushover and IDA results of a 5-story building with varying and constant wall strength. Although this comparison is done only for this single archetype, the results indicate that there is no significant difference between the two cases. Indeed, based on the fact that the system is non-redundant, this similarity in the seismic performance is expected.

6.2. Application for taller buildings

Even though according to current codes, the system cannot be applied in buildings taller than 5 stories, the investigations are extended to buildings with up to 10 stories. With respect to structural behavior, the light-gauge shear wall is capable in taller buildings, too, as the results in Table 6-1 confirms.

However, two important observations can be made: i) the ACMR value is decreasing with increasing height and ii) when considering archetypes with more than 5 stories as separate performance group, the average ACMR exceeds the limit associated with the 10% probability of collapse, even though the individual buildings each meet the 20% limit. Accordingly, for buildings with 6~10 stories, smaller R-factors may be appropriate, or alternatively, limiting building heights to 8 stories would satisfy the limit.

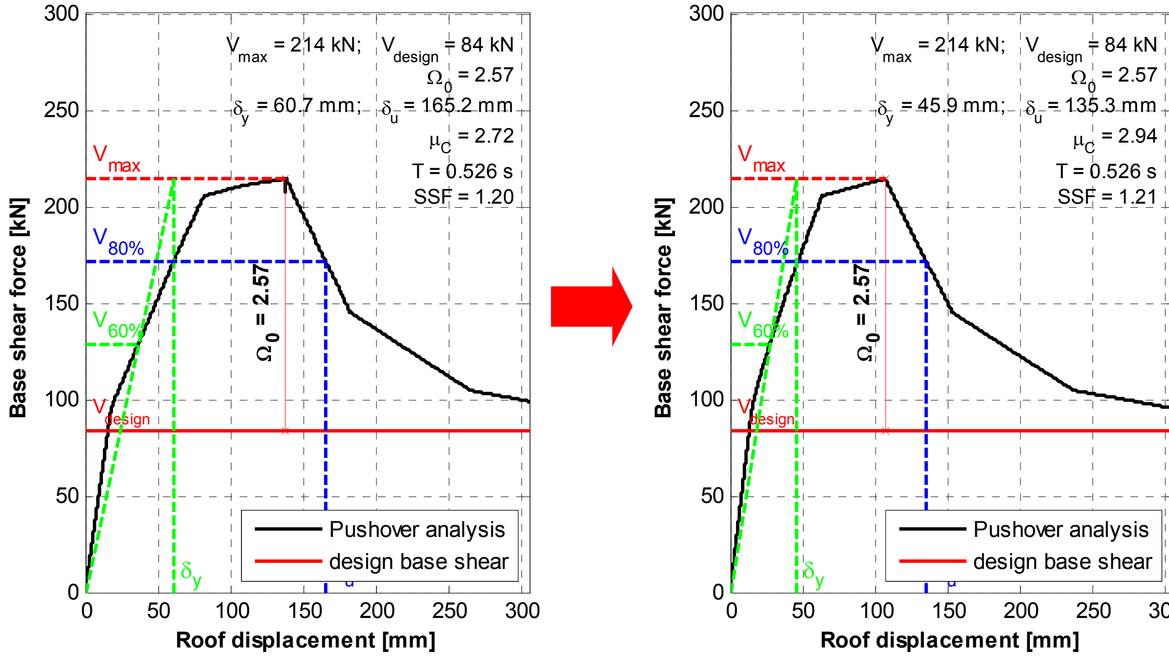

a) varying wall strength b) constant wall strength

Figure 6-1. Capacity curve – Archetypes #15 and #1501 (5-story).

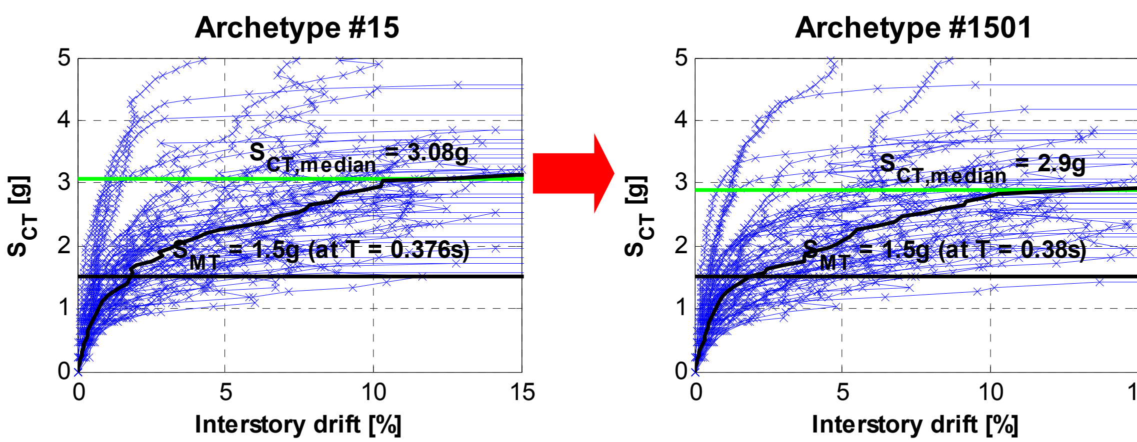

a) varying wall strength b) constant wall strength

Figure 6-2. IDA curve – Archetypes #15 and #1501 (5-story).

Table 6-1. Summary of collapse results – Including taller buildings.

R = 4 High seismic (SDC Dmax)

S_S = 1.5, S_1 = 0.9 (S_{DS} = 1.0, S_{D1} = 0.6)

Archetype	Storey #	Function	Ω [-]	μ_C [-]	SSF [-]	S_{MT} (T_{design}) [g]	SF_{anchor} [-]	β_{tot} [-]	$\hat{S}_{CT}$ [g]	CMR [-]	ACMR [-]		ACMR limit [-]	check (pass/fail)
2	1	1&2 family	9.91	10.38	1.33	1.50	2.60	0.70	**4.85**	3.24	**4.30**	>	**1.76**	**Pass**
6	2	1&2 family	4.91	7.34	1.31	1.50	1.97	0.70	**4.44**	2.96	**3.89**	>	**1.76**	**Pass**
10	3	multi-family	2.52	6.95	1.30	1.50	1.88	0.70	**3.34**	2.23	**2.90**	>	**1.76**	**Pass**
13	4	multi-family	2.56	4.93	1.25	1.50	1.95	0.70	**3.01**	2.01	**2.50**	>	**1.76**	**Pass**
15	5	multi-family	2.57	4.75	1.24	1.50	2.00	0.70	**3.08**	2.05	**2.55**	>	**1.76**	**Pass**
										Mean	**3.23**	>	**2.38**	**Pass**
17	6	multi-family	2.57	3.91	1.22	1.50	2.05	0.70	**2.98**	1.98	**2.41**	>	**1.76**	**Pass**
18	7	multi-family	2.08	4.19	1.23	1.50	2.02	0.70	**2.97**	1.98	**2.43**	>	**1.76**	**Pass**
19	8	multi-family	2.34	3.42	1.20	1.50	2.14	0.70	**2.79**	1.86	**2.22**	>	**1.76**	**Pass**
20	9	multi-family	2.56	3.00	1.18	1.50	2.40	0.70	**2.61**	1.74	**2.05**	>	**1.76**	**Pass**
21	10	multi-family	2.42	2.91	1.18	1.42	2.44	0.70	**2.30**	1.62	**1.90**	>	**1.76**	**Pass**
										Mean #17-21	**2.20**	>	**2.38**	**Fail**
										Mean #2-21	**2.72**	>	**2.38**	**Pass**

6.3. Comparison of scaling method

Figure 6-3 and 6-4 illustrate the effect of scaling on the IDA results. As is expected, in the case of component scaling the dispersion in elastic and quasi-elastic stage is smaller than at ATC scaling. As a consequence, the median drift ratio at the MCE level is a bit smaller. Note that the overall characteristics (maximum drifts, intensities, dispersion in plastic region, etc.) hardly changes.

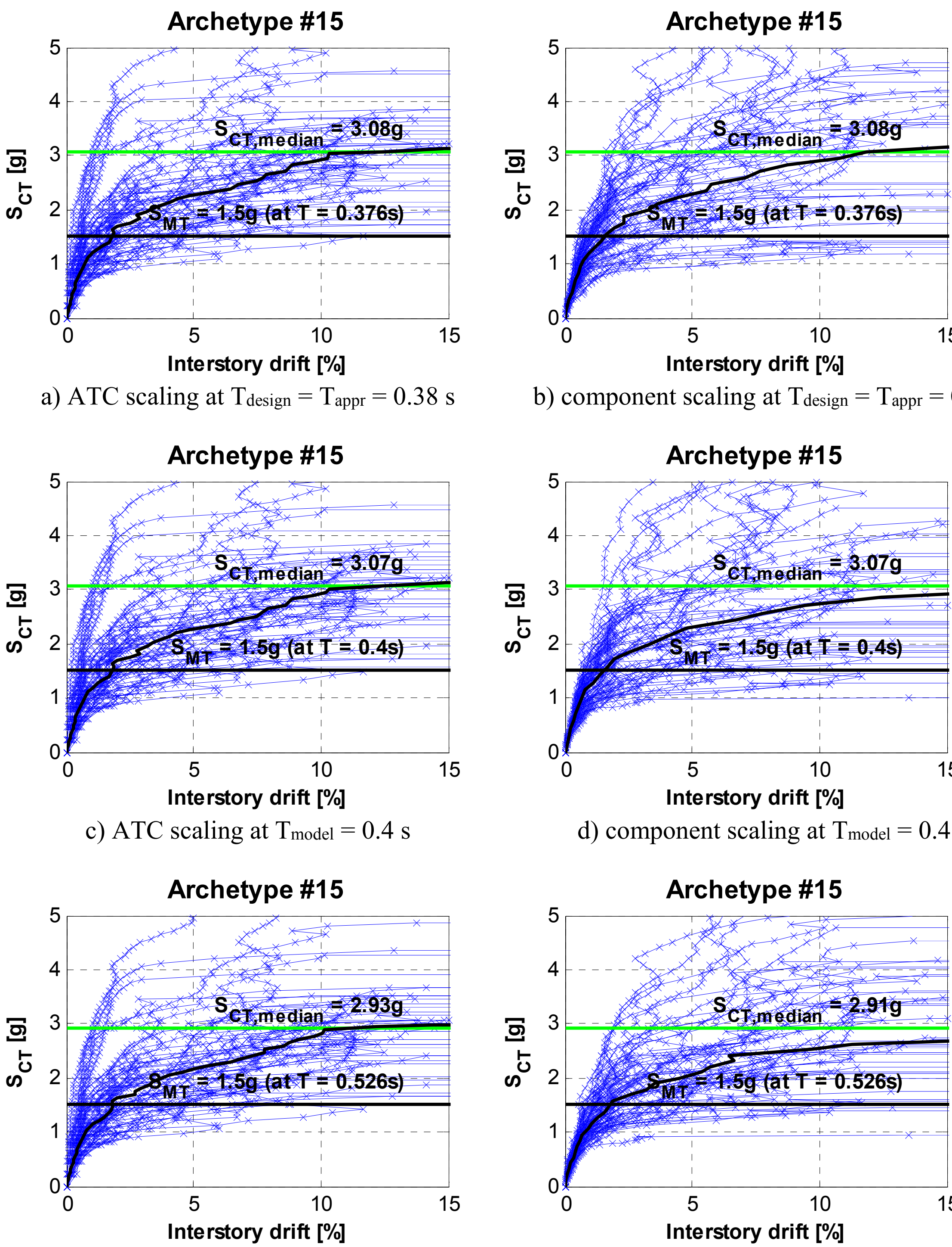

a) ATC scaling at $T_{design} = T_{appr} = 0.38$ s

b) component scaling at $T_{design} = T_{appr} = 0.38$ s

c) ATC scaling at $T_{model} = 0.4$ s

d) component scaling at $T_{model} = 0.4$ s

e) ATC scaling at $T_{upper} = 0.53$ s

f) component scaling at $T_{upper} = 0.53$ s

Figure 6-3. Comparison of scaling methods – Archetype #15.

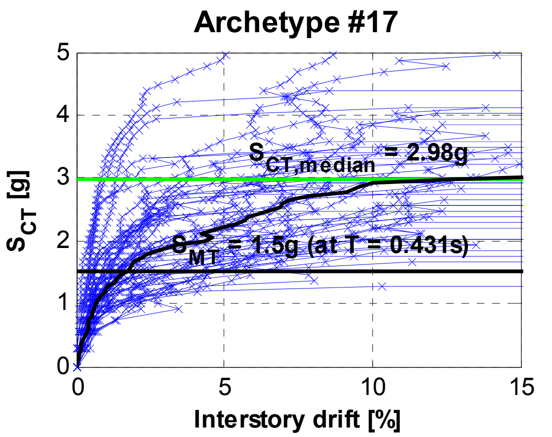

a) ATC scaling at $T_{design} = T_{appr} = 0.43$ s

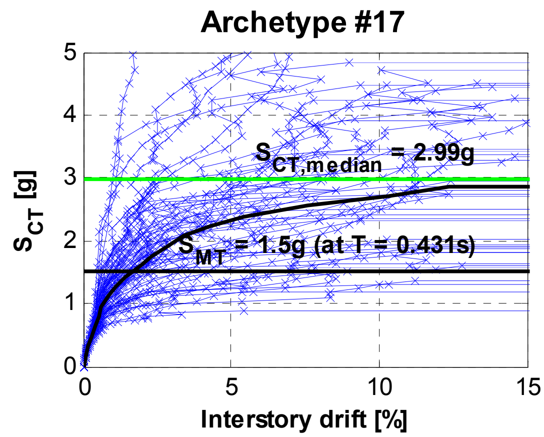

b) component scaling at $T_{design} = T_{appr} = 0.43$ s

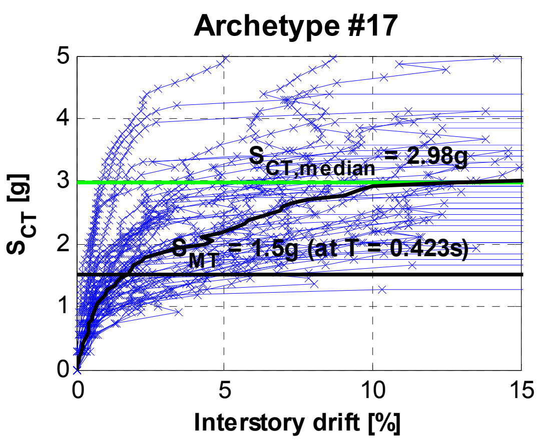

c) ATC scaling at $T_{model} = 0.42$ s

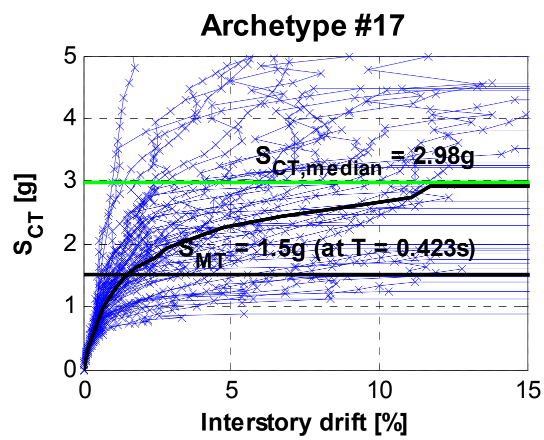

d) component scaling at $T_{model} = 0.42$ s

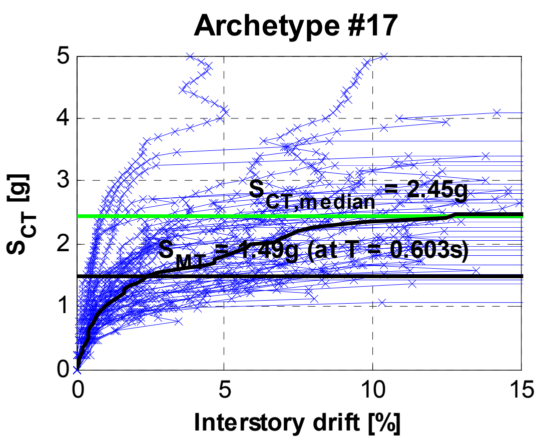

e) ATC scaling at $T_{upper} = 0.60$ s

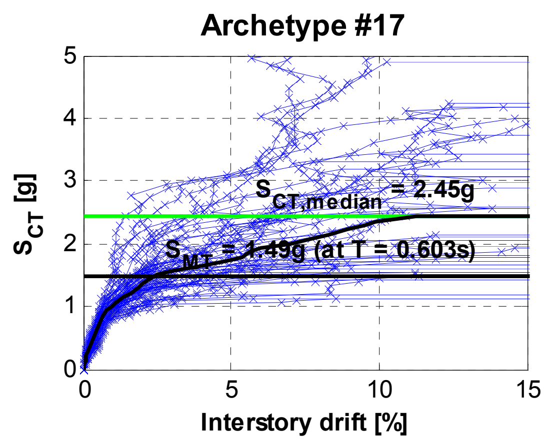

f) component scaling at $T_{upper} = 0.60$ s

Figure 6-4. Comparison of scaling methods – Archetype #17.

6.4. Period sensitivity – Effect of scaling period

The scaling and thus the IDA results can be sensitive to the period chosen for scaling. Figures 6-3 ~ 6-5 illustrate that collapse intensity may significantly vary with the scaling period (all archetypes are designed on the approximate period bases). The results demonstrate that it is important that a) archetype design and ground motion scaling shall be based on the same reference fundamental period; b) the model shall capture the real behavior in terms of fundamental period, too, or with other words, the model and design should be coherent with each other.

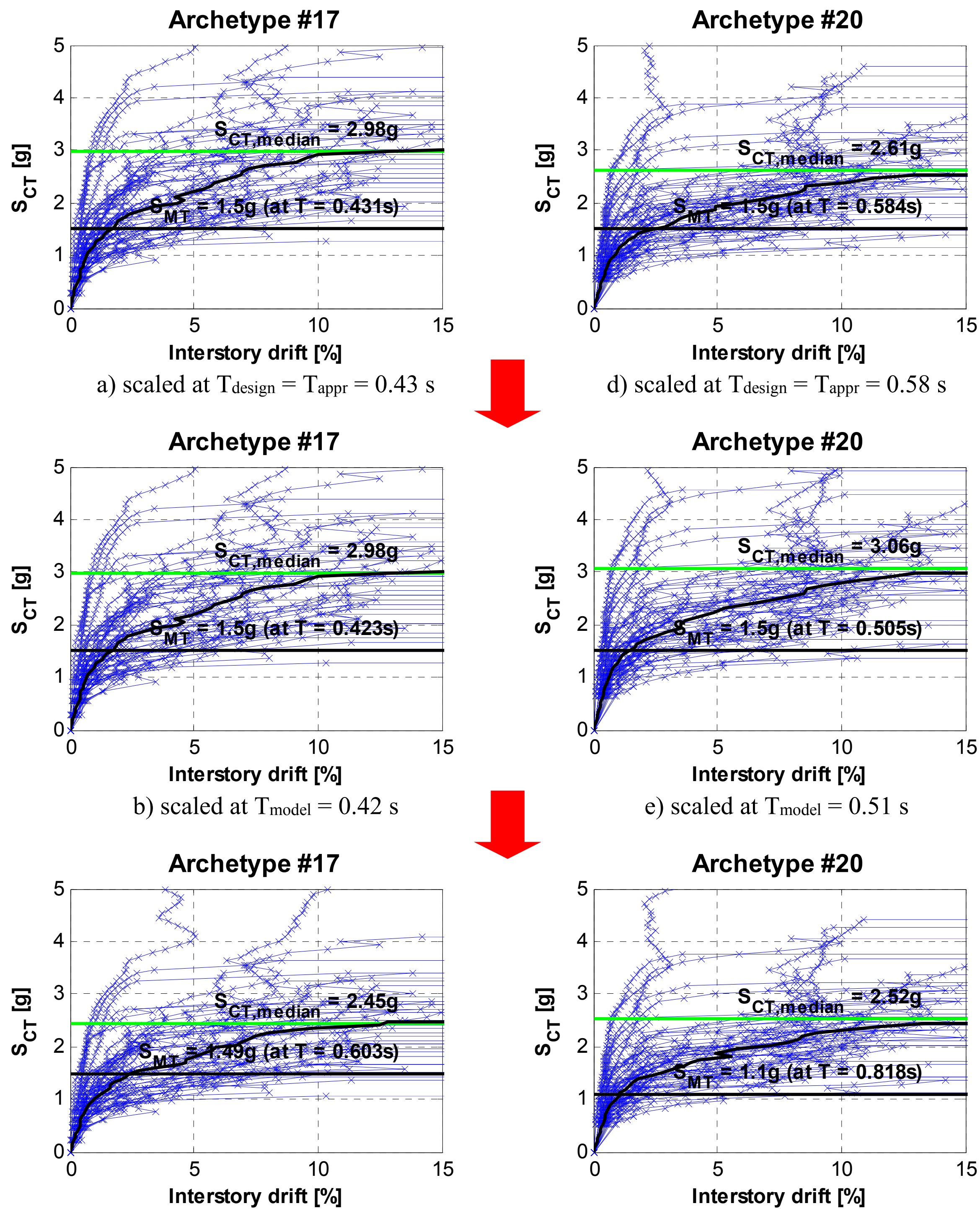

a) scaled at $T_{design} = T_{appr} = 0.43$ s

d) scaled at $T_{design} = T_{appr} = 0.58$ s

b) scaled at $T_{model} = 0.42$ s

e) scaled at $T_{model} = 0.51$ s

c) scaled at $T_{upper} = 0.60$ s

f) scaled at $T_{upper} = 0.89$ s

Figure 6-5. Effect of scaling period.

6.5. Model parameter sensitivity on collapse intensity

As discussed, there are uncertainties in the calibration, because the monotonic backbone curve had to be estimated in lack of experimental data. In a separate sensitivity analysis, the effect of some of the material model parameters is studied on Archetype #5.

As indicated in Table 6-2, drastically changing the capping displacement (by 50%) and the post-capping slope (to 1/3) results in just 6% increase in the collapse intensity. Similarly, changing the pinching parameters resulting in a larger hysteresis loop or favorably modifying the initial stiffness provides slightly increased collapse intensity. It can be concluded that the performance is most sensitive for the shear strength of the wall: 40% larger strength leads to 30% increase in the value of the collapse intensity. Considering the failure mechanism and sequence of a building (as pointed out in Chapter 5), this observation is reasonable: short period, moderate ductility and limited redistribution characterize the structure. After reaching the shear strength at any floor in a dynamic analysis, collapse due to global instability shortly follows as displacements rapidly increase. Note that combining with other structural system that may allow the redistribution of forces (e.g. continuity of boundary members) may favorably change the performance.

Based on these results, the calibrated models can be assumed relatively reliable if the shear strength determination is accurate, despite the other uncertainties in the monotonic performance.

Table 6-2. Model parameter sensitivity on collapse intensity – Archetype #5.

Parameter	**Variation**			**Change in collapse intensity**
capping displacement and capping slope	50 mm -0.15	→	75 mm -0.05	+6%
α_P and β_P	0.75 0.25	→	0.40 0.21	+8%
adjusted initial stiffness				+6%
strength			x 1.4	+30%

6.6. Effect of other structural and non-structural components

The wood shear wall study discussed in [2] confirms that finish materials (e.g. gypsum boards) and other non-structural components in the building may highly improve the performance. The cited study shows that the response modification factor may be increased from 4 to even 6 when considering the additional components.

6.7. Comparison to wooden shear wall systems

The steel corrugated shear wall performance – both on component and global archetype level – shows similarities to the wood shear wall studied in [2].

On the component level, both systems have pinching characteristics (Figure 6-5). Additionally, strength and ductility are also comparable.

Similarities in the IDA results are illustrated in Figure 6-6. The overall ductility, strength, median performance is similar in the two cases. These observations confirm that the steel shear wall is comparable to the wood shear wall on the archetype level as well, and indicates that similar *R* factor can be applied for both systems.

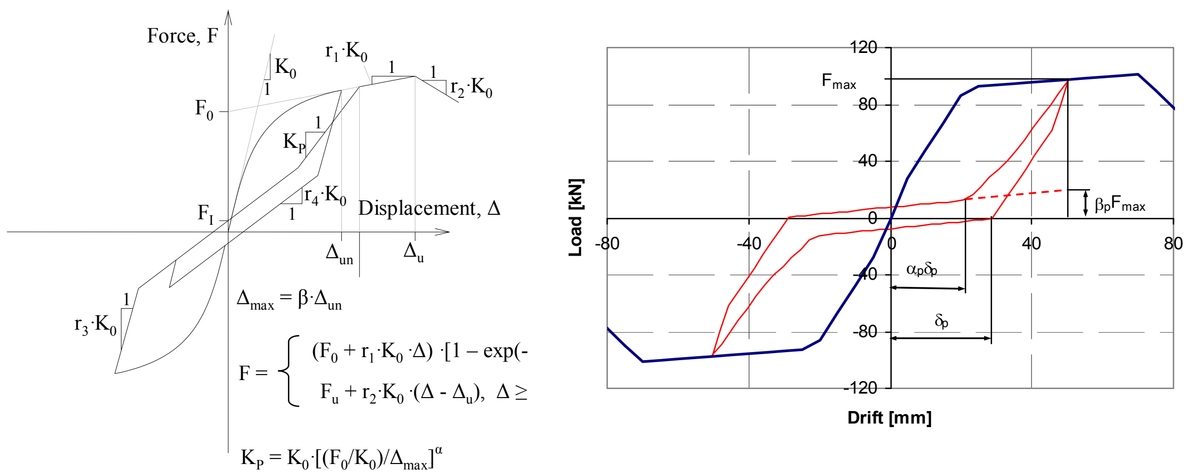

a) wood shear wall [2] b) corrugated shear wall

Figure 6-6. Comparison of wood and steel shear wall – Component level.

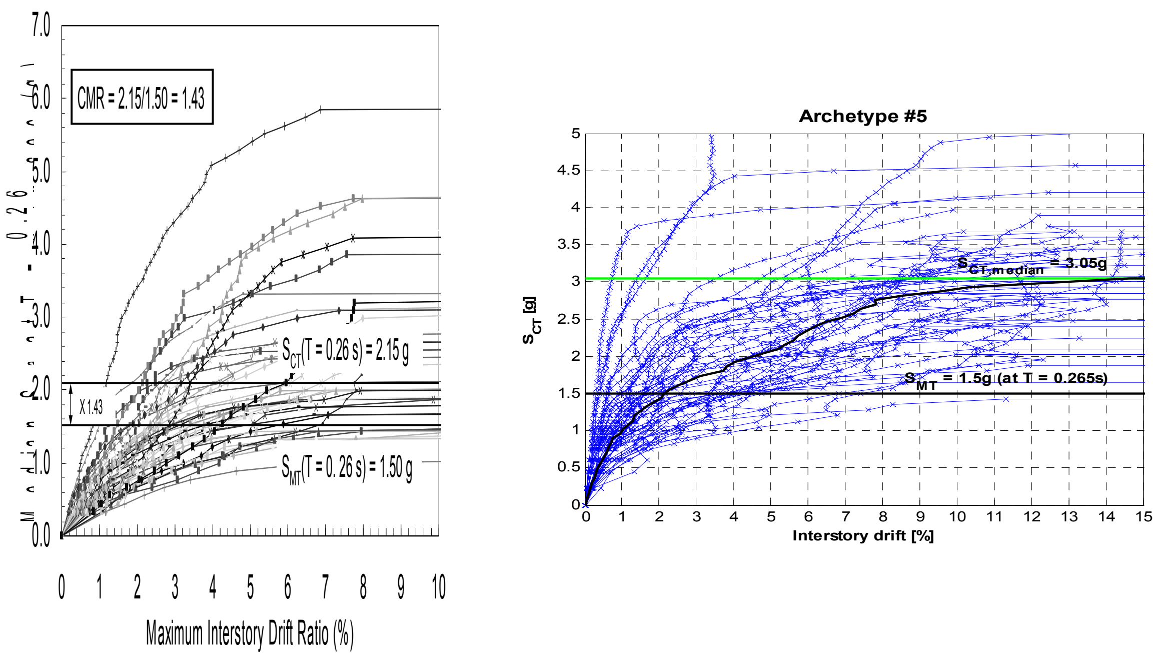

a) wood shear wall [2] b) corrugated shear wall

Figure 6-7. Comparison of wood and steel shear wall – Archetype performance.

7. Summary and conclusions

The FEMA P695 seismic performance evaluation method was presented through a practical example of steel shear wall system. While the methodology is comprehensive and relatively objective, it nevertheless requires one to exercise considerable judgment in

(a) establishing the design archetypes and performance groups,

(b) developing and calibrating the non-linear analysis models, and

(c) establishing appropriate quality ratings (for design requirements, test data, and model accuracy).

In this study, monotonic behavior of the shear wall is investigated by shell-element model. The non-linear analysis helped to determine the monotonic backbone curve of each shear wall type for use in simpler nonlinear spring models model of the entire building. Parameters for the complex cyclic material model are determined by optimization using genetic algorithm. Parameter sensitivity analysis confirms that uncertainties in the model parameters do not lead high variation in the collapse intensity; the model is relatively reliable if the shear strength determination is accurate.

The seismic performance assessment is completed on the basis of pushover and IDA analysis for each archetype. The study indicates that appropriate seismic performance factors for the steel shear wall system are as follows: $R = C_d = 4$ and $\Omega_0 = 3$. These values are based on the available test data and the implied quality ratings of "fair" for design requirements and test data and "good" for the analysis model. If more test data were available to more fully characterize the response (e.g., monotonic backbone curve, longer wall panels), and if the quality ratings were judged to be higher than assumed herein, then higher values for R may be justified.

Further studies confirm that:

- Designing constant wall strength along the building height does not necessarily influence the seismic performance (collapse intensity), as the system is non-redundant.

- For buildings with 6~10 stories (considering them as separate performance group), smaller R-factors may be appropriate. Alternatively, building height can be limited to 8 stories, to keep the obtained R-factor.
- In case of component scaling of the earthquake records the dispersion in elastic and quasi-elastic stage is smaller than at ATC scaling. The overall characteristics (maximum drifts, intensities, dispersion in plastic region, etc.) hardly changes.
- Scaling and IDA results can be sensitive to the period chosen for the scaling. Archetype design and ground motion scaling should preferably be based on the same reference fundamental period. The model shall capture the real behavior in terms of fundamental period, too, or with other words, the model and design should be coherent with each other.
- Response modification factor can be drastically increased when considering additional (non-structural) components. Note that, however, these components are typically non-engineered components.
- With respect to seismic performance, the steel shear wall is comparable to the wood shear wall of [2], both on the component and the archetype levels. It can be presumed that similar *R* factor can be applied for both systems.

It is important to note that this study does not constitute a full implementation of the FEMA P695 procedures, but instead only exercises the analysis aspects of the methodology. A complete implementation of the FEMA P695 methodology would require an independent peer review panel to review the supporting design provisions and test data and a more comprehensive set of system archetypes (e.g. including archetypes for lower seismic regions).

References

[1] Stojadinovic, B., Tipping, S., Structural Testing of Corrugated Sheet Steel Shear Walls. Research report, University of California, Berkeley. 2007

[2] FEMA P695, Quantification of Building System Performance and Response Parameters. FEMA P695, June 2009.

[3] Deierlein GG, Liel AB, Haselton CB, Kircher ChA. Assessing Building System Collapse Performance and Associated Requirements for Seismic Design. Proc. SEAOC 2007 Convention. 2007

[4] ANSYS Structural analysis guide, online documentation. ANSYS Inc.

[5] Fülöp LA, Dubina D. Design Criteria for Seam and Sheeting-to-Framing Connections of Cold-Formed Steel Shear Panels. Journal of Structural Engineering, Vol. 132, No. 4. pp. 582–590. 2006

[6] EN 1993-1-3:2007: Eurocode 3: Design of steel structures. Part 1-3: General rules. Supplementary rules for cold formed members and sheeting. CEN, Brussels. 2007

[7] OpenSees: Open Systems for Earthquake Engineering Simulation, http://opensees.berkeley.edu

[8] Ibarra L, Medina R, Krawinkler H. Hysteretic models that incorporate strength and stiffness deterioration. Eq. Eng. and Struct. Dynamics, Vol 34, No.12. pp.1489-1511. 2005

[9] ASCE 7-10: Minimum Design Loads for Buildings and Other Structures. American Society of Civil Engineers, Reston, VA, 2010.

[10] Matt Eiler PE. Specifying Screws Per the 2011 North American Specification Highlights Need for Manufacturers to Publish Tested Screw Capacities. Newsletter for the Light Gauge Steel Engineers Association. pp. 4-5. 2005

[11] EN 1993-1-5:2007: Eurocode 3: Design of steel structures. Part 1-5: Plated structural elements. CEN, Brussels. 2007

[12] AC154:2000 (editorially revised 2005) Acceptance criteria for cyclic racking shear tests for metal-sheathed shear walls with steel framing. ICC Evaluation service, Inc. Whittier, CA. 2005

[13] AC130:2004 Acceptance criteria for prefabricated wood shear panels. ICC Evaluation service, Inc. Whittier, CA. 2004

Unit conversion

Imperial	Metric
1” (inch)	25.4 mm (millimeter)
1’ (feet, ft)	0.3048 m (meter)
1 sqft (square foot)	0.092903 m^2 (square meter)
1 kip (kilopound)	4.448 kN (kilonewton)
1 psi (pound-force/square inch)	6.8947573 kN/m^2
1 psf (pound-force/square foot)	0.0478803 kN/m^2
1 plf (pounds of force per linear foot, lbf/ft)	14.59390 N/m

Appendix A – Sample design of shear wall

Design of shear wall
Archetype #15

1. General building data

Number of stories: $nr_{st} := 5$ MULTI-FAMILY

Storey height: $h_i := i \cdot 10 \cdot ft$ $h = \begin{pmatrix} 10 \\ 20 \\ 30 \\ 40 \\ 50 \end{pmatrix} ft$

Total height: $H := h_{nr_{st}}$ $H = 50\,ft$ $h_n := \frac{H}{ft}$

Shear wall length: $L := 20ft$

Tributary width: $B := 12.5ft$

Tributary area for seismic mass: $A_{fl} := 40ft \cdot 12.5ft$ $A_{fl} = 500\,sqft$

2. Loading (effective seismic weight)

Load on roof (DL+LL): $q_{roof} := 30psf$

Load on typical floor (DL+LL): $q_{floor} := 30psf$

$i := 1 .. nr_{st}$ $x := 1 .. nr_{st}$

$q_i := \text{if}\left(i < nr_{st}, q_{floor}, q_{roof}\right)$

$w_i := q_i \cdot A_{fl}$

Total effective seismic weight:

$W := \sum_i w_i$ $W = 75\,kip$

3. Seismic design parameters

Procedure: equivalent lateral force procedure

Seismic design category: High D

$$S_{DS} := 1.0 \qquad (\quad S_S := 1.5 \ )$$

$$S_{D1} := 0.6 \qquad (\quad S_1 := 0.9 \ )$$

$$T_0 := 0.2 \cdot \frac{S_{D1}}{S_{DS}} \qquad T_0 = 0.12$$

$$T_S := \frac{S_{D1}}{S_{DS}} \qquad T_S = 0.6$$

$T_L := 12$ (long-period transition period, Region 1, San Francisco)

Importance factor: $I := 1.00$

Response modification coefficient: $R := 4.0$

4. Seismic demand - Base shear force

4.1 Approximate fundamental period

Structure type: all other

$C_t := 0.02$ (0.0488 for metric units)

$x_c := 0.75$

Fundamental period: $T_a := C_t \cdot h_n^{\,x_c}$ $\qquad T_a = 0.376$

Upper limit on period: $C_u := 1.4$

$$T := C_u \cdot T_a \qquad T = 0.526$$

4.2 Seismic response coefficient

Constant acc.: Constant velocity: Constant displ.:

$$C_{s.1} := \frac{S_{DS}}{\left(\frac{R}{I}\right)} \qquad C_{s.2} := \frac{S_{D1}}{T_a \cdot \left(\frac{R}{I}\right)} \qquad C_{s.3} := \frac{S_{D1} \cdot T_L}{T_a^{\,2} \cdot \left(\frac{R}{I}\right)} \qquad C_s := \min\left(C_{s.1}, C_{s.2}, C_{s.3}\right)$$

$$C_{s.1} = 0.25 \qquad C_{s.2} = 0.399 \qquad C_{s.3} = 12.728 \qquad C_s = 0.25$$

Minimum coefficients:

$$C_{s.min.1} := \frac{0.5 \cdot S_1}{\left(\frac{R}{I}\right)} \qquad C_{s.min.1} = 0.113 \qquad \text{(since S1>=0.6g)}$$

$$C_{s.min.2} := 0.01$$

$$C_s := \max\left(C_s, C_{s.min.1}, C_{s.min.2}\right) \qquad C_s = 0.25$$

4.3 Seismic base shear

$$V := C_s \cdot W \qquad V = 18.75\ \text{kip}$$

4.4 Seismic force distribution

$k := 1$ (structure having period less than 1s)

$$C_{v_x} := \frac{w_x \cdot \left(h_x\right)^k}{\sum_i w_i \cdot \left(h_i\right)^k} \qquad F_x := C_{v_x} \cdot V \qquad C_v = \begin{pmatrix} 0.067 \\ 0.133 \\ 0.2 \\ 0.267 \\ 0.333 \end{pmatrix} \qquad F = \begin{pmatrix} 1.25 \\ 2.5 \\ 3.75 \\ 5 \\ 6.25 \end{pmatrix} \text{kip}$$

$$\sum C_v = 1$$

4.5 Shear force per level

$$V_{v_x} := \sum_{j=x}^{nr_{st}} F_j$$

$$V_v = \begin{pmatrix} 18.75 \\ 17.5 \\ 15 \\ 11.25 \\ 6.25 \end{pmatrix} \text{kip} \qquad v_v = \begin{pmatrix} 937 \\ 875 \\ 750 \\ 563 \\ 312 \end{pmatrix} \text{plf}$$

5. Earthquake resisting system - Shear walls

5.1 Shear wall types and design strength

$group_1 =$	$v_{u.ASD_1} =$		$v_{u.LRFD_1} =$		
1	469	plf	657	plf	(note: LRFD = 1.4xASD)
25	602		843		
7	734		1028		
3	866		1212		
6	1291		1807		
8	1316		1842		
13	1658		2321		
14	2065		2891		
16	2350		3290		

5.2 Shear wall schedule

Shear wall type: Shear wall length: Capacity:

$$SWtype := \begin{pmatrix} 3 \\ 3 \\ 2 \\ 1 \\ 1 \end{pmatrix} \qquad L = 20\,ft \qquad v_{u_i} := v_{u.LRFD_{(SWtype_i)}} \qquad v_u = \begin{pmatrix} 1028 \\ 1028 \\ 843 \\ 657 \\ 657 \end{pmatrix} plf$$

(1 - #1; 2 - #25; 3 - #7; 4 - #3; 5 - #6; 6 - #8; 7 - #13; 8 - #14; 9 - #16)

5.3 Check & Utilization factor

$$UF_x := \frac{v_{v_x}}{v_{u_x}} \qquad UF = \begin{pmatrix} 91 \\ 85 \\ 89 \\ 86 \\ 48 \end{pmatrix} \% \qquad check = \begin{pmatrix} \text{"ok"} \\ \text{"ok"} \\ \text{"ok"} \\ \text{"ok"} \\ \text{"ok"} \end{pmatrix}$$

Appendix B – Capacity curve of archetypes

Archetype #1

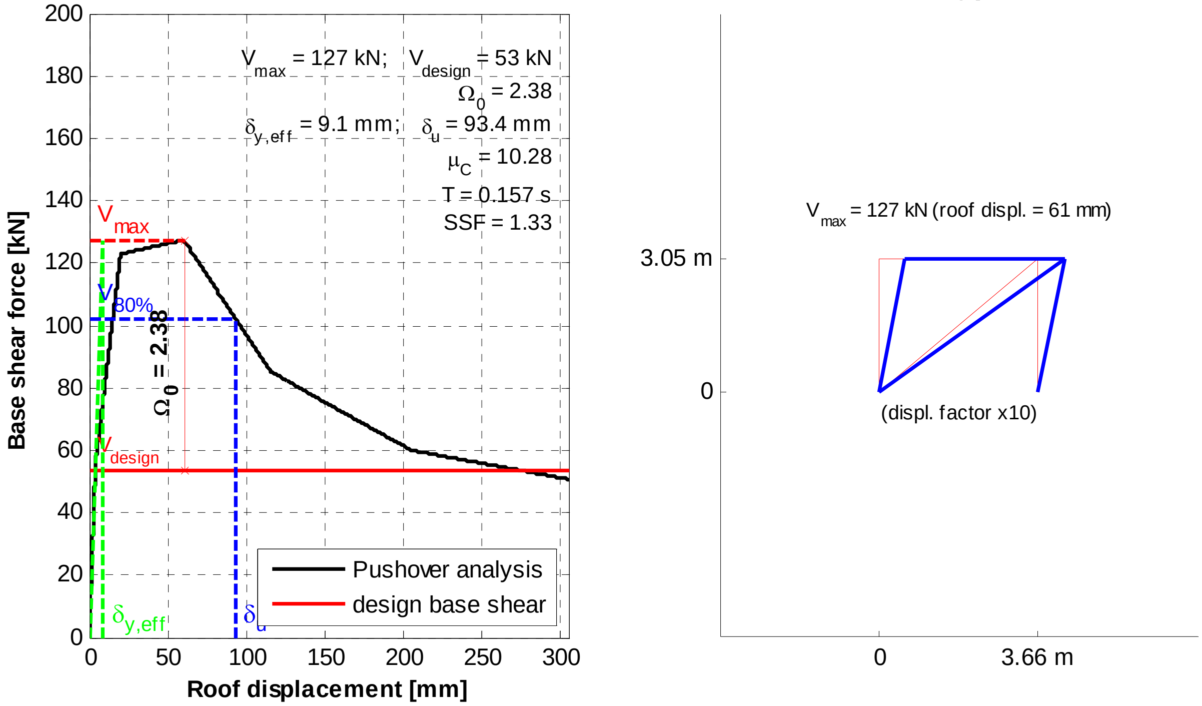

Archetype #5

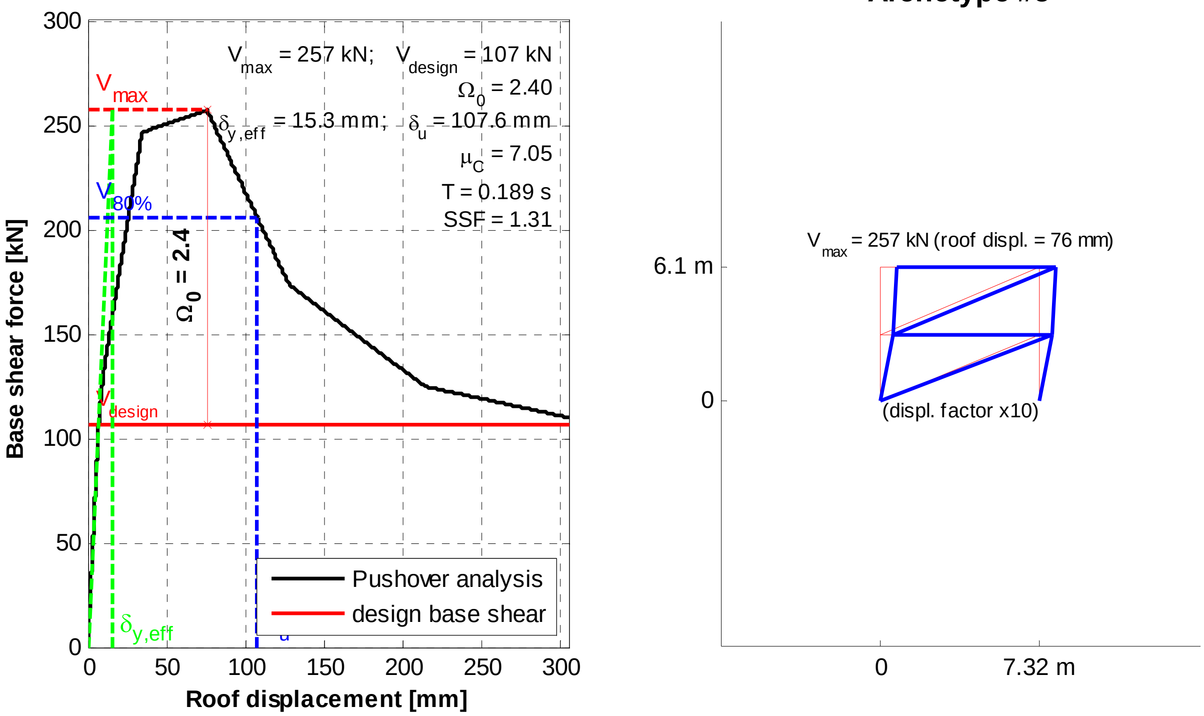

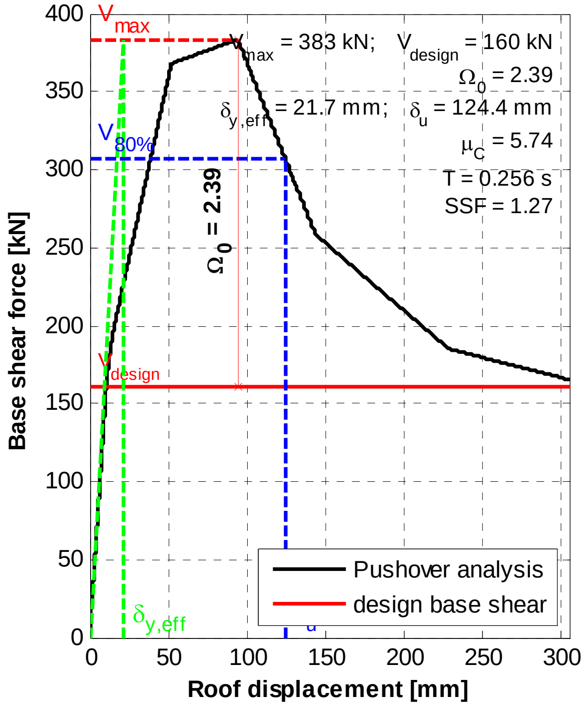

V_{max} = 383 kN; V_{design} = 160 kN
Ω_0 = 2.39
$\delta_{y,eff}$ = 21.7 mm; δ_u = 124.4 mm
μ_C = 5.74
T = 0.256 s
SSF = 1.27
V_{max}
$V_{80\%}$
V_{design}
Ω_0 = 2.39
$\delta_{y,eff}$
Pushover analysis
design base shear
Base shear force [kN]
Roof displacement [mm]

Archetype #9

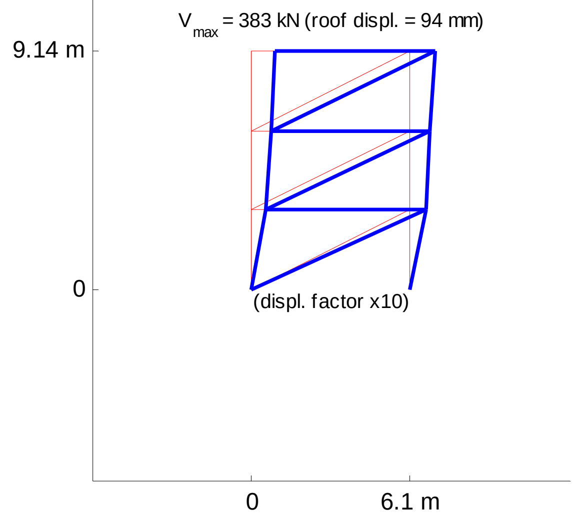

V_{max} = 383 kN (roof displ. = 94 mm)
9.14 m
0
(displ. factor x10)
0
6.1 m

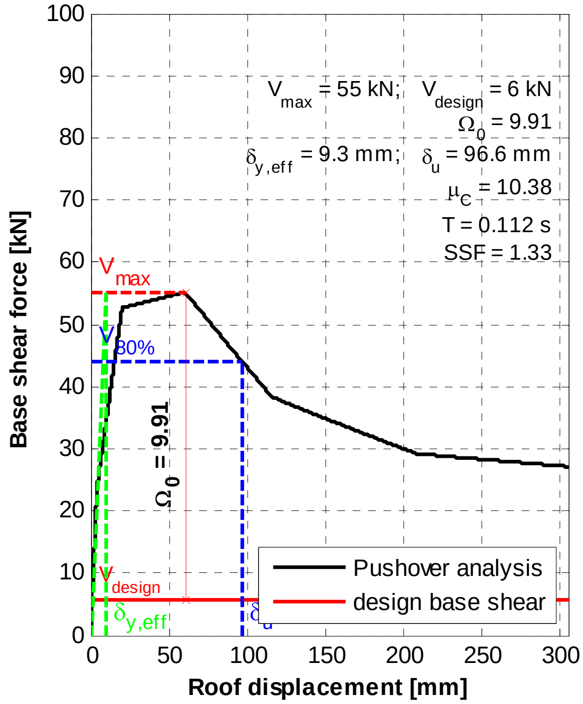
V max = 55 kN; V design = 6 kN
Ω 0 = 9.91
δ y,eff = 9.3 mm; δ u = 96.6 mm
μ C = 10.38
T = 0.112 s
SSF = 1.33
V max
V 80%
Ω 0 = 9.91
V design
δ y,eff
δ u
Pushover analysis
design base shear
Base shear force [kN]
Roof displacement [mm]

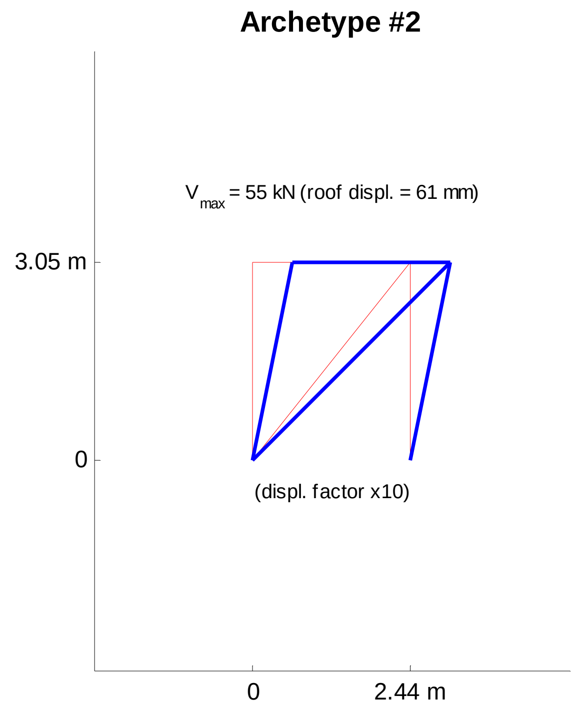
Archetype #2
V max = 55 kN (roof displ. = 61 mm)
3.05 m
0
(displ. factor x10)
0
2.44 m

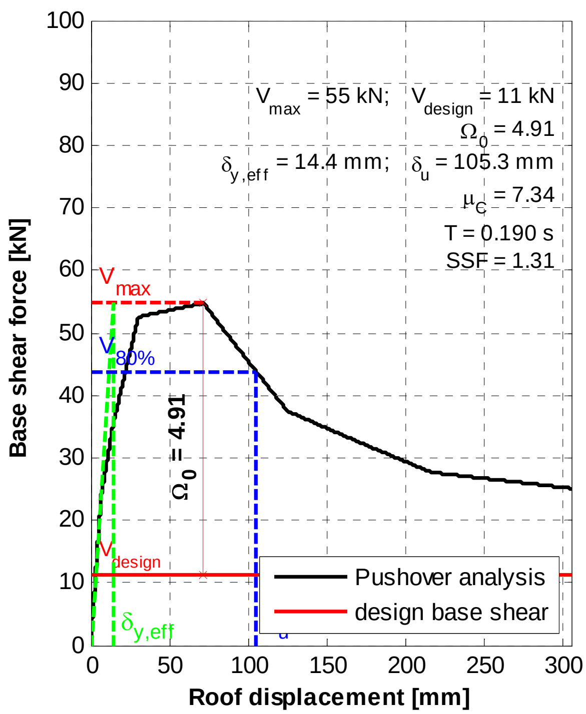
V max = 55 kN; V design = 11 kN
Ω 0 = 4.91
δ y,eff = 14.4 mm; δ u = 105.3 mm
μ C = 7.34
T = 0.190 s
SSF = 1.31
V max
V 80%
Ω 0 = 4.91
V design
δ y,eff
Pushover analysis
design base shear
Base shear force [kN]
Roof displacement [mm]

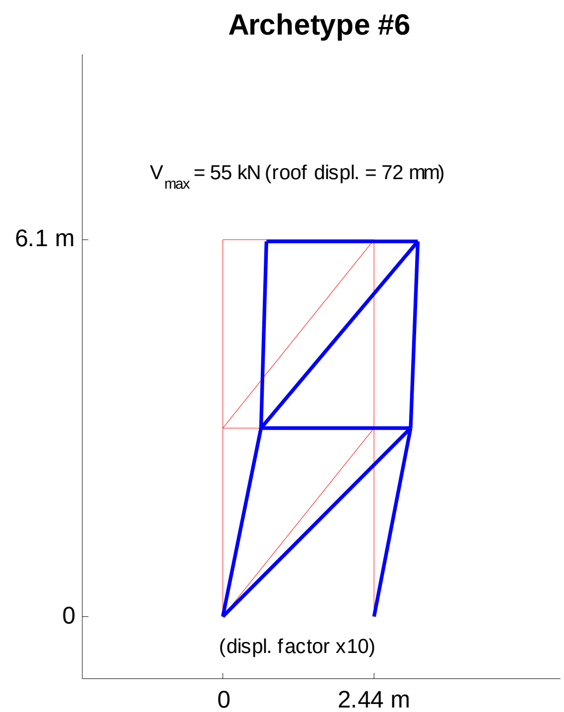
Archetype #6
V max = 55 kN (roof displ. = 72 mm)
6.1 m
0
(displ. factor x10)
0
2.44 m

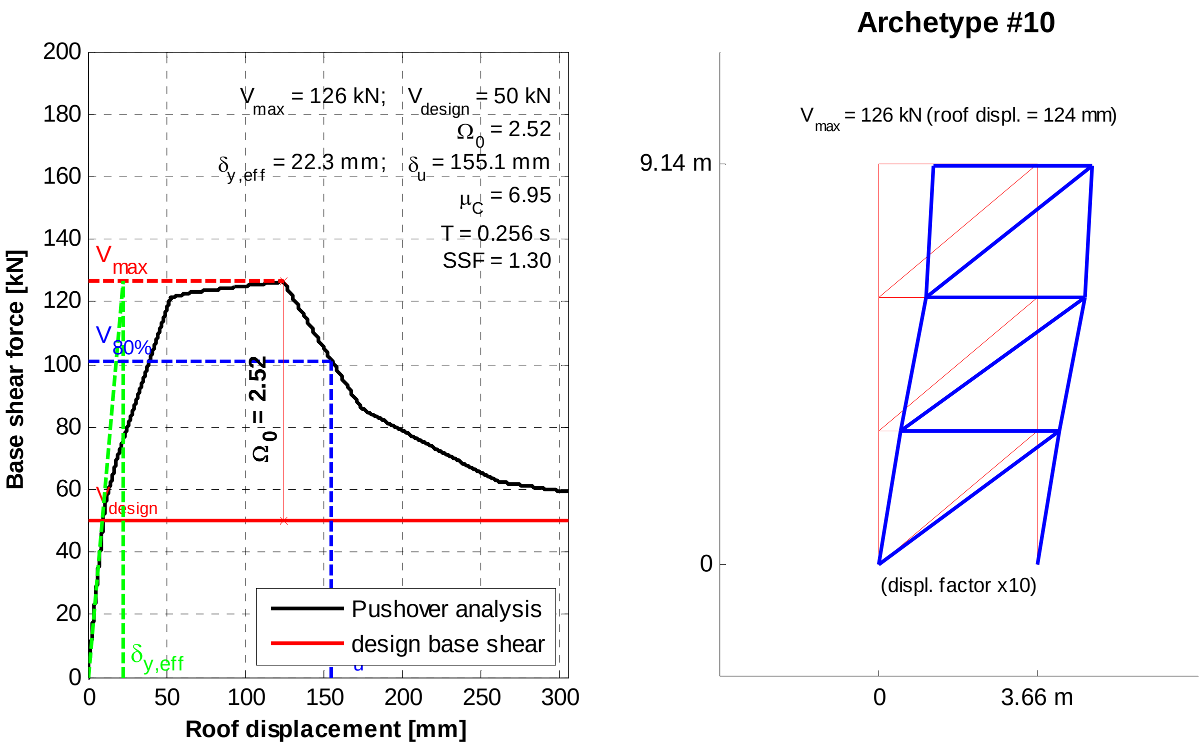
Archetype #10
V max = 126 kN; V design = 50 kN
Ω0 = 2.52
δy,eff = 22.3 mm; δu = 155.1 mm
μC = 6.95
T = 0.256 s
SSF = 1.30
V max
V 80%
V design
δy,eff
Ω0 = 2.52
Pushover analysis
design base shear
Base shear force [kN]
Roof displacement [mm]
V max = 126 kN (roof displ. = 124 mm)
9.14 m
0
(displ. factor x10)
3.66 m

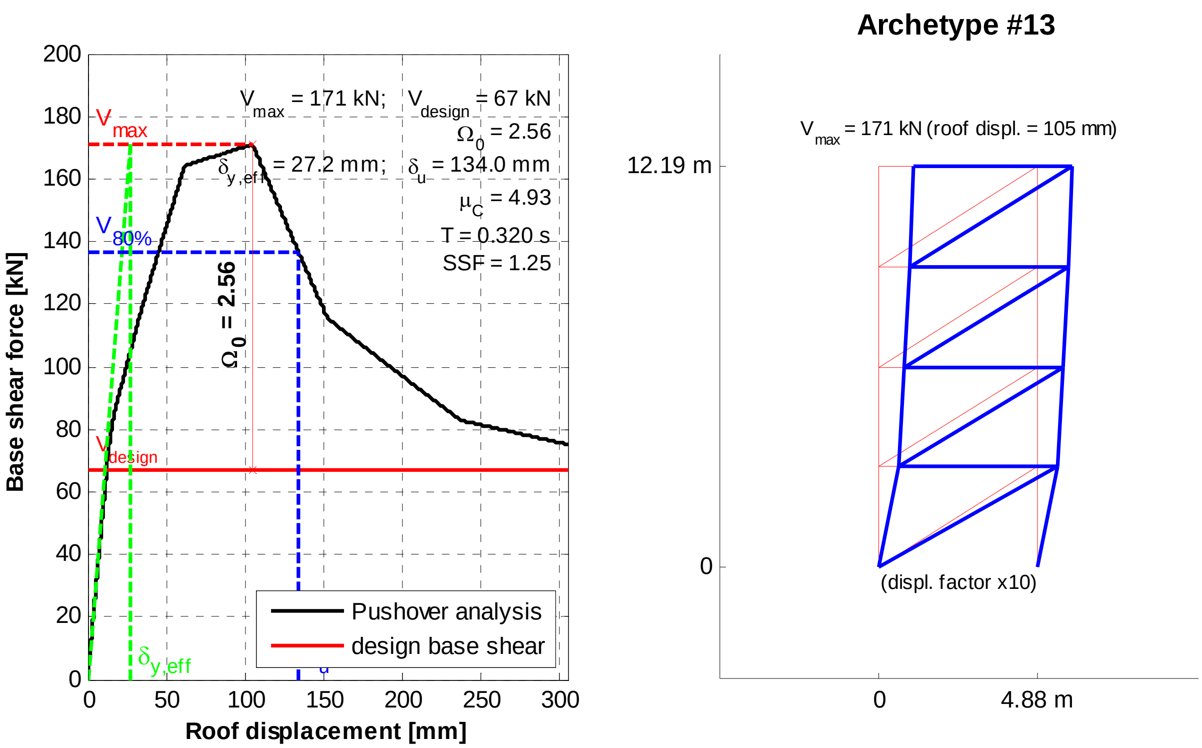
Archetype #13
V max = 171 kN; V design = 67 kN
Ω0 = 2.56
δy,eff = 27.2 mm; δu = 134.0 mm
μC = 4.93
T = 0.320 s
SSF = 1.25
V max
V 80%
V design
δy,eff
Ω0 = 2.56
Pushover analysis
design base shear
Base shear force [kN]
Roof displacement [mm]
V max = 171 kN (roof displ. = 105 mm)
12.19 m
0
(displ. factor x10)
4.88 m

Archetype #15

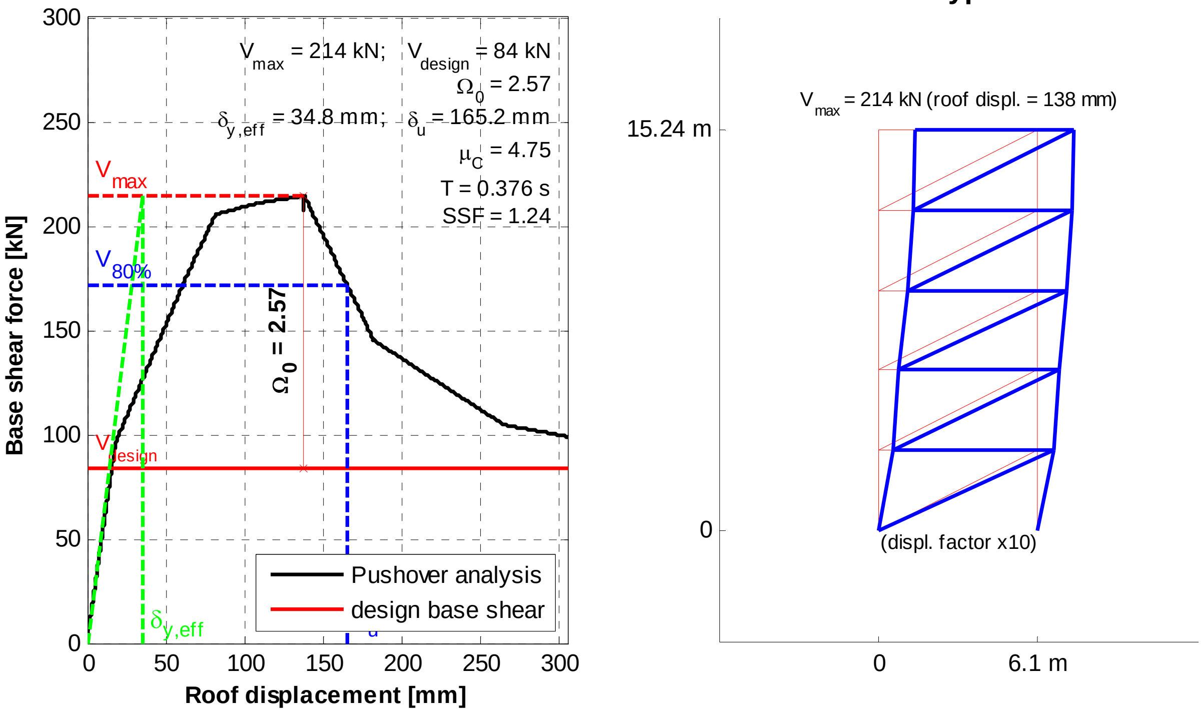

Archetype #1501

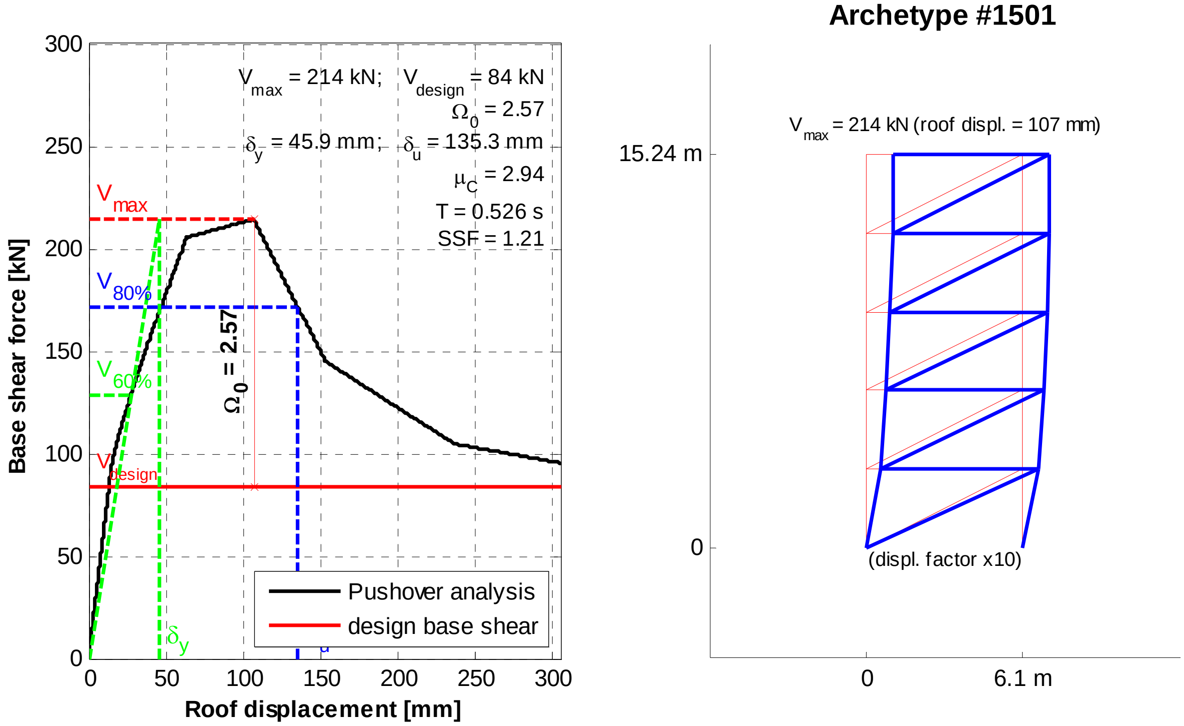

Archetype #17

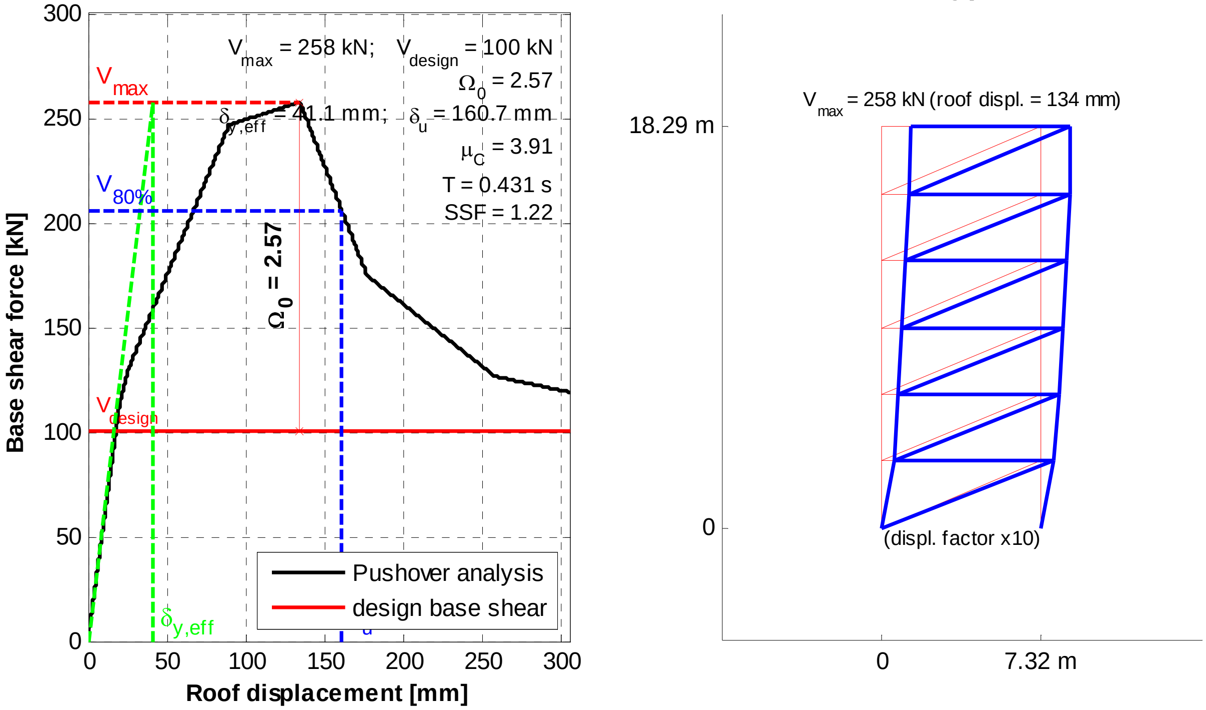

Archetype #18

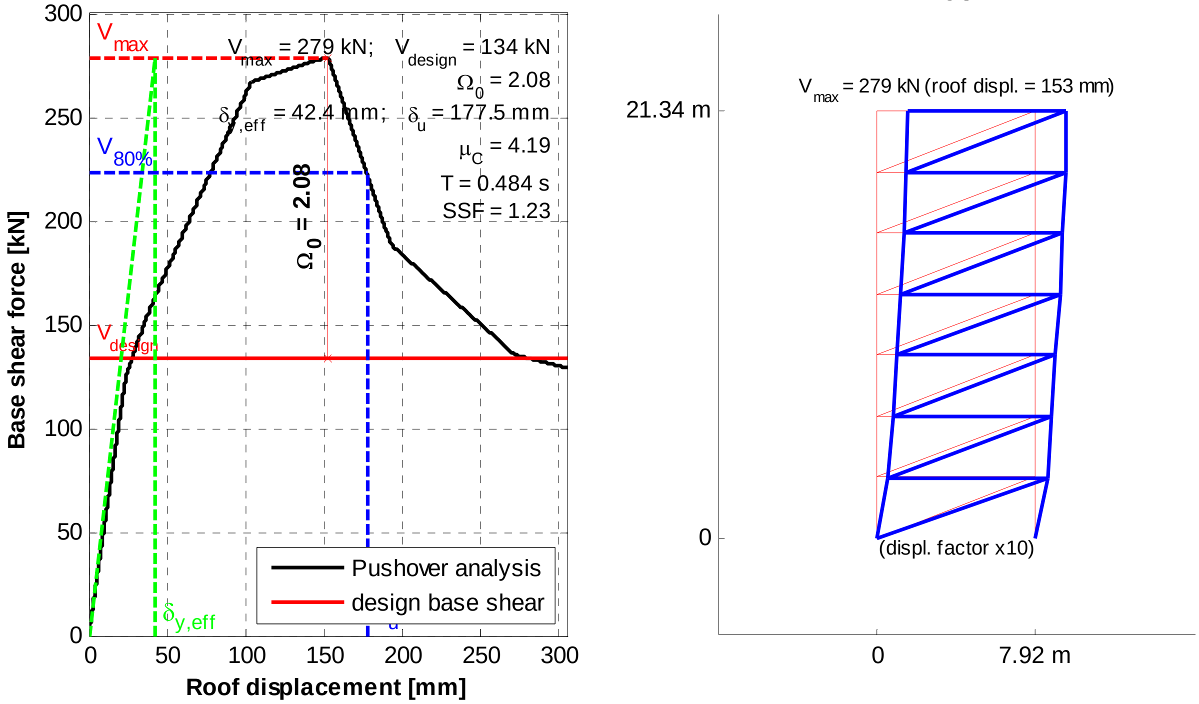

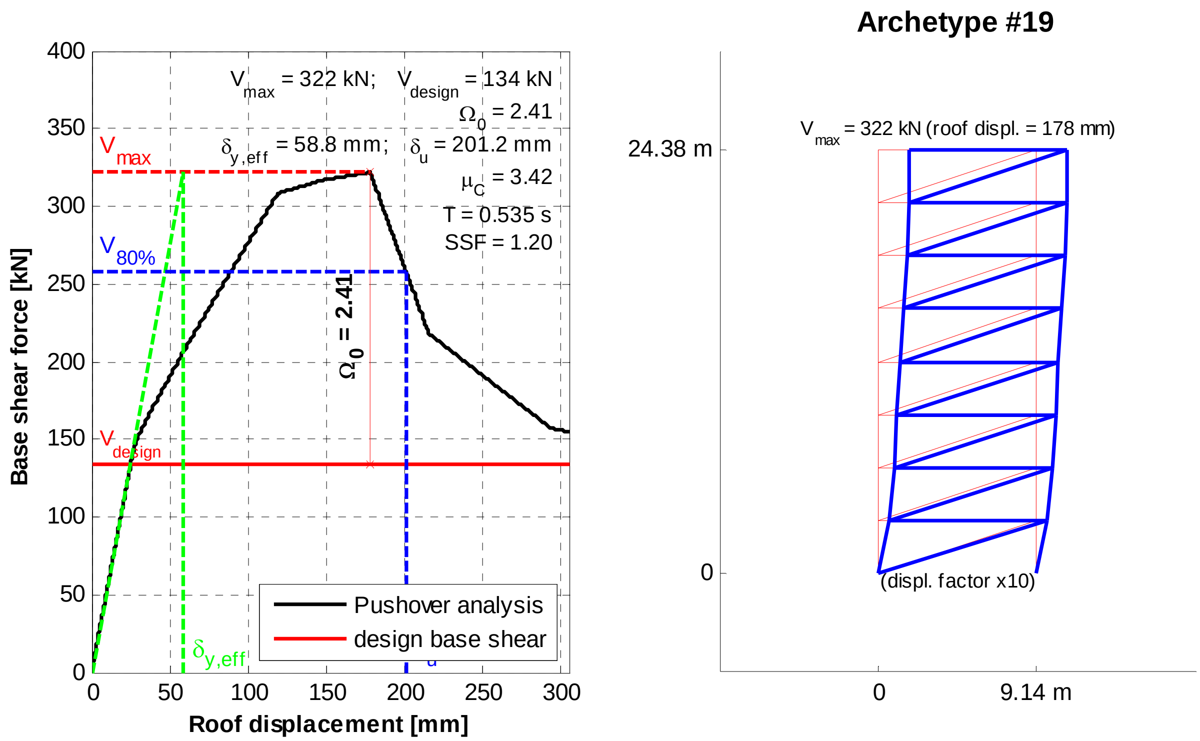
Archetype #19
Vmax = 322 kN; Vdesign = 134 kN
Ω0 = 2.41
δy,eff = 58.8 mm; δu = 201.2 mm
μC = 3.42
T = 0.535 s
SSF = 1.20
Vmax
V80%
Vdesign
Ω0 = 2.41
δy,eff
Pushover analysis
design base shear
Base shear force [kN]
Roof displacement [mm]
Vmax = 322 kN (roof displ. = 178 mm)
24.38 m
(displ. factor x10)
9.14 m

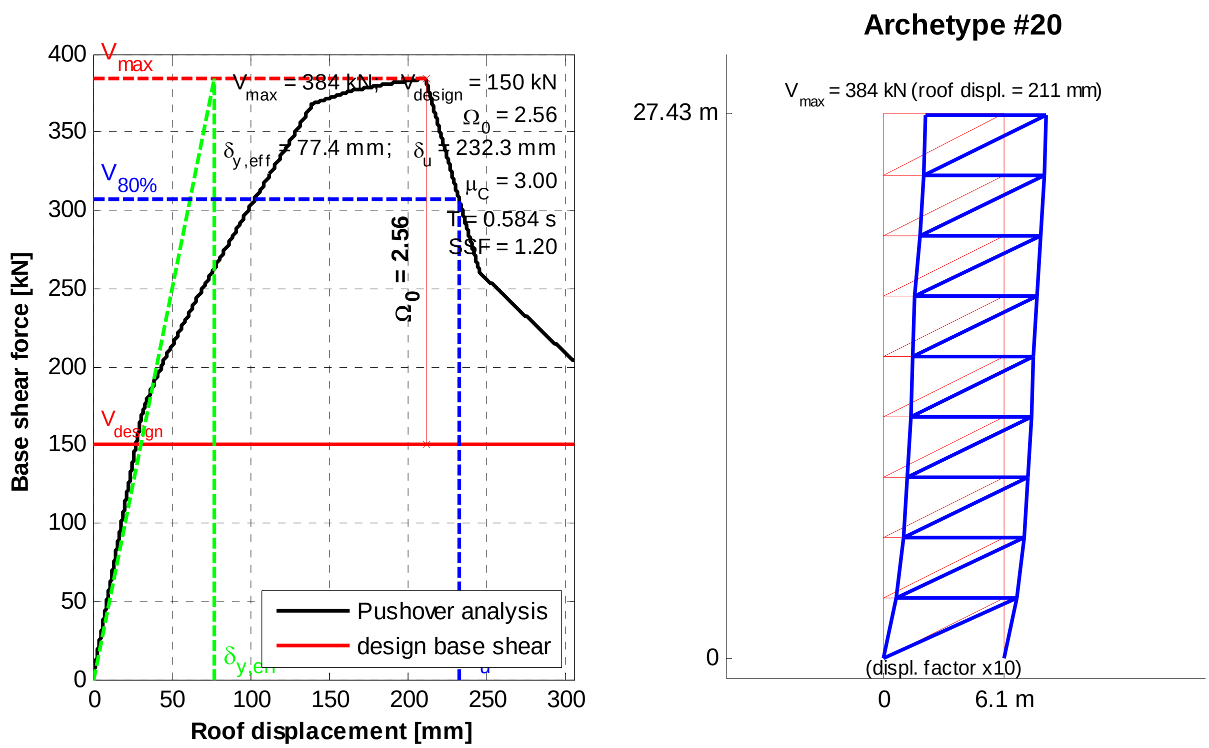
Archetype #20
Vmax = 384 kN; Vdesign = 150 kN
Ω0 = 2.56
δy,eff = 77.4 mm; δu = 232.3 mm
μC = 3.00
T = 0.584 s
SSF = 1.20
Vmax
V80%
Vdesign
Ω0 = 2.56
Pushover analysis
design base shear
Base shear force [kN]
Roof displacement [mm]
Vmax = 384 kN (roof displ. = 211 mm)
27.43 m
(displ. factor x10)
6.1 m

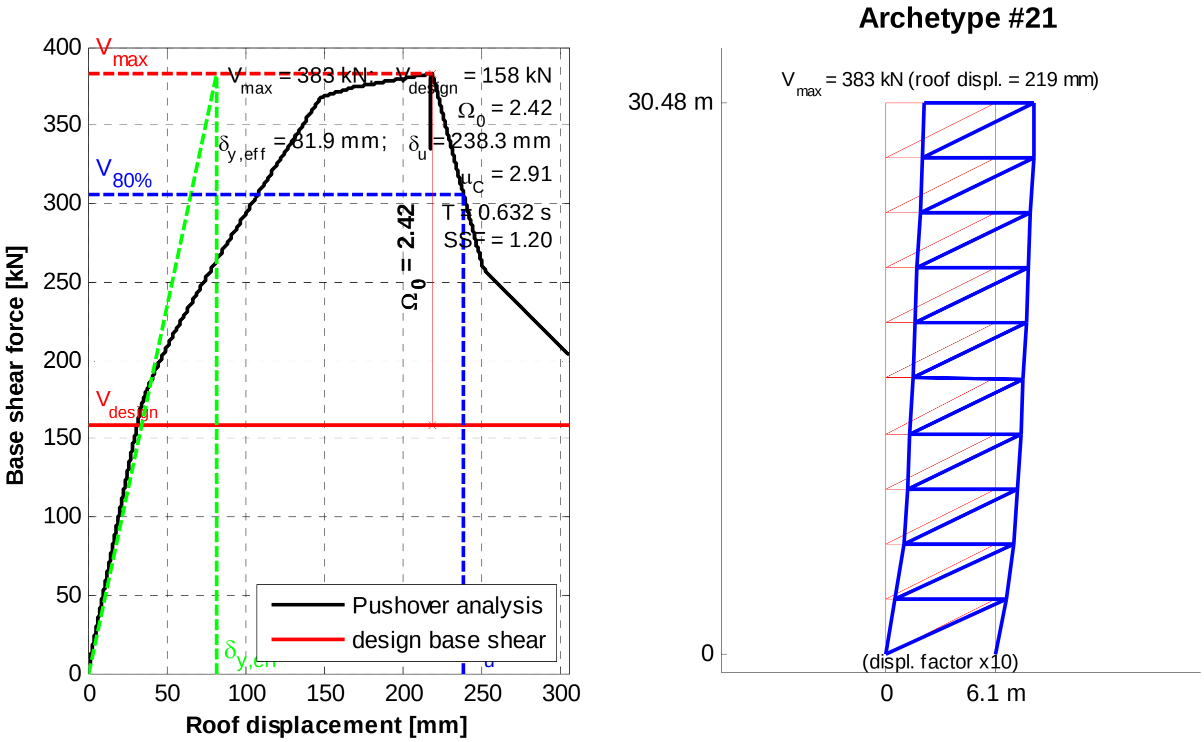

Archetype #21
V_{max}
V_{max} = 383 kN; V_{design} = 158 kN
Ω_0 = 2.42
$\delta_{y,eff}$ = 81.9 mm; δ_u = 238.3 mm
μ_C = 2.91
T = 0.632 s
SSF = 1.20
$V_{80\%}$
Ω_0 = 2.42
V_{design}
$\delta_{y,eff}$
Pushover analysis
design base shear
Base shear force [kN]
Roof displacement [mm]
V_{max} = 383 kN (roof displ. = 219 mm)
30.48 m
0
(displ. factor x10)
6.1 m

Appendix C – IDA results for each archetype

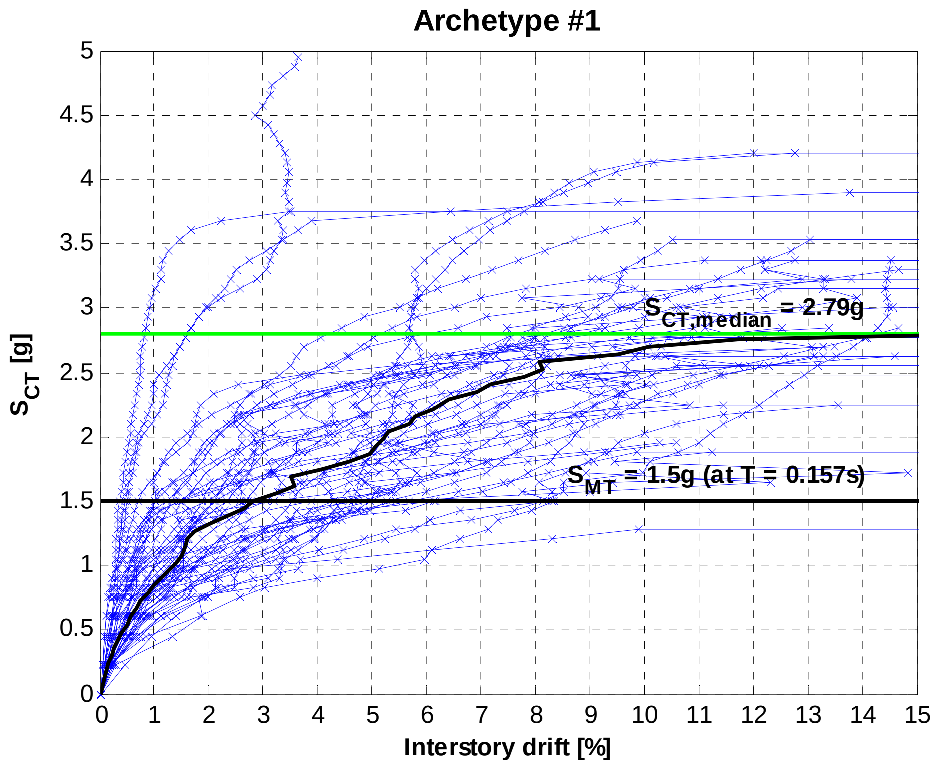

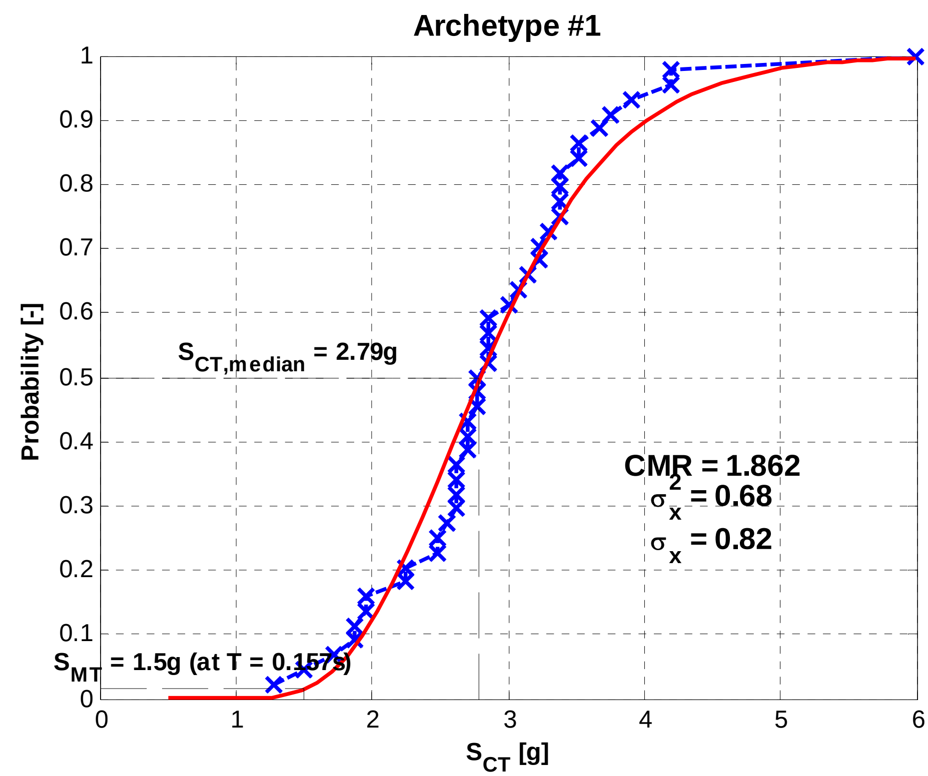

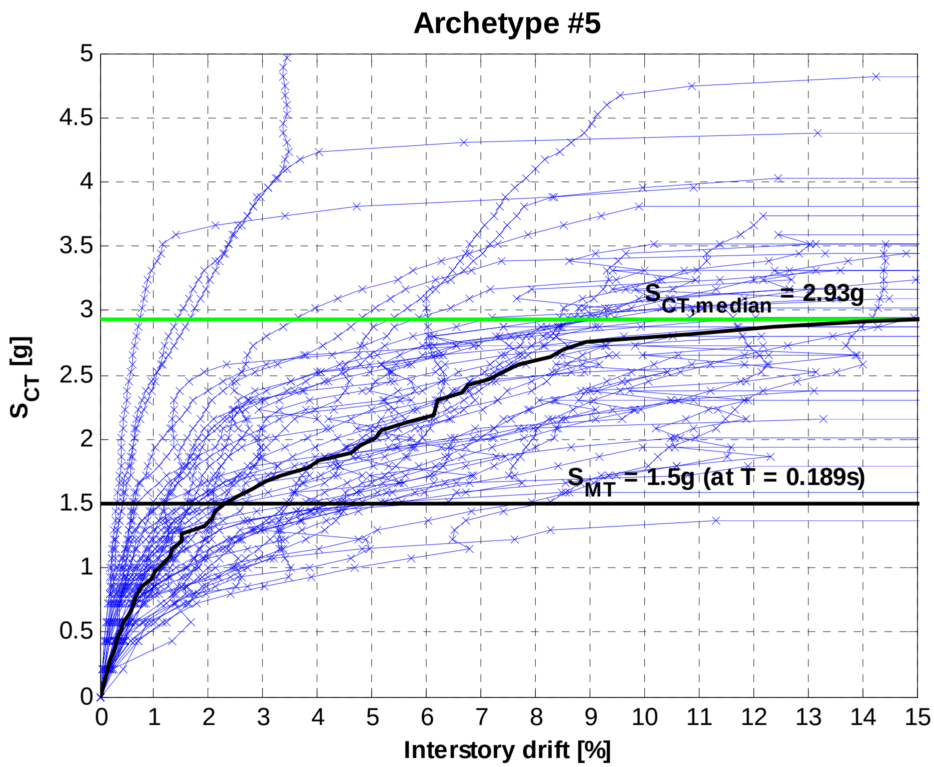
Archetype #5
$S_{CT,median}$ = 2.93g
S_{MT} = 1.5g (at T = 0.189s)
S_{CT} [g]
Interstory drift [%]

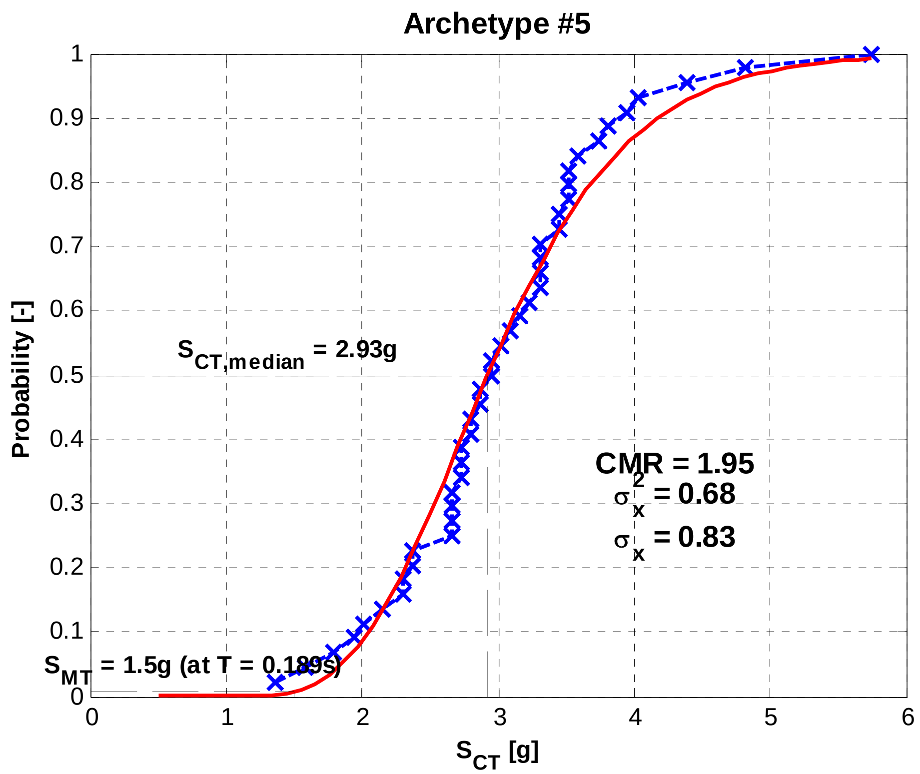
Archetype #5
$S_{CT,median}$ = 2.93g
CMR = 1.95
σ_x^2 = 0.68
σ_x = 0.83
S_{MT} = 1.5g (at T = 0.189s)
Probability [-]
S_{CT} [g]

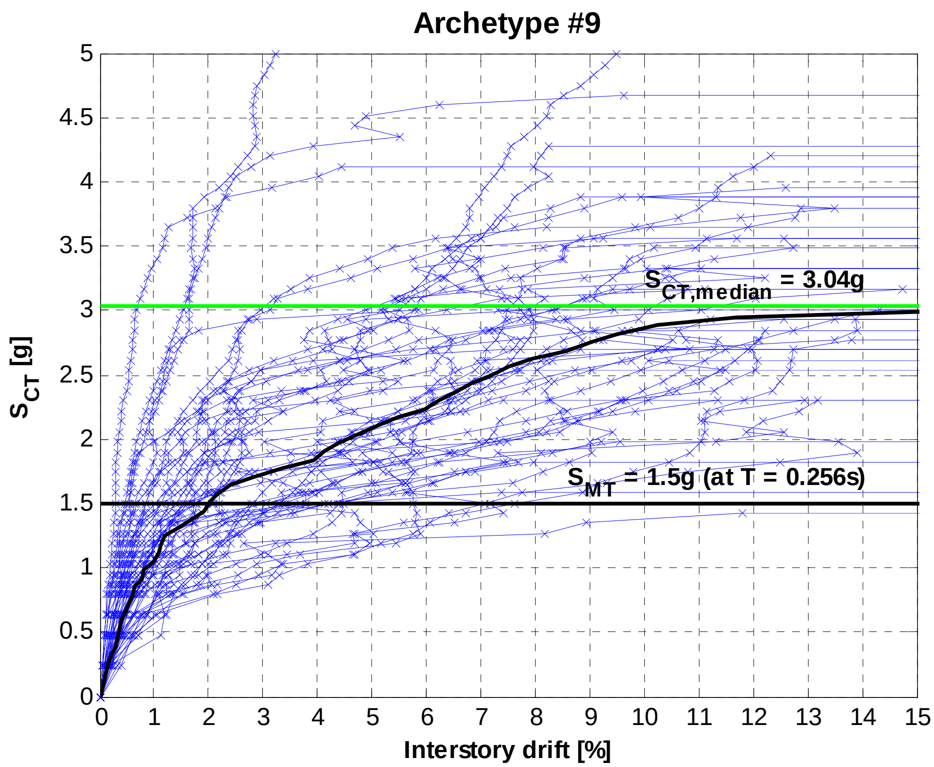

Archetype #9
$S_{CT,median}$ = 3.04g
S_{MT} = 1.5g (at T = 0.256s)
S_{CT} [g]
Interstory drift [%]

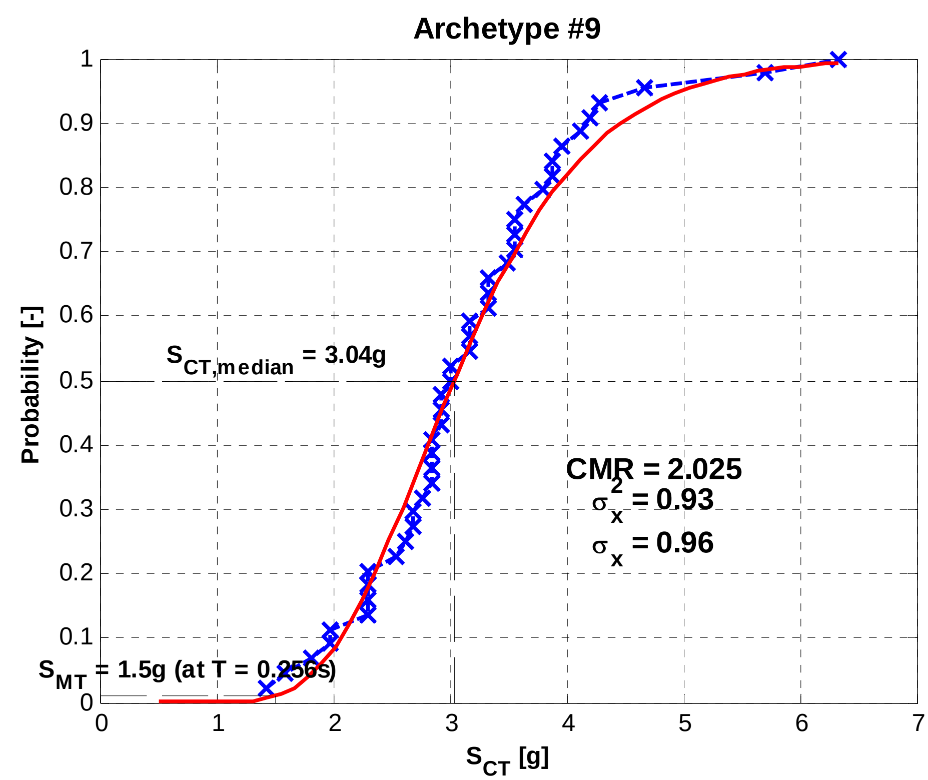

Archetype #9
$S_{CT,median}$ = 3.04g
CMR = 2.025
σ_x^2 = 0.93
σ_x = 0.96
S_{MT} = 1.5g (at T = 0.256s)
Probability [-]
S_{CT} [g]

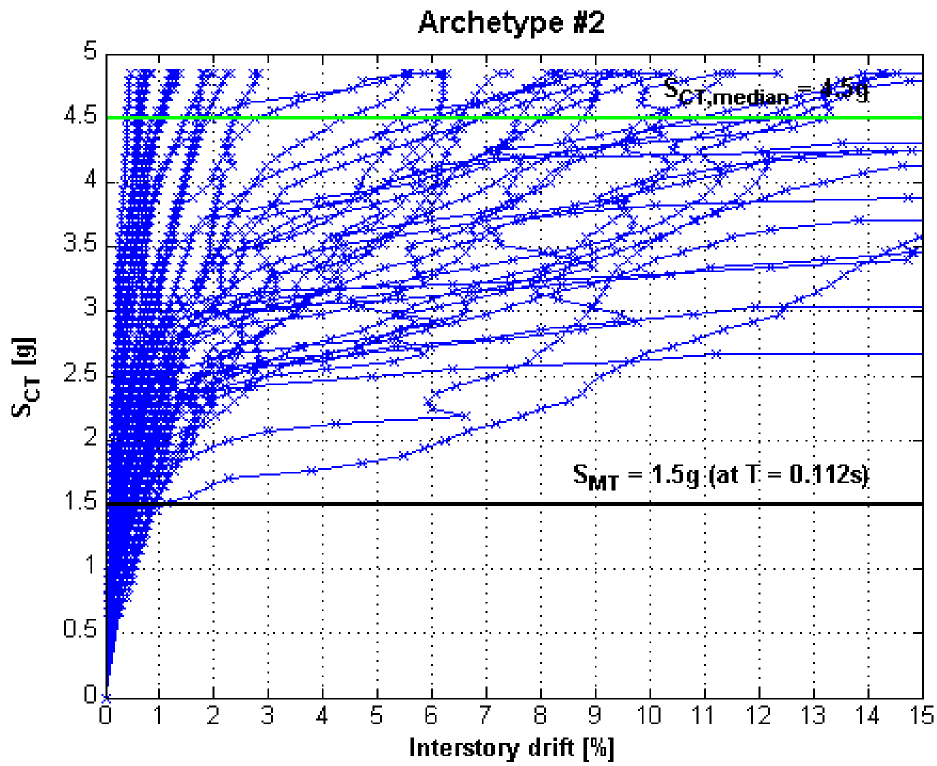

Archetype #2
$S_{CT,median}$ = 4.5g
S_{MT} = 1.5g (at T = 0.112s)
S_{CT} [g]
Interstory drift [%]

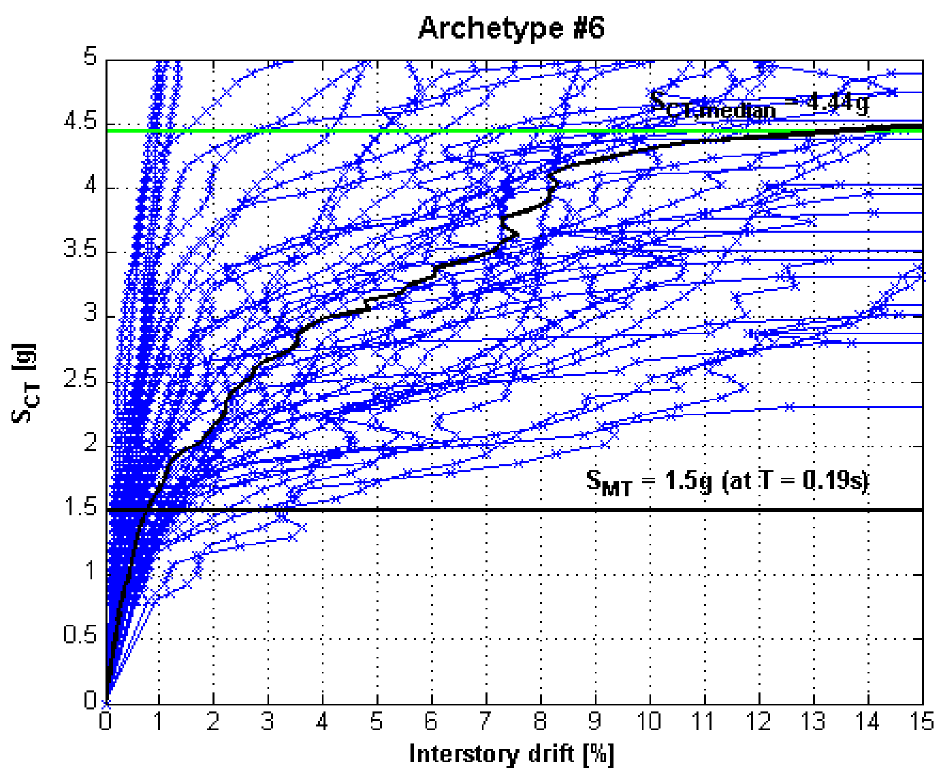

Archetype #6
$S_{CT,median}$ = 4.44g
S_{MT} = 1.5g (at T = 0.19s)
S_{CT} [g]
Interstory drift [%]

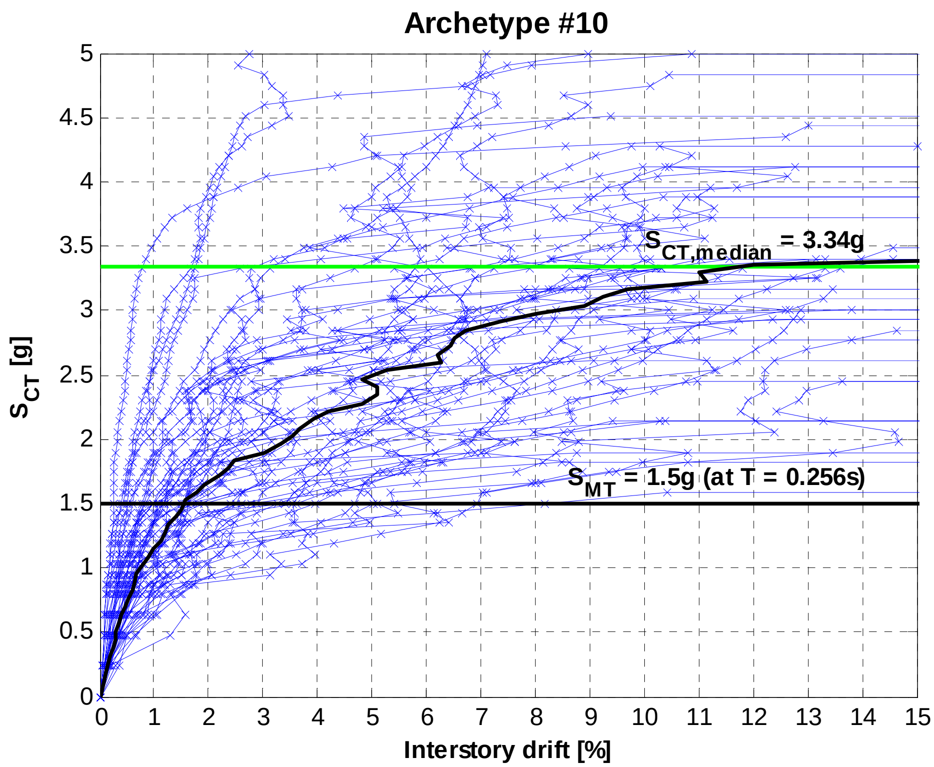

Archetype #10
S_CT [g]
Interstory drift [%]
S_CT,median = 3.34g
S_MT = 1.5g (at T = 0.256s)

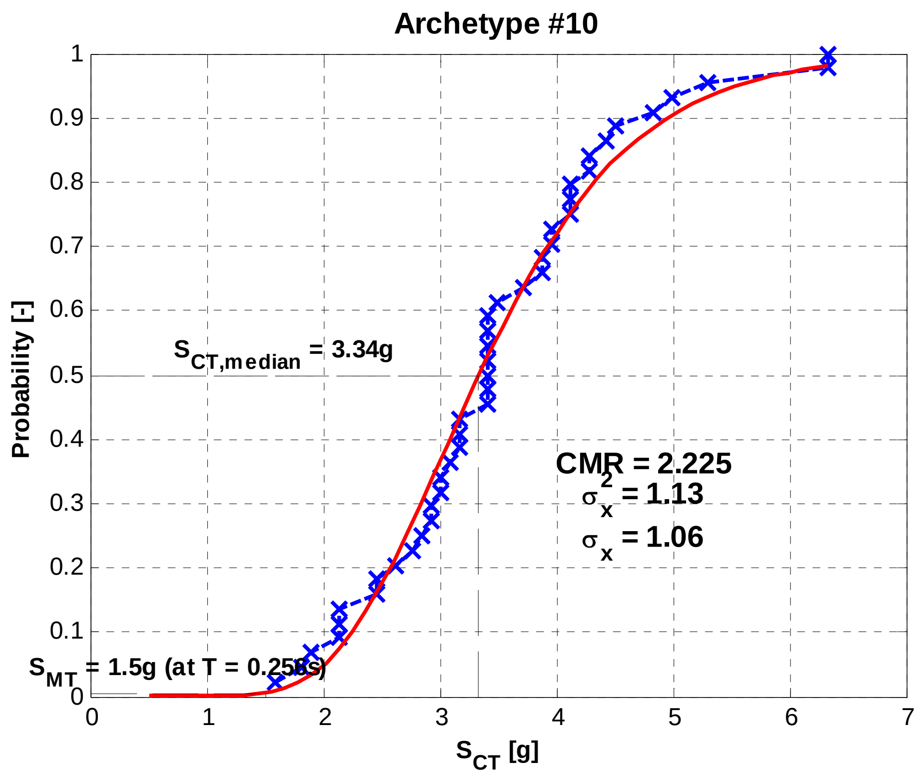

Archetype #10
Probability [-]
S_CT [g]
S_CT,median = 3.34g
CMR = 2.225
σ_x^2 = 1.13
σ_x = 1.06
S_MT = 1.5g (at T = 0.256s)

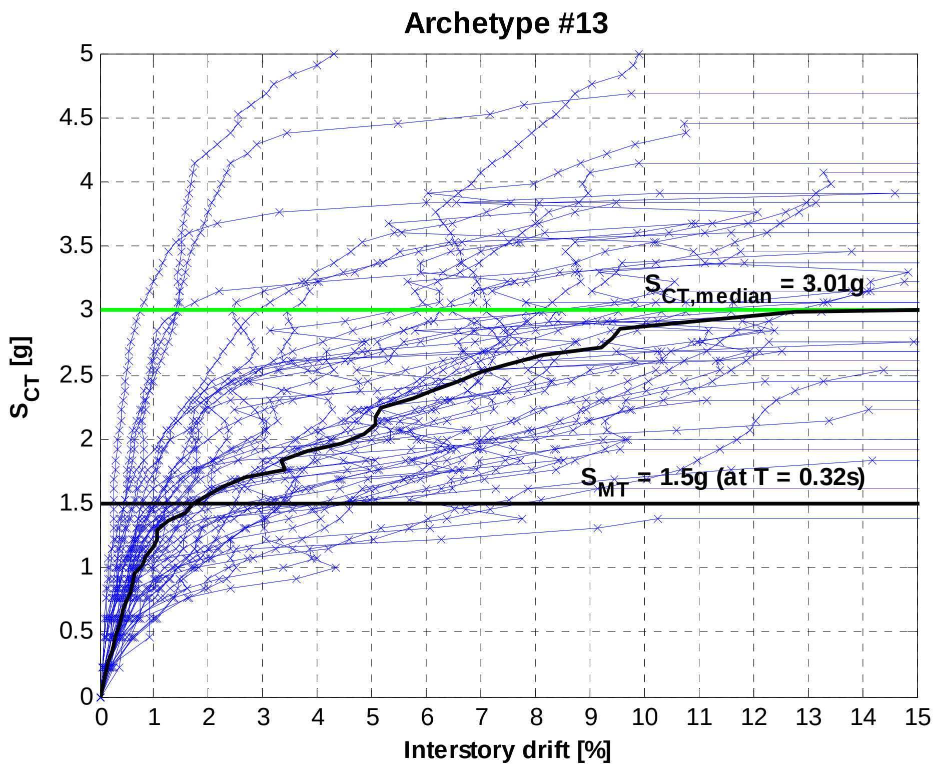

Archetype #13
S_{CT} [g]
Interstory drift [%]
$S_{CT,median}$ = 3.01g
S_{MT} = 1.5g (at T = 0.32s)

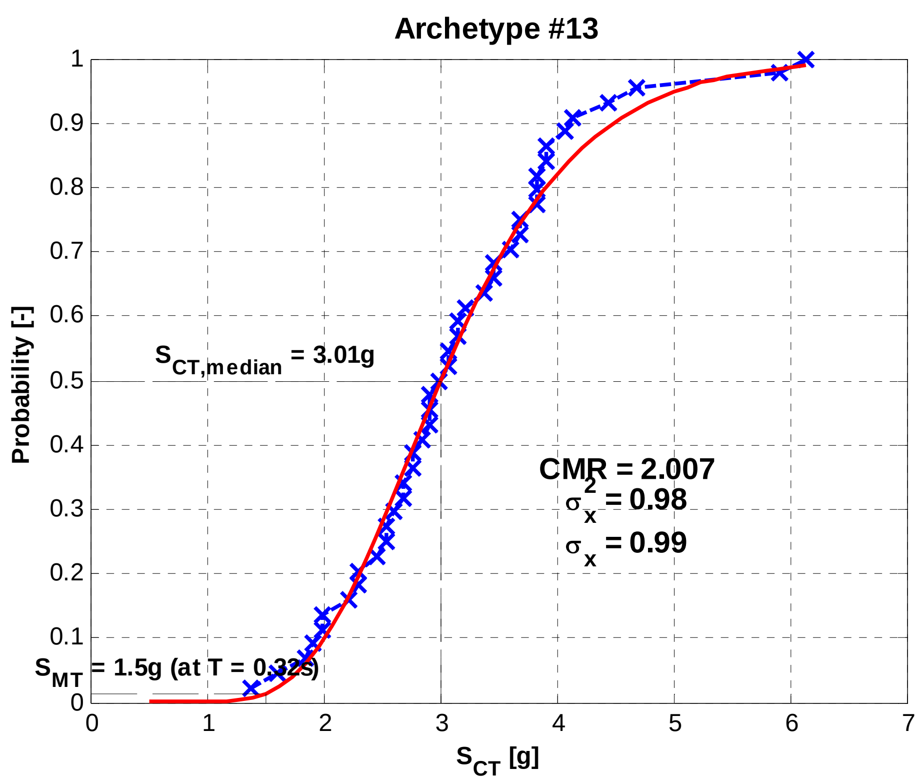

Archetype #13
Probability [-]
S_{CT} [g]
$S_{CT,median}$ = 3.01g
CMR = 2.007
σ_x^2 = 0.98
σ_x = 0.99
S_{MT} = 1.5g (at T = 0.32s)

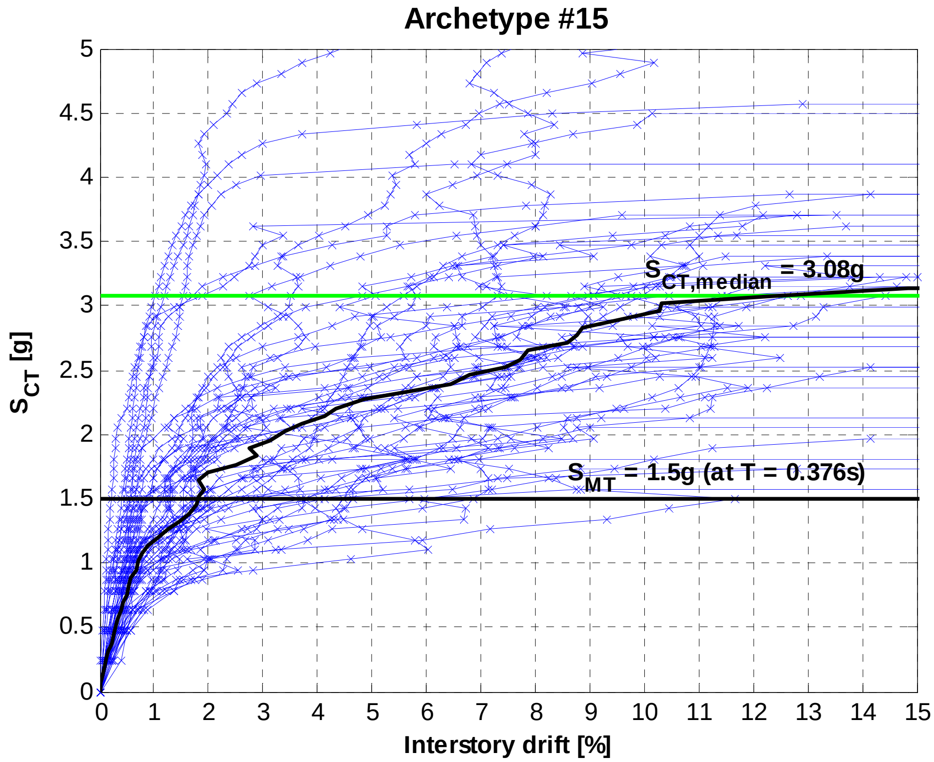
Archetype #15
5
4.5
4
3.5
3
2.5
2
1.5
1
0.5
0
S_CT [g]
S_CT,median = 3.08g
S_MT = 1.5g (at T = 0.376s)
0 1 2 3 4 5 6 7 8 9 10 11 12 13 14 15
Interstory drift [%]

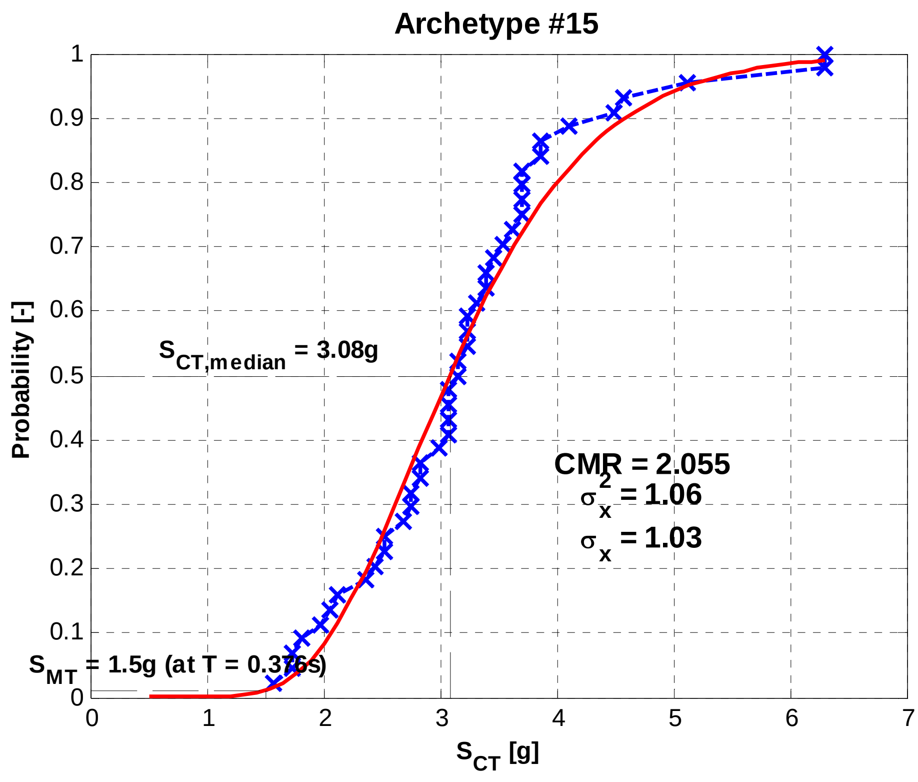
Archetype #15
1
0.9
0.8
0.7
0.6
0.5
0.4
0.3
0.2
0.1
0
Probability [-]
S_CT,median = 3.08g
CMR = 2.055
σ_x^2 = 1.06
σ_x = 1.03
S_MT = 1.5g (at T = 0.376s)
0 1 2 3 4 5 6 7
S_CT [g]

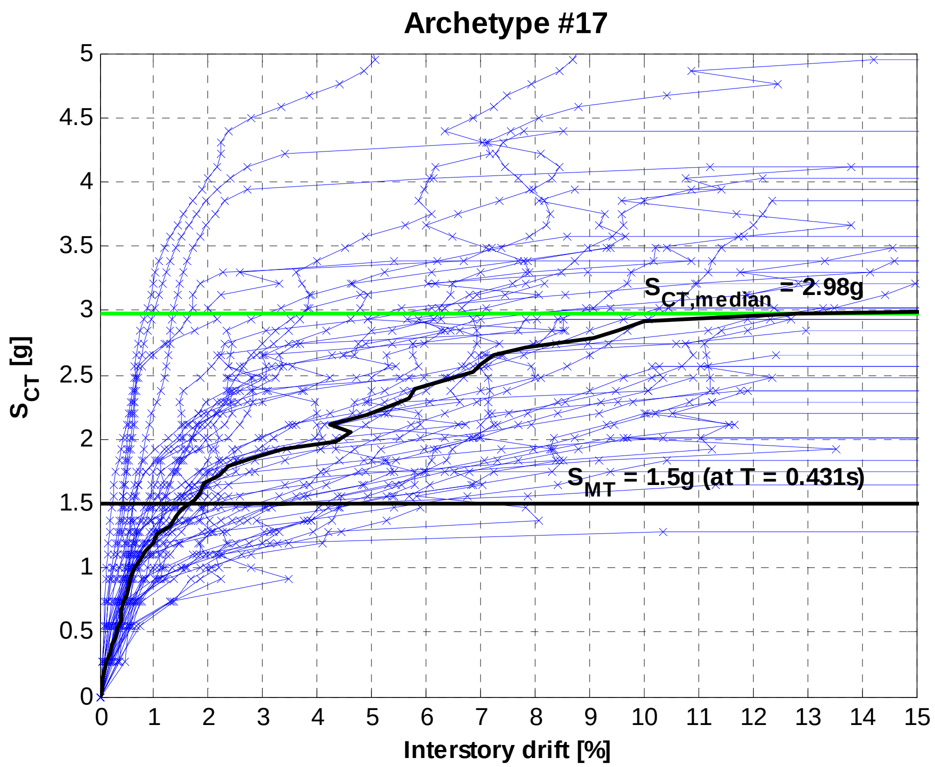

Archetype #17
$S_{CT,median}$ = 2.98g
S_{MT} = 1.5g (at T = 0.431s)
S_{CT} [g]
Interstory drift [%]

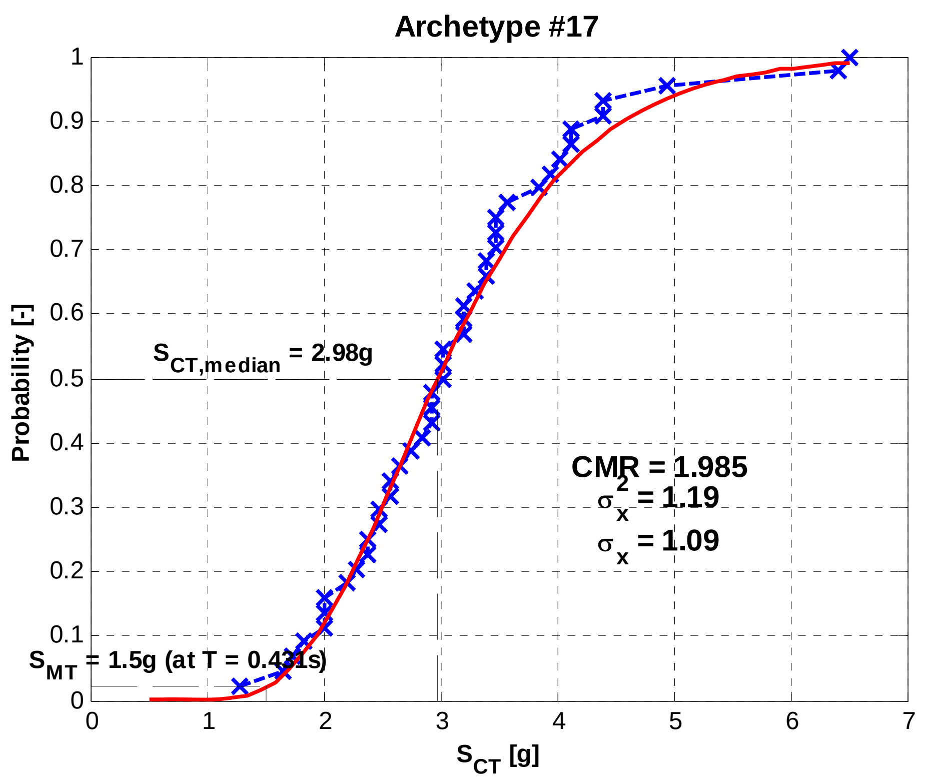

Archetype #17
$S_{CT,median}$ = 2.98g
S_{MT} = 1.5g (at T = 0.431s)
CMR = 1.985
σ_x^2 = 1.19
σ_x = 1.09
Probability [-]
S_{CT} [g]

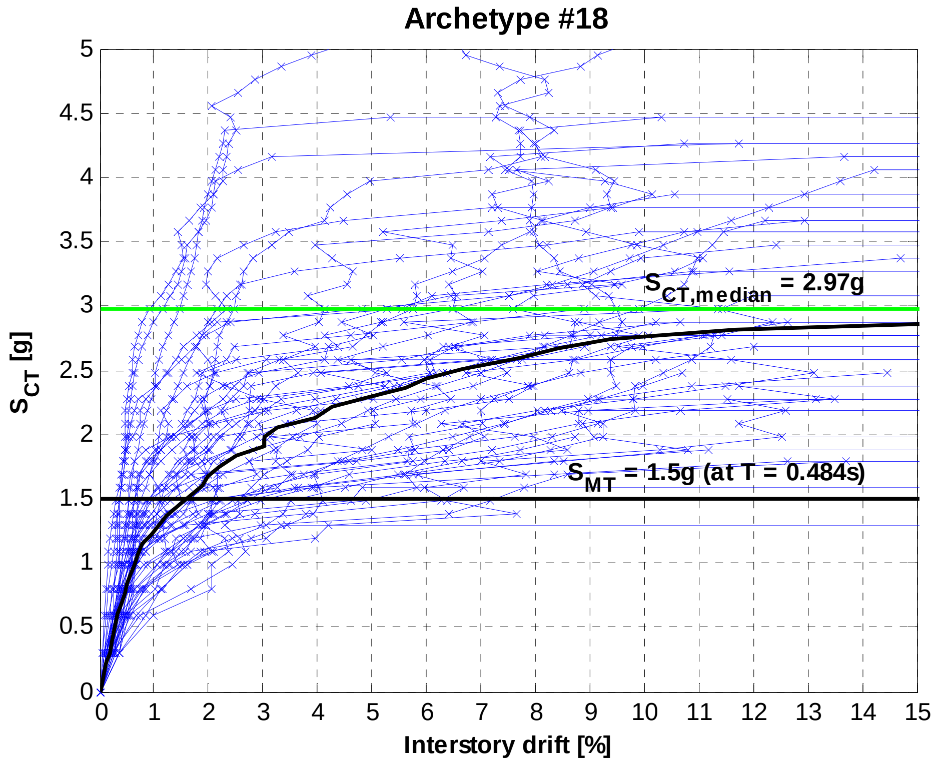

Archetype #18
$S_{CT,median}$ = 2.97g
S_{MT} = 1.5g (at T = 0.484s)
S_{CT} [g]
Interstory drift [%]

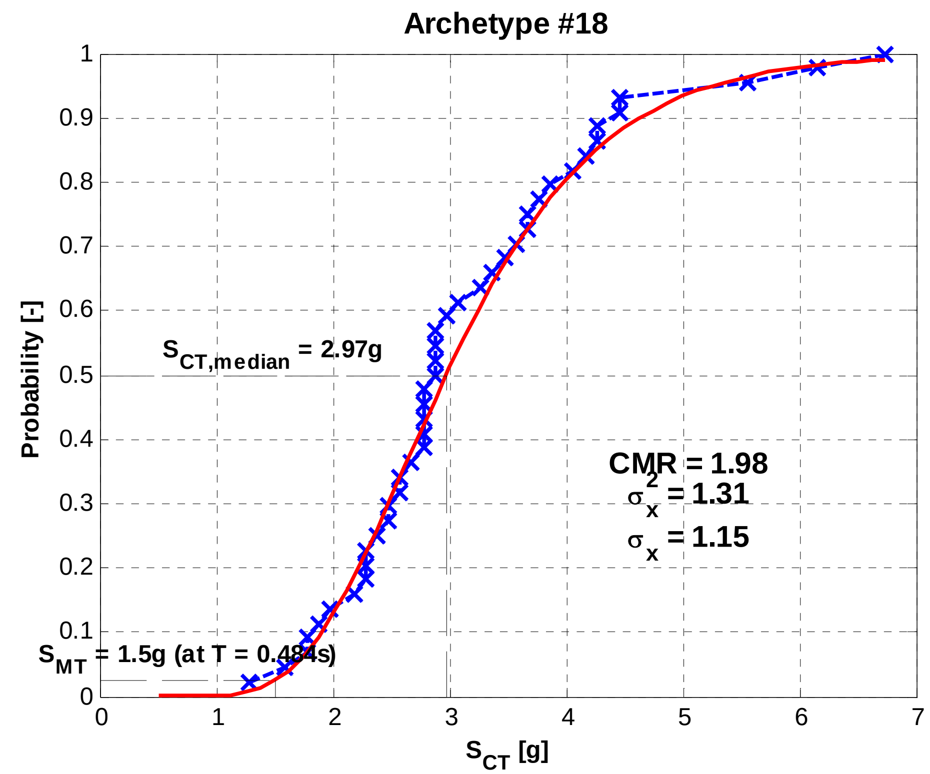

Archetype #18
$S_{CT,median}$ = 2.97g
CMR = 1.98
σ_x^2 = 1.31
σ_x = 1.15
S_{MT} = 1.5g (at T = 0.484s)
Probability [-]
S_{CT} [g]

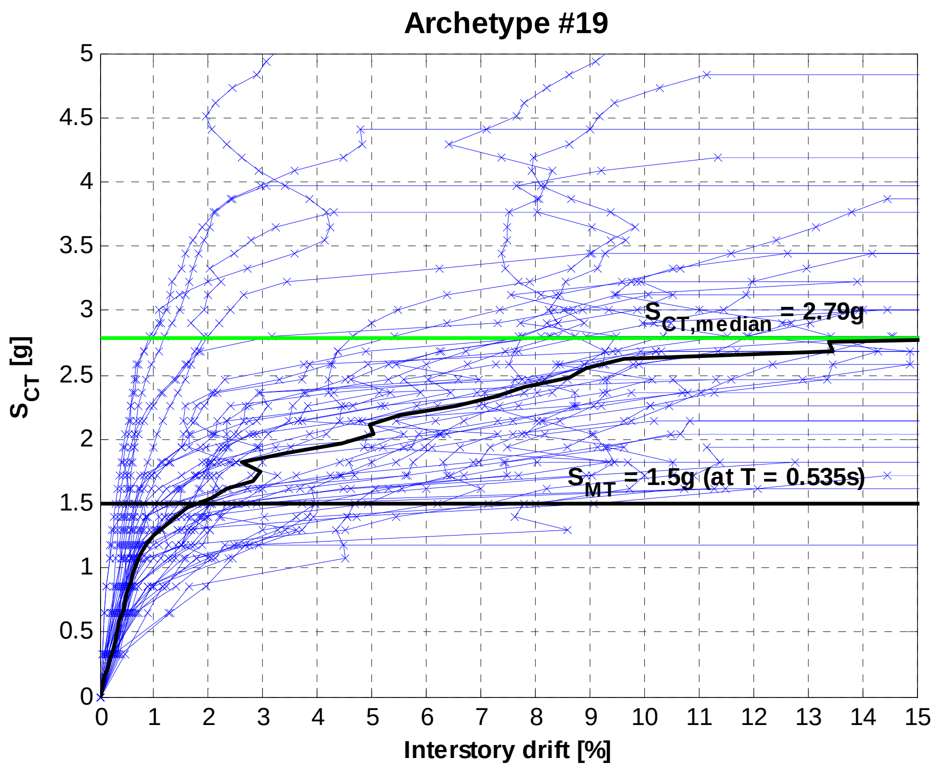
Archetype #19
S_{CT} [g]
Interstory drift [%]
$S_{CT,median}$ = 2.79g
S_{MT} = 1.5g (at T = 0.535s)

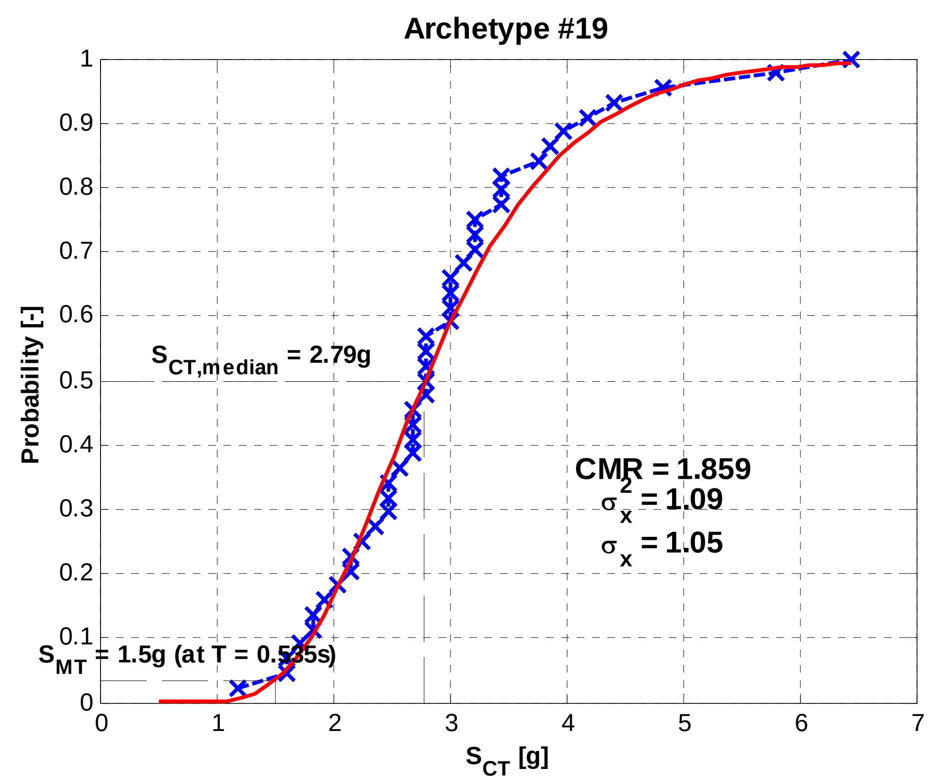
Archetype #19
Probability [-]
S_{CT} [g]
$S_{CT,median}$ = 2.79g
S_{MT} = 1.5g (at T = 0.535s)
CMR = 1.859
σ_x^2 = 1.09
σ_x = 1.05

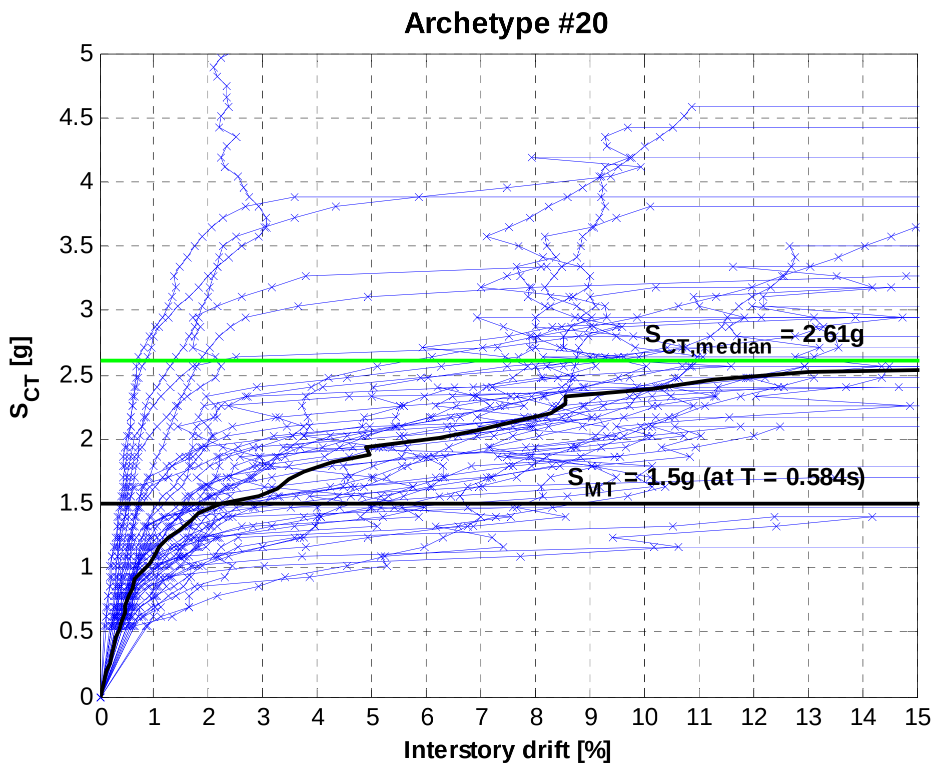
Archetype #20
$S_{CT,median}$ = 2.61g
S_{MT} = 1.5g (at T = 0.584s)
S_{CT} [g]
Interstory drift [%]

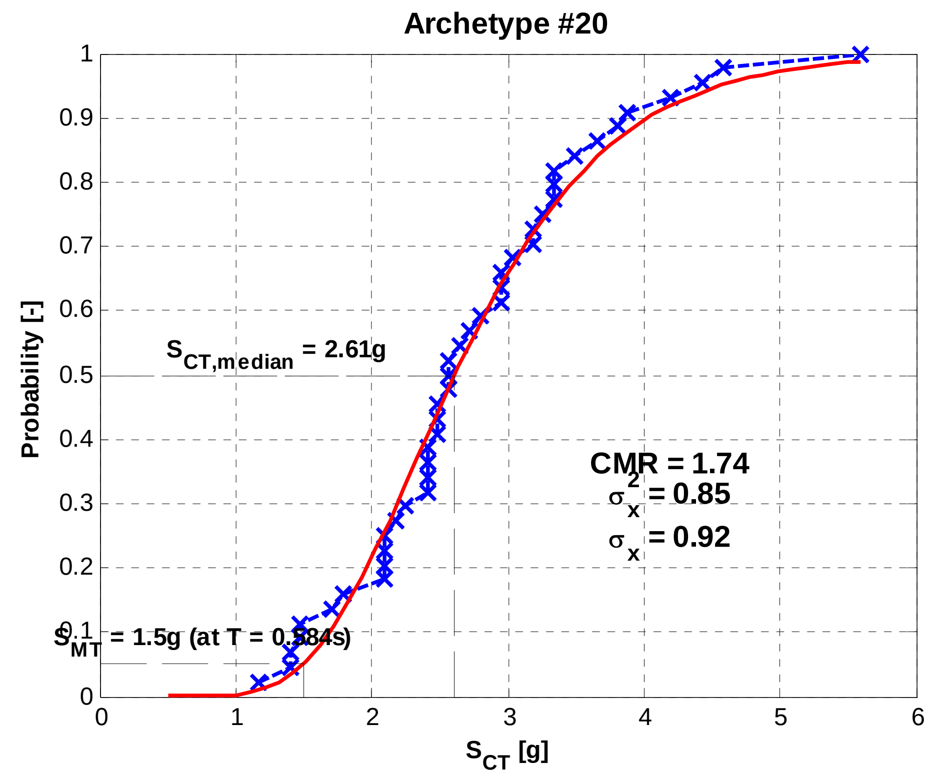
Archetype #20
$S_{CT,median}$ = 2.61g
CMR = 1.74
σ_x^2 = 0.85
σ_x = 0.92
S_{MT} = 1.5g (at T = 0.584s)
Probability [-]
S_{CT} [g]

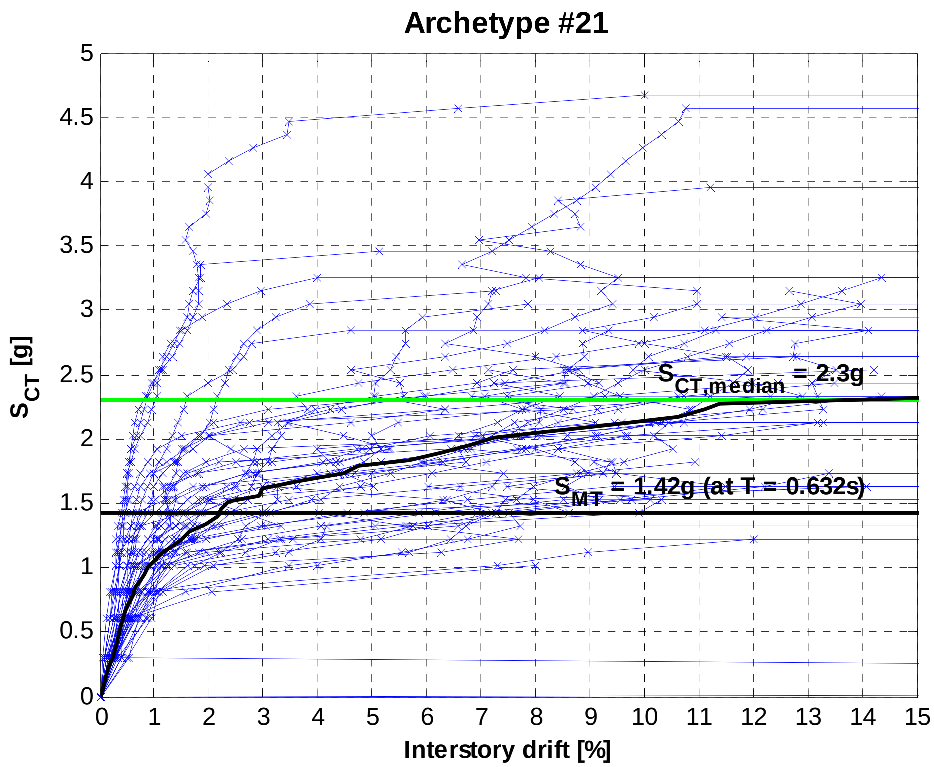
Archetype #21
S_{CT} [g]
Interstory drift [%]
$S_{CT,median}$ = 2.3g
S_{MT} = 1.42g (at T = 0.632s)

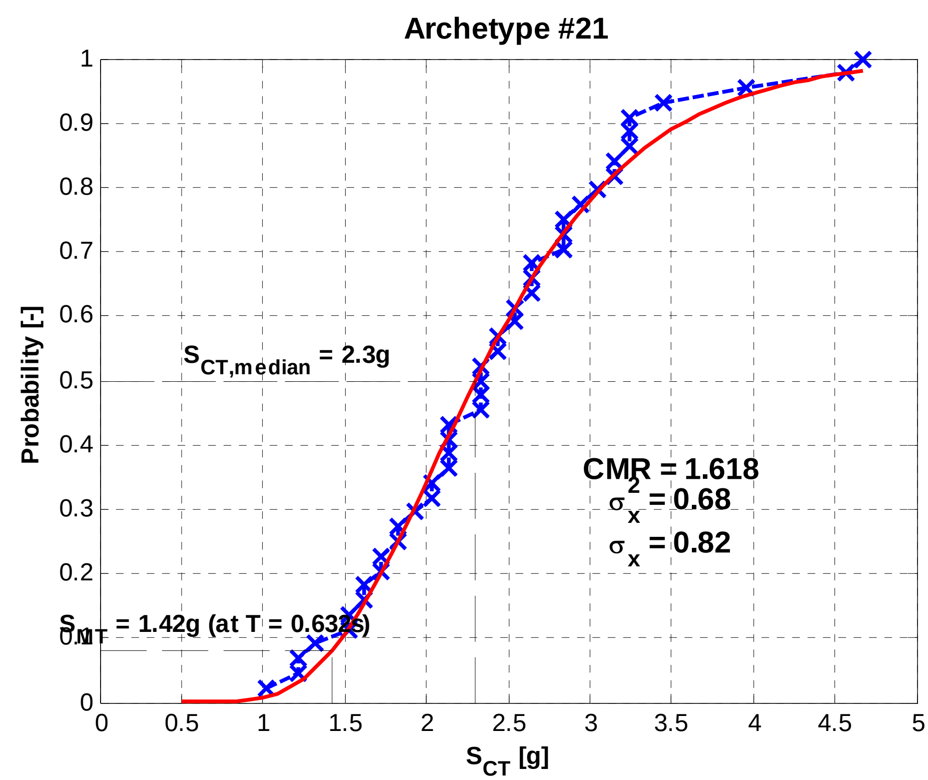
Archetype #21
Probability [-]
S_{CT} [g]
$S_{CT,median}$ = 2.3g
S_{MT} = 1.42g (at T = 0.632s)
CMR = 1.618
σ_x^2 = 0.68
σ_x = 0.82

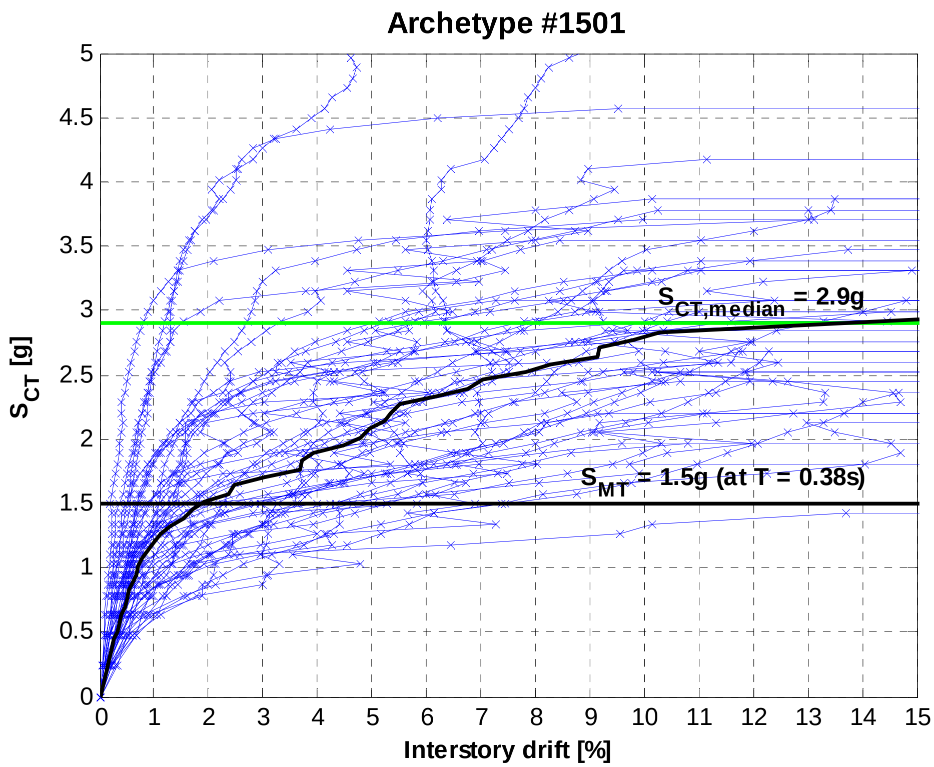
Archetype #1501
5
4.5
4
3.5
3
2.5
2
1.5
1
0.5
0
S_CT [g]
0 1 2 3 4 5 6 7 8 9 10 11 12 13 14 15
Interstory drift [%]
S_CT,median = 2.9g
S_MT = 1.5g (at T = 0.38s)

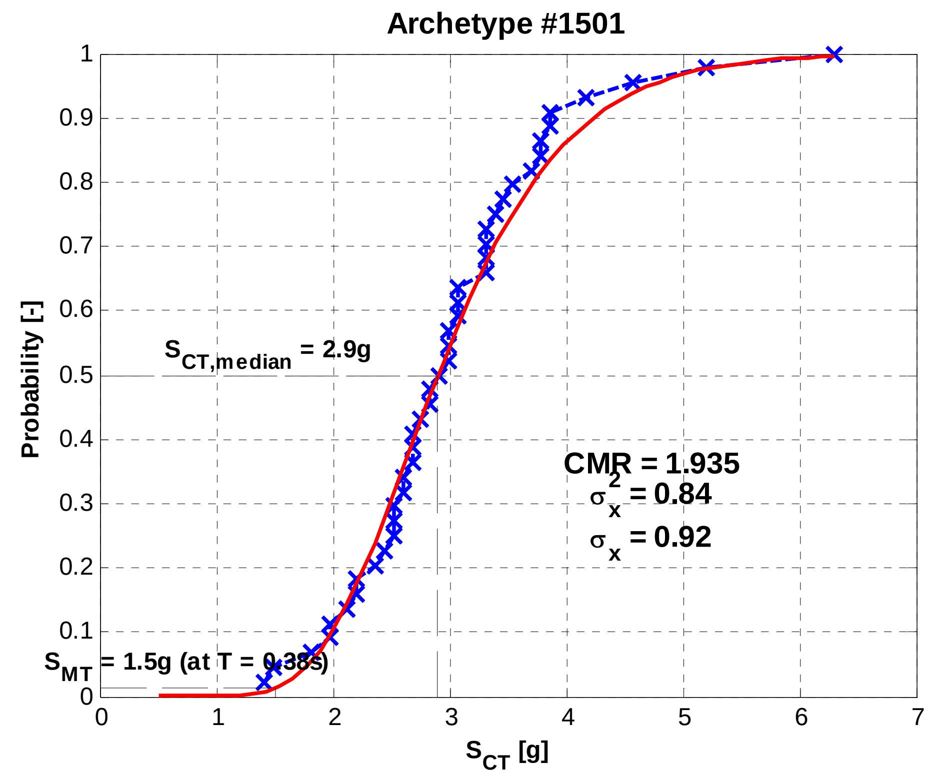
Archetype #1501
1
0.9
0.8
0.7
0.6
0.5
0.4
0.3
0.2
0.1
0
Probability [-]
0 1 2 3 4 5 6 7
S_CT [g]
S_CT,median = 2.9g
S_MT = 1.5g (at T = 0.38s)
CMR = 1.935
σ_x^2 = 0.84
σ_x = 0.92